Fracture Mechanics Evaluation of
Recirculation System Piping Welds in
Browns Ferry Unit 2 Nuclear Power Plant

STRUCTURAL INTEGRITY ASSOCIATES, INC.

3150 ALMADEN EXPRESSWAY SUITE 226 • SAN JOSE, CALIFORNIA 95118 • (408) 978-8200 • TELEX 17-1618 STRUCT

Report No.: SIR-85-008
Revision 0
SI Project No: TVA-06
June 14, 1985

Fracture Mechanics Evaluation of Recirculation System Piping Welds in Browns Ferry Unit 2 Nuclear Power Plant

Prepared by:

Structural Integrity Associates
San Jose, California

Prepared for:

Tennessee Valley Authority

Prepared by: An-Yu Kuo — A. Y. Kuo — Date: 6/13/85

S. S. Tang — Date: 6/13/85

Reviewed and Approved by: P. C. Riccardella, Project Manager — Date: 6/13/85

STRUCTURAL INTEGRITY ASSOCIATES, INC.

REVISION CONTROL SHEET

SECTION	PARAGRAPH(S)	DATE	REVISION	REMARKS
All	All	6/14/85	0	Initial Issue

STRUCTURAL INTEGRITY ASSOCIATES, INC.

TABLE OF CONTENTS

STRUCTURAL INTEGRITY ASSOCIATES, INC.

LIST OF TABLES

LIST OF FIGURES

LIST OF FIGURES (continued)

LIST OF FIGURES (continued)

1.0 INTRODUCTION

During the 1984/85 outage at the Browns Ferry Unit 2 Nuclear Power Plant, ultrasonic (UT) examination of the recirculation system piping produced indications at four weld joints which are believed to result from intergranular stress corrosion cracking (IGSCC). Similar indications have been observed at a number of other Boiling Water Reactors (BWRs) in the U.S. and overseas.

These four welds have been evaluated to demonstrate their acceptability in accordance with ASME Section XI requirements, supplemented by the recommendations of NRC Generic Letter 84-11. The welds were also analyzed using Elastic Plastic Fracture Mechanics Tearing Instability methodology to account for possible effects of low toughness weld metal. All of the welds were treated by induction heating stress improvement (IHSI) to inhibit further IGSCC propagation.

Structural Integrity Associates (SI) was contracted by the Tennessee Valley Authority (TVA) to perform the evaluations of the four weld joints. This report documents the results of the analyses, which demonstrate that design basis safety margins are maintained in these welds, considering worst case interpretation of the UT indications.

Section 2 of this report summarizes the inspection results. Section 3 describes the flaw evaluation methodology used to evaluate the welds, and Section 4 presents the evaluation results. Section 5 presents the conclusion of the evaluation regarding the continued, safe operation of the plant.

2.0 SUMMARY OF INSPECTION RESULTS

After a thorough in-service inspection of the recirculation and associated stainless steel piping systems, IGSCC-like indications were found in three ring header-to-sweepolet welds and one ring header-to-end cap weld. Figures 2-1 to 2-4 provide a weld-by-weld summary of these indications, including indication sizes detected after IHSI treatment*. All the indications are circumferentially oriented, and have been conservatively assumed to be cracks or crack-like for purposes of this evaluation.

Upper bound crack dimensions and worst case positions with respect to the applied stresses were used in the crack growth calculations and are tabulated in Table 2-1.

*Some changes in indication sizes occured between the pre- and post-IHSI inspections of these welds, but they were not significant.

TABLE 2-1

Upper Bound Crack Sizes and Worst Case Crack Locations

Weld No.	Crack Depth (% Wall Thickness)	Crack Length (inches)	Worst Applied Stress Location (degrees)*
KR-2-14	12.6	2.1	80**
KR-2-36	25	2.2	80**
KR-2-41	19	4	60**
KR-2-37	12	5	any position

* 0^{o} is along the 9:00 direction and 90^{o} is along the 12:00 direction in Figures 2-1 to 2-4.

** the highest stress location (see Section 3.1).

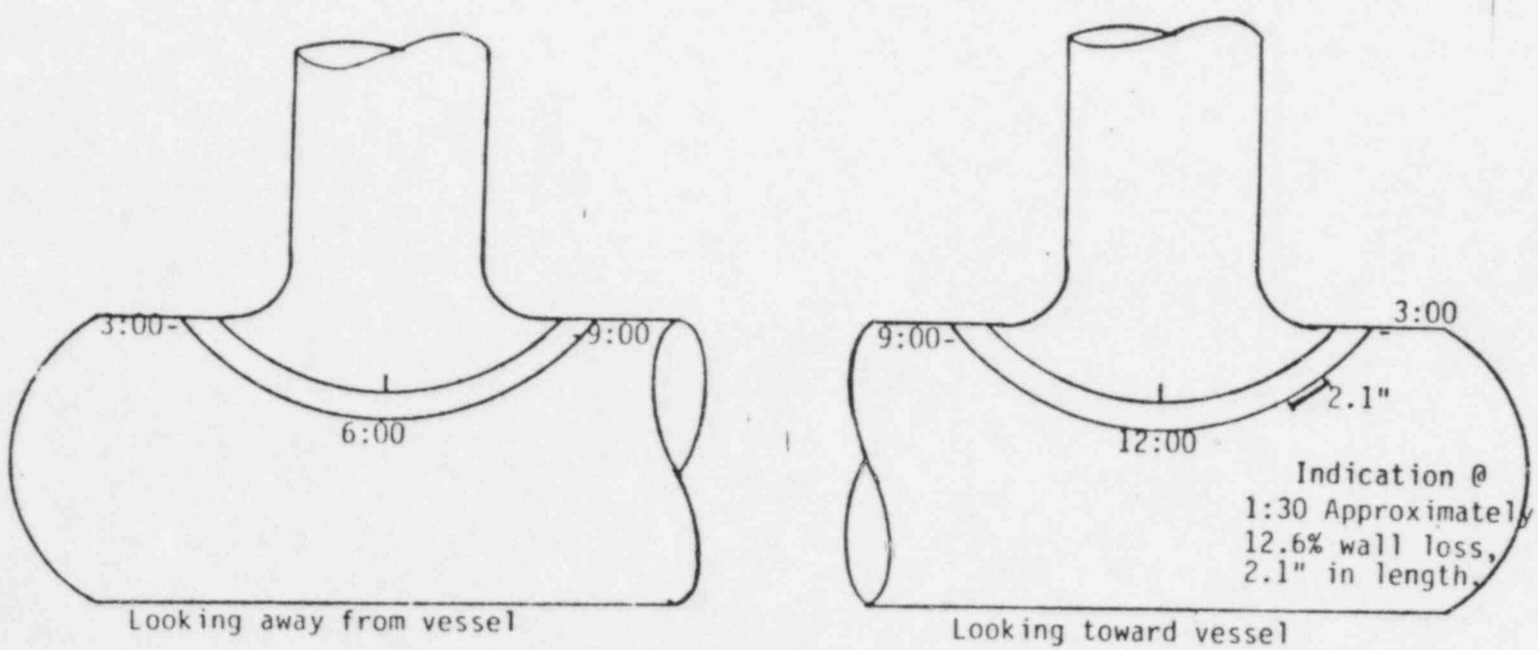

Figure 2-1. Flaw Indications in Weld KR-2-14

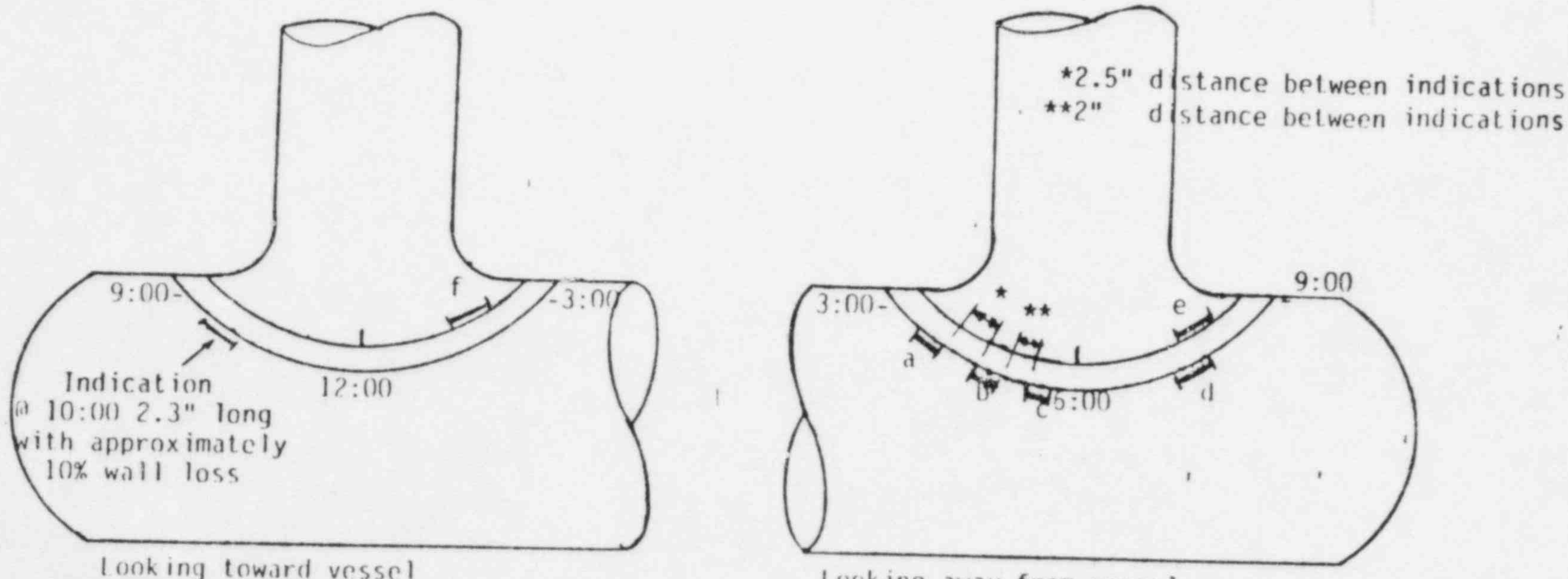

Indications	@	Approx. Wall Loss	Length
a	4:00	15%	1.2"
b	4:30	15%	1.2"
c	6:00	15%	1.1"
d	7:30	25%	2.2"
e	8:00	14%	1.0"
f	1:30	17%	1.0"

Figures 2-2. Flaw Indications in Weld KR-2-36

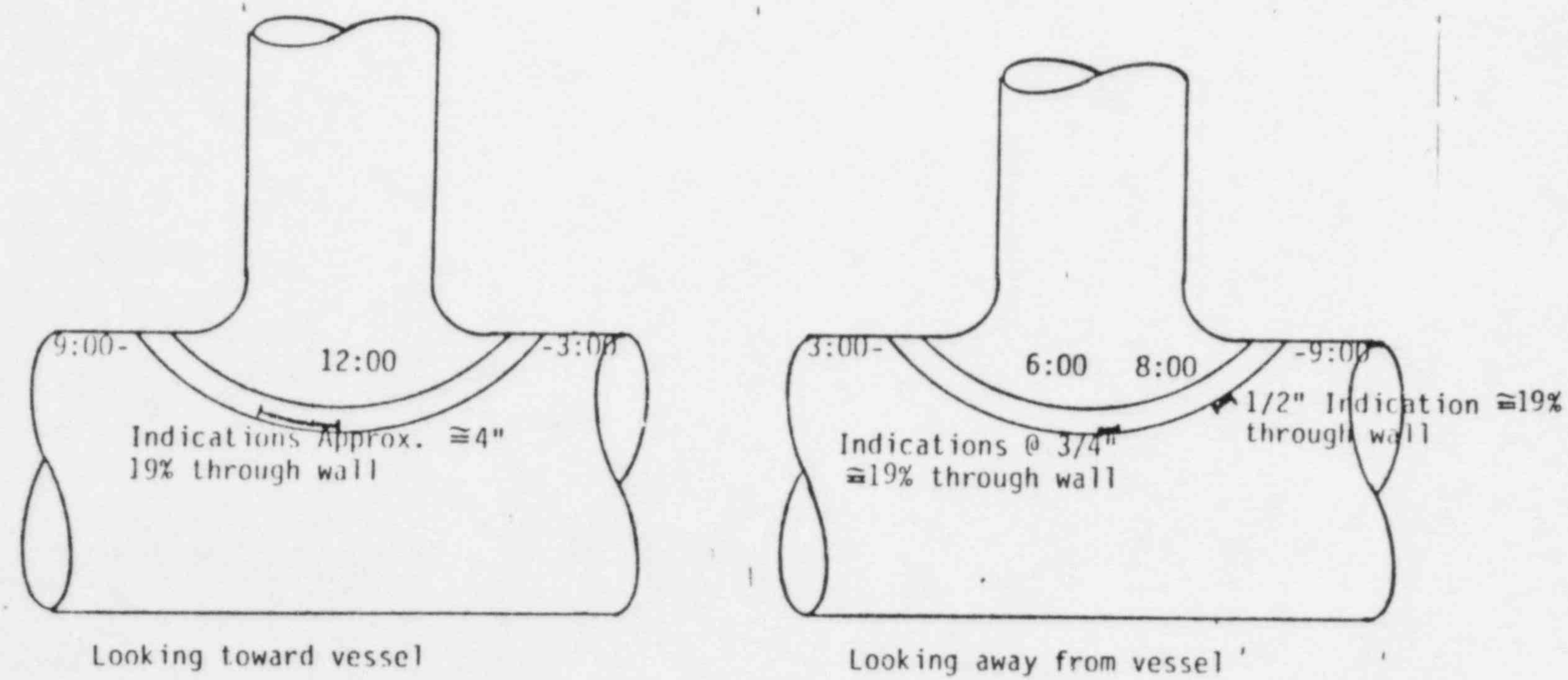

Figure 2-3. Flaw Indications in Weld KR-2-41

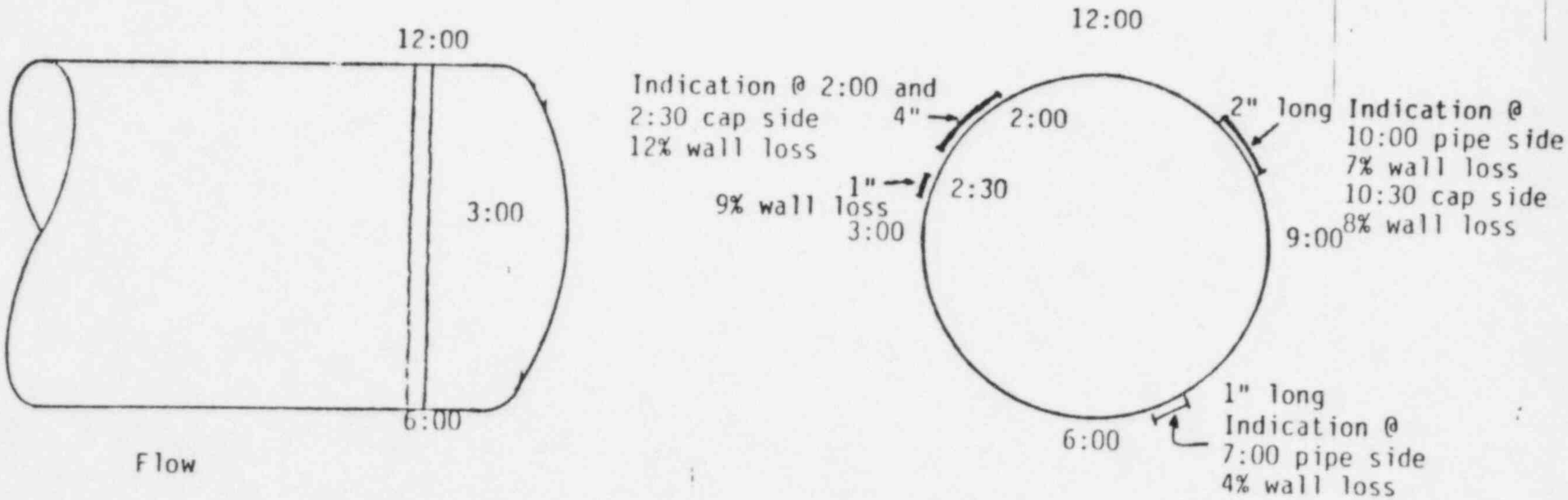

Figure 2-4. Flaw Indications in Weld KR-2-37

3.0 EVALUATION METHODOLOGY

3.1 Applied Stresses

Two major types of stresses are considered in this evaluation, stresses due to operational loadings and residual stresses. The operational stresses include pressure, deadweight, shrinkage due to weld overlay repair of weld GR-2-15, thermal, and seismic. Residual stresses were evaluated considering the beneficial effects of the IHSI treatment which was performed on these welds. These stresses are described in more detail in the following sections.

3.1.1 Stresses Due to Operational Loadings

The applied moments on sweep-o-lets KR-2-14, KR-2-36 and KR-2-41 were provided by TVA (Ref. 1). Due to the complexity of the sweep-o-let geometry, the stress due to these moments varies in a non-linear fashion along the azimuthal location of the weld between the ring header and the sweep-o-let. Also, the stress varies with distance from the crotch region of the sweep-o-let (Ref. 2). The highest stress location in a sweep-o-let is at the crotch region, and the stress decays rapidly as one moves away from that region.

Since the weld seam between the sweep-o-let and the ring header is somewhat removed from the crotch region, it does not see the full stress concentration attributable to the crotch region, but the stresses are still higher than the nominal bending stresses caused by the pipe applied moments. A stress concentration methodology for such a sweep-o-let weldment location was developed in Reference 2, and is used in this evaluation to obtain the appropriate stresses.

Table 3-1 to 3-3 present the applied stresses due to the various applied loadings for welds KR-2-14, KR-2-36 and KR-2-41 calculated in accordance with the Reference 2 methodology. As azimuthal angle increases from 0^{o} (longitudinal section) to 90^{o} (transverse sections), the stress concentration factor on bending moment increases from 1 to 3. The corresponding stress concentration factor for pressure increases from 0.6 to 1. These inside surface concentration factors also include local through-wall bending stress effects on the moment terms. At the weld location, the magnitude of the outside surface stress is approximately two-thirds of the inside surface stress and is compressive (Ref. 2).

Tables 3-1 to 3-3 also give the resultant through-wall membrane and bending stresses, and the ASME Code stress ratio $(P_m + P_b)/S_m$ for normal and faulted conditions. The maximum normal condition membrane stress is seen to be 15.4 ksi for all welds and locations, which corresponds to a maximum stress ratio of 0.91. Note that this stress ratio conservatively includes thermal expansion and weld overlay shrinkage stresses as a primary stress term. The maximum faulted condition stress ratio is only negligibly higher (0.925) and, therefore, normal conditions will govern the allowable flaw size calculations.

3.1.2 Residual Stresses

Residual stresses are known to play a significant role in IGSCC. A favorable residual stress pattern can arrest further crack growth, while an unfavorable one can accelerate crack growth. A general survey of available analytical and experimental results was performed to establish the most appropriate residual stress profile for use in the subsequent crack growth analysis. In evaluating the indications two representative post-IHSI residual stress distributions, one for the sweep-o-let welds and one for the end cap weld, are considered.

Rybicki, et al (Ref. 3) have presented extensive analytical results on induction heating of welded stainless steel pipes. These analytical results cover a wide range of piping welds and fittings. Also Ishikawajima-Harima Heavy Industries (IHI) Company in Japan did an in-depth study to qualify and verify the IHSI process for boiling water reactor piping (Ref. 4).

Figures 3-1 to 3-4 present computed and experimentally measured residual stresses for a sweep-o-let weld with IHSI treatment. Figures 3-1 and 3-2 present the inner surface stresses, circumferential and longitudinal, versus distance from the weld centerline. The measured stresses compare very favorably to the analytical results. As shown in the figures, the surface residual stress in a 12-inch sweep-o-let is about 20 to 40 ksi compressive.

Figures 3-3 and 3-4 present through-wall analytical results, from two different finite element models. They give about the same magnitude surface stress, as compared to each other and to those in Figures 3-1 and 3-2. The two finite element models also give similar through-wall residual stress patterns.

Finally, Figure 3-5 presents test data on 12 inch sweep-o-let weld to a 22 inch pipe, from Reference 5. The test data give only inside and outside surface stresses, but at three different azimuthal angles; 0°, 45°, 90°. Since no through-wall test data are available from that test, linear through-wall stress profiles are assumed. Of the three angles examined, the inside surface stress at 0° had the least compressive stress, but all three through-wall stress profiles are similar. Also, the surface stresses agree reasonably with the previous analytical and experimental results. Thus, for conservatism, the 0° residual stress distribution of Figure 3-5 was used for sweep-o-lets in this evaluation.

Figures 3-6 and 3-7 present an analytical model and IHSI residual stress results for a 16-inch end cap (Ref. 4). No results, either analytical or experimental, are available for a 22 inch end cap. Therefore, the 16 inch end cap analytical IHSI residual stress is assumed for the 22 inch end cap in the recirculation system. Figure 3-6 presents the finite element model identifying all the dimensions, boundary conditions and length of the heating coil. Figure 3-7 presents the inside and outside surface stresses as a function of the distance from the weld centerline. Near the weld centerline, the compressive surface stresses are on the order of 30 ksi. Since no through-wall data are available, a linear through-wall stress profile is assumed for the subsequent end cap crack growth analysis.

3.2 Stress Intensity Factors

Pipe dimensions used in this analysis are as follows (Ref. 1):

	22 Inch Pipe	12 Inch Pipe
Outside Diameter (in.)	22	12.75
Inside Diameter (in.)	19.75	11.592
Pipe Wall Thickness (in.)	1.125	0.579

An analytical model of a 360° circumferential crack in a cylinder of radius to thickness ratio of 10:1 (Ref. 6) was used for the fracture mechanics crack growth evaluation. The applied loading consists of piping loads due to shrinkage, dead weight, pressure, thermal expansion, and seismic and the residual stress distributions discussed in Section 3.2. For the piping loads, the loading consists of the piping stresses tabulated in Tables 3-1 to 3-3 for the sweep-o-lets, or just internal pressure stress for the 22 inch end cap (5.662 ksi axial, 11.324 ksi circumferential). The post-IHSI residual stress distributions are given in Figures 3-5 and 3-7.

For purposes of the fracture mechanics analysis, the axial stress distributions from these loading cases have been expressed in terms of third degree polynomials of the form:

$$\sigma = A_0 + A_1 x + A_2 x^2 + A_3 x^3 \qquad (1)$$

where σ is axial stress in the units of ksi, x is the distance from the inside surface, and A_0 - A_3 are the coefficients resulting from the curvefit.

The stress intensity factor for a circumferential crack in a cylinder of radius to thickness ratio of 10:1 can be expressed as follows (Ref. 6):

$$K_1 = \sqrt{\pi a}\,(A_0 F_1 + \frac{2a}{\pi} A_1 F_2 + \frac{a^2}{2} A_2 F_3 + \frac{4}{3\pi} a^3 A_3 F_4) \qquad (2)$$

where F_1, F_2, F_3, and F_4 are magnification factors and a is crack depth as shown in Figure 3-8. For the linear elastic fracture mechanics portion of the analysis, the stress intensity factors can be calculated independently for piping stress and post-IHSI residual stress distributions, and the resultant stress intensity factor is the superposition of the two loading cases.

3.3 Crack Growth

A large body of laboratory data exist on stress corrosion crack growth rates for sensitized stainless steels in simulated BWR environments. These data are summarized in Figure 3-9, taken from Reference 7. These data were obtained using fracture mechanics type specimens with different crack sizes and loadings, which can be characterized by the crack tip stress intensity factor K. The data represent a wide variation in material sensitization, as well as levels of dissolved oxygen in the water. While subject to some criticism because the simulated water chemistry in these tests did not contain levels of impurities (chlorides, sulfates, etc.) that could exist in operating BWRs, the "best estimate" curve of Figure 3-9 is widely believed to provide a reasonably conservative bound of stress corrosion crack growth rate for weld sensitized 304 stainless steel in BWR environments. This curve can be described by a power law representation of the form:

$$da/dt = 2.27 \times 10^{-8}(K)^{2.26} \qquad (3)$$

where a is the crack depth in units of inches, t is time in units of hours, and K is the stress intensity factor in units of Ksi $\sqrt{in.}$

Crack growth analyses typically make use of one of the two assumptions illustrated in Figure 3-10 regarding crack length extension, self-similar crack growth or constant aspect ratio crack growth. The former assumes that the incremental crack extension is the same at all points on the crack front, while the latter assumes that the ratio of depth to length remains constant during crack extension. Considering field and laboratory experience with circumferential crack extension, it appears that the self-similar assumption may underpredict crack length versus time, while the constant aspect ratio assumption overpredicts.

Recent work by Gerber (Ref. 8) under contract to EPRI provides a new approach for addressing circumferential crack extension which is more technically defensible than the above self-similar or constant aspect ratio approaches. This approach utilizes data generated in a laboratory stress corrosion test of a 26 inch diameter welded pipe specimen at Battelle Pacific Northwest

Laboratories (Ref. 9). IGSCC was induced in this pipe through loading to a high applied stress in a simulated BWR environment, which was accelerated by the use of graphite wool to create an artificial crevice. Crack growth occurred and was monitored both during operation and at several scheduled shutdown intervals for the test. A number of small cracks initiated early in the test, the length of which was periodically measured and the initiation of new cracks was noted and their lengths subsequently tracked as well. At the completion of the test, there were a total of 63 cracks with a combined length of 32.57 inches.

The average effective circumferential crack extension observed in this test is presented in Figure 3-11. This rate includes both growth of existing cracks as well as new defects initiating and contributing to the effective crack growth rate in each inspection interval. Examination of Figure 3-11 suggests that an average effective circumferential crack growth rate of 0.5 mils/hour should give a reasonably conservative estimate. Thus, 0.5 mils/hours was used as the crack length growth rate in this report. It should be pointed out, however, that although this is an average effective rate, it is based on a laboratory test in which the local environment, load and cycles were all intentionally modified to accelerate IGSCC relative to actual plant conditions. Test and analytical data (Reference 4) have also shown that the IHSI will suppress not only crack initiation but also crack propagation for cracks in both the length and depth directions.

3.4 Allowable Flaw Size (IWB-3640)

Based on detailed calculations presented in References 10 and 11, allowable flaw sizes for various levels of primary and applied loading ($P_m + P_b$) have been specified in ASME Section XI, IWB-3640 (Ref. 12). A tabulation of allowable flaw sizes as a function of applied load is given in Table 3-4, which is taken directly from Section XI, IWB-3640. Note that this table permits very large defects in some cases (as great as 75% of pipe wall) and does not include consideration of any stress other than primary, notably secondary and peak stresses from the design stress report as well as any weld residual stresses or misalignment/fit-up stresses which might exist from construction. The argument for this exclusion is that, given the extremely high ductility of austenitic stainless steel, these strain controlled effects will self-relieve after a small amount of plastic deformation and/or stable crack extension, and will have little or no impact on the loads and flaw sizes needed to cause unstable crack propagation or pipe rupture.

However, some recent fracture toughness data may invalidate the above argument, at least for some classes of austenitic weld metal (Ref. 13). To account for possibility of low ductility weld metal, secondary stresses from stress report were also included in the IWB-3640 allowable flaw size determinations in this report, although it is not required by the ASME Code.

It is important to note that the very low measured toughness occurred only in a small percentage of the materials addressed in Reference 13, and may be of only limited concern from a probabilistic viewpoint. Indeed, most IGSCC observed to date has been restricted to weld heat affected zones, which should exhibit the high toughness attributed to base material. Also, the low toughness data to date has been limited to flux types of weldments (submerged arc or shielded metal arc), which are not used in current construction practice nor in weld overlay repairs of pipe cacks. Nevertheless, tc address these possible concerns, the analysis procedure used in this report includes thermal expansion effects as a primary stress condition in determining allowable flaw size from Table 3-4.

3.5 Allowable Flaw Size (EPFM)

Methodologies from References 14 and 15 are also used in this report to calculate applied J and T values for circumferential through-wall or part-through-wall cracks in pipes as functions of applied loading. Details of the methodology used are provided below. These computed, applied J and T values are then compared to a J/T material curve on a J/T stability diagram (as in Figure 3-12) to provide a second means of determining allowable flaw size.

3.5.1 360° Part-Through-Wall Cracks in Tension

As shown in Figure 3-13, consider a cylinder with an inner radius R_i, outer radius R_o, and wall thickness $t = R_o - R_i$, containing an internal axisymmetric part-through crack of depth a. σ^{∞} denotes the far field uniform tensile stress and c = t-a the uncracked ligament. A radius to thickness ratio (R_i/t) of 10 is used in this report, which corresonds approximately to the Schedule 80 piping used in service. The elastic-plastic formulae for J-applied in this case have been obtained from Reference 14 and are as follows:

$$J_{appl} = J_e + J_p$$
$$= f_1\,(a_e, R_i/R_o)(P^2/E') + \alpha\,\sigma_o\,\varepsilon_o\,C\,(a/t)\,h_1\,(P/P_o)^{n+1} \qquad (4)$$

where:

$$f_1(a_e, R_i/R_o) = \frac{a\,F^2}{\pi(R_o^2 - R_i^2)^2}$$

$E' = E/(1-\nu^2)$

E = Young's Modulus

ν = Poisson's Ratio

σ_o= Yield Stress

ε_o= Yield Strain

α,n= Material constants of Ramberg-Osgood Model

$$a_e = a + [1 + (P/P_o)^2]^{-1}\,[(\frac{n-1}{n+1})\,(\frac{K}{\sigma_o})^2/(2\pi)]$$

$K = \sigma^{\infty}\sqrt{\pi a} \cdot F$

$P_o = 2/\sqrt{3}\,\sigma_o\,[R_o^2 - (R_i + a)^2]$

$P = \sigma^{\infty}\pi(R_o^2 - R_i^2)$

F = function given in Table 3-5

h_1 = function given in Table 3-6

For materials with n values between 1 and 10 but not exactly as provided in Table 3-6, the corresponding h_1 values can be calculated by interpolation.

The non-dimensional tearing modulus, T_{appl} is calculated by:

$$T_{appl} = (\frac{E'}{\sigma_o^2})\,(d\,J_{appl}/da) \qquad (5)$$

where T_{appl} is the applied tearing modulus from loading and all the other quantities are defined in the same manner as those in Equation (4).

The applied tearing modulus can be determined numerically by applying a finite difference scheme on the above definition of T_{appl}, e.g.,

$$T_{appl} = \left(\frac{E'}{\sigma_o^2}\right) \frac{J(a+da) - J(a)}{da} \qquad (6)$$

where da is a small crack length increment.

3.2 Through-Wall Cracks in Tension

As a second case, consider a cylinder containing a circumferential through-wall crack of length 2a, and subjected to remote uniform tension as shown in Figure 3-14. In this figure, R denotes the mean radius, t the wall thickness, 2γ the total angle span of the crack, and 2a = 2Rγ the total length of the crack. 2b = 2πR is the pipe circumference, and P is the applied load. Load is applied by a uniform stress field at its ends given by

$$\sigma^{\infty} = P/(2\pi Rt) \qquad (7)$$

Again, a radius to thickness ratio of 10 is used to approximate service piping. For a Ramberg-Osgood material, the elastic-plastic J-integral estimation has been obtained from Reference 15 and is given as follows:

$$J_{appl} = J_e + J_p$$

$$J_{appl} = f_1\left(a_e, \frac{R}{t}\right)(P^2/E) + \alpha\sigma_0\,\varepsilon_0\,C\,(a/b)\,h_1\,(P/P_o)^{n+1} \qquad (8)$$

where:

$f_1(a_e, \frac{R}{t}) = a\,F^2/(4\pi R^2 t^2)$

E = Young's modulus

σ_0 = Yield stress

ε_0 = Yield strain

α,n = material constants of Ramberg-Osgood Model

STRUCTURAL INTEGRITY ASSOCIATES, INC.

$$a_e = a + [1 + (P/P_0)^2]^{-1} [(\frac{n-1}{n+1})(\frac{K}{\sigma_0})^2]/(\beta\pi)$$

$$K = \sigma^{\infty}\sqrt{\pi a}\ F$$

$$P_0 = 2\ \sigma_0\ Rt\ [\pi - \gamma - 2\ \sin^{-1}(1/2\ \sin\gamma)]$$

F = function given in Table 3-7

h_1 = function given in Table 3-8

Interpolation is again used for materials with n values between 1 and 7, but n t exactly as provided in Table 3-8.

The non-dimensional tearing modulus T_{appl} can be evaluated by differen- t ation of J_{appl} in the same manner as described in Section 3.5.1 for part- t ough-wall cracks.

.3 Limitations for J-Controlled Growth

order for the above tearing modulus stability concept to be valid, certain itations on the theory must be checked. These limitations are necessary ensure that the incremental crack growth and non-proportional loading ne in the immediate vicinity of the crack tip are sufficiently small to ustify use of the J-integral in the analysis of crack growth, a condition which is defined in Reference 16 as "J-controlled growth". These conditions e generally satisfied, in the large scale yielding range, if the uncracked gament of the cracked cross-section (b) is sufficiently large to satisfy e following criteria:

$$\omega = \frac{b}{J}\ \frac{dJ}{da} >> 1 \tag{9}$$

and

$$\rho = \frac{b\sigma_0}{J} >> 1 \tag{10}$$

While there are no generally accepted rules for how much greater than 1 these p ameters must be to ensure J-controlled growth, a value of ω=5 to 10 i suggested as a quate for Equation (9) and a value of ρ=25 has been used n a number of sources for Equation (10). These parameters are thus calculated in the J-T analyses which follow, and compared to the above values to provide an assessment of the validity of the calculations.

3.5.4 Stress-Strain Laws Considered

The primary material stress-strain law used in this report is based on test data for stainless steel weldments and base metal reported by Westinghouse, (Ref. 17). Figure 3-15 illustrates these stress-strain data at operating temperature and their Ramberg-Osgood representations. A complete tabulation of material tensile properties and corresponding Ramberg-Osgood parameters for these materials are listed in Table 3-9 at both 75°F and 550°F. The weldment material properties at 550°F are used in this report as the primary basis for the J-T analysis results.

However, since studies have shown J-T analyses to be extremely sensitive to the specific material stress-strain law characteristics used in the analysis, Ramberg-Osgood constants have been obtained for a number of different stainless steel weldment materials. Table 3-10 lists three commonly used data sets for weldment material at 550°F. As a parametric study, allowable flaw size results have been calculated using all three data sets.

3.5.5 Weld Metal Toughness Data

Data on the elastic-plastic toughness properties of austenitic stainless steel welds are presented in References 17 to 21 in the form of J-resistance curves, J-T values, and/or tabulated J_{Ic} and J-Resistance curve slope values. These data have been used to determine lower bound J-T material toughness curves for comparison with applied values to assess crack instability and allowable flaw size by the J-T method. The effects and results of welding process have been considered in establishing lower bound toughness properties for such stability evaluations.

A compilation of applicable material toughness J-T curves from the above references is shown in Figure 3-16. These curves represent wrought stainless steel base metal toughness, along with the toughness of stainless steel weld metal representing submerged arc welding (SAW), stick or shielded metal arc welding (SMAW), and gas tungsten arc welding (GTAW) or tungsten inert gas (TIG) welding processes. With the exception of the data from Reference 20, the J-T curves in Figure 3-16 were derived from J vs. crack extension (Δa) curves (J-R curves) and the following equation.

$$T = \frac{E'}{\sigma_f^2} \quad \frac{dJ}{da} \quad , \qquad (11)$$

where T = tearing modulus

$E' = E/(1 - \nu^2)$

E = elastic modulus = 30,000,000 psi

ν = Poisson's ratio = 0.3

σ_f = material flow stress = 50,000 psi

dJ/da = slope of J-R curve at specific Δa

Because of the absence of tensile properties in many cases, the above values of flow stress and elastic modulus were assumed throughout. J-R curves and tensile properties were not available from Reference 20, so J-T curves were used directly from this reference.

Figure 3-17 presents lower bounds of the toughness data for the various categories of material in Figure 3-16. It can be seen that there are distinct differences in lower bound material toughness between the wrought base metal and the various weld metals. The base metal is the toughest material (largest values of J and T), with the SAW and SMAW weld metals being the least tough, and the TIG weld metal having intermediate toughness.

As shown in the previous figures, SAW and SMAW welds possess lower toughness than TIG weld metal. Differences in the welding processes, primarily heat input differences and the use of flux versus inert gas shielding, can be used to explain such toughness differences. Key features of the TIG (GTAW), SMAW and SAW processes (Ref. 22) are given in Table 3-11, along with the relationship to weld metal toughness. Essentially, SAW is a high heat input, flux-shielded process which can result in relatively coarse microstructures and relatively heavy slag/non-metallic inclusion contents. Such microstructures would tend to give reduced toughness (Ref. 23). In comparison, TIG is a low heat input process with inert gas shielding rather than flux. Therefore, TIG welds should be of superior toughness. SMAW has intermediate heat input and shielding by gas and molten flux from the electrode covering. Thus, SMAW welds are expected to have intermediate toughness - lower than TIG and slightly higher than SAW. Figure 3-16 generally illustrates this expected trend.

Lower bound J-T toughness curves for use in this analysis were derived from data of Figure 3-16 and 3-17. Essentially, the data were divided into three categories based on the preceding toughness discussions: base material, TIG weld metal, and SAW and SMAW weld metal. For each of these categories, the lower bound curves at low J values were corrected for specimen size effects, and merged with the lower bound curves at higher J values from Reference 20 in a conservative manner.

To account for the effects of specimen size and geometry in the small specimen data of References 17, 18, 19 and 21, a modified J approach, known as J_m, was used along with a modified T, T_m (Ref. 24 and 25). Reference 24 shows that J_m and T_m can correlate data for test situations in which the conditions for J-controlled crack growth described in Section 3.5.3 are grossly violated. This approach is applied here to adjust the lower bound data of Figure 3-17.

From Reference 23, J_m is computed for the compact tension specimen as follows:

$$J_m = J + \int_{a_o}^{a} \gamma \, \frac{J_p}{b} \, da \qquad (12)$$

$$\gamma = \left(1 + 0.76 \left(\frac{b}{W}\right)\right) \qquad (13)$$

where J_p is the nonlinear part of the deformation theory J, b is the remaining ligament, W is the specimen width, a_o and a are the initial and extended crack lengths respectively, and γ is as defined above. Also, from Reference 24, T_m is evaluated as:

$$T_m = T + \frac{E}{\sigma_f^2} \cdot \frac{\gamma}{b} J_p \qquad (14)$$

In the preceding equations for J_m and T_m, J and J_p must be defined as functions of crack extension for each material evaluated. Such definitions have been obtained from the power law curve-fits of the J-R data of the lower bound materials in References 17, 18, 19 and 21. The resulting values of J_m-T_m for the lower bound curves for each material category of Figure 3-17 are illustrated in Figure 3-18. In each case the J_m-T_m curve branches upward from the respective J-T curve at a prescribed point on the curve.

Finally, lower bound J_m - T_m curves of Figure 3-18 are then faired into the high J, large Δa data of Reference 20 to obtain the lower bound J-T curves shown in Figure 3-19 for each material. Again, it can be seen in Figure 3-19 that three distinct levels of material toughness exist: the toughest-base material, the intermediate toughness - TIG welds, and the lowest toughness SAW and SMAW welds. These lower bound curves of Figure 3-19 are employed in this report to determine predicted fracture stresses for the subject pipe welds using elastic-plastic fracture mechanics analyses.

In order to make crack growth corrections to applied J-integral values, a reference J-R curve was derived from the lower bound J-T curve in Figure 3-19. Since the tearing modulus (T) is a function of the slope of the J-R curve (dJ/da), the reference J-R curve in Figure 3-20 was obtained by integrating the lower bound J-T curve in Figure 3-19. The lower data points at small Δa in Figure 3-20 represent the raw data from the unmodified J-R curve for the lower bound material toughness. Figure 3-21 shows an expanded scale of this low Δa regime comparing the raw data (FUC-9) with the extrapolated J_m data. It can be seen that, in validating the raw data, J_m gives significant toughness advantages over the deformation J (raw data).

3.5.6 Critical Flaw Size Determination

The above J-integral estimation methods and material data are then used to establish allowable flaw sizes for the subject welds for comparison to the allowable flaw sizes for these welds based on ASME Section XI, IWB-3640 methodology discussed previously (Section 3.4). The basic technique is illustrated in Figure 3-12. The intersection of the applied and material J-T curves in this figure yields a critical value of J for predicted instability of the weld. This critical value of J uniquely defines a critical stress for a given flaw size, or conversely, a critical flaw size for a given stress level. The later definition is used here.

At this point, it must be noted that the IWB-3640 tables for permissible flaw sizes were developed based on an inherent safety factor of 2.773 on stress or load to net section collapse of the cracked cross-section (Ref. 11). Thus, in order to provide a consistent basis for comparison, the applied loading on each pipe weld to be evaluated (Ref. 1) is multiplied by a factor of 2.773 before applying the J-T critical flaw size determination described above. Allowable sizes for 360° part-through-wall cracks and finite length, through-wall cracks, defined in this manner, are thus used as end-points to prescribe a second allowable flaw size locus for the subject welds, with the same safety margins, but under the assumption of lower bound, flux-type material toughness from Figure 3-18. The new allowable flaw size loci are constructed by drawing a smooth curve parallel to the corresponding allowable locus from IWB-3640 between the two end points. Since such a critical flaw size determination potentially reflects less than full limit load ductility in the pipe cross-section, it is also appropriate to include global secondary stress terms (such as thermal expansion) in the above applied loading.

Critical flaw size loci have been determined in this manner for the four welds with UT indications in Section 4.0 of this report. They are then compared to the IWB-3640 based allowable flaw sizes, as well as to the observed flaw sizes, plus predicted IGSCC crack propagation during subsequent operation.

TABLE 3-1

Summary of Applied Stress at Weld KR-2-14

BRANCH MOMENTS

LOAD CASES	Myy (FT-LBS)	Mzz (FT-LBS)
DW	-2222	6560
THERMAL	16119	-47473
OBE-XY	2441	2467
OBE-ZY	3190	3506
SSE-XY	4134	4115
SSE-ZY	4683	5173
SHRINKAGE	5241	-3835

12" PIPE

PRESSURE=	1150	PSI
THK=	0.579	IN
OD=	12.75	IN
Z=	64.5	IN**3
SM=	16950	PSI

STRESSES NORMAL TO WELD DUE TO BRANCH MOMENTS (PSI)

		ANGLE (DEGREE) 0	10	20	30	40	50	60	70	80	90
LOAD CASES	SCF MOMENT	1	1	1.05	1.17	1.24	1.42	1.8	2.12	2.69	3
	PRES	0.6	0.61	0.64	0.67	0.69	0.75	0.86	0.89	0.95	1
INSIDE SURFACE	PRESSURE	7597.150	7723.769	8103.626	8483.484	8736.722	9496.437	10889.24	11269.10	12028.82	12661.91
	DW	1220.465	1273.708	1352.664	1478.472	1488.813	1563.674	1742.838	1708.483	1665.235	1240.186
	THERMAL	8832.186	9218.755	9791.479	10703.55	10779.93	11323.78	12623.76	12378.28	12070.07	8996.651
	SHRINKAGE	713.4883	871.9679	054.150	1293.357	1454.924	1711.906	2162.122	2459.821	2916.369	2925.209
	OBE	1111.255	1276.292	1472.676	1738.641	1890.595	2153.900	2633.220	2892.782	3294.388	3142.883
	SSE	1728	1986.595	2294.070	2710.513	2948.888	3361.615	4112.297	4520.807	5152.735	4921.116
OUTSIDE SURFACE	PRESSURE	7597.150	7723.769	8103.626	8483.484	8736.722	9496.437	10889.24	11269.10	12028.82	12661.91
	DW	-813.643	-849.139	-901.776	-985.648	-992.542	-1042.44	-1161.89	-1138.98	-1110.15	-826.790
	THERMAL	-5888.12	-6145.83	-6527.65	-7135.70	-7186.62	-7549.19	-8415.84	-8252.19	-8046.71	-5997.76
	SHRINKAGE	-475.658	-581.311	-702.767	-862.238	-969.949	-1141.27	-1441.41	-1639.88	-1944.24	-1950.13
	OBE	-740.837	-850.861	-981.784	-1159.22	-1260.39	-1435.93	-1755.48	-1928.52	-2196.25	-2095.25
	SSE	-1152	-1324.39	-1529.38	-1807.00	-1965.92	-2241.07	-2741.52	-3013.87	-3435.15	-3280.74
PRESSURE + DW + THERMAL + SHRINKAGE											
MEMBRANE		9391.506	9617.841	10136.67	10729.38	11024.00	11929.66	13644.03	14026.87	14804.10	14855.59
BENDING		8971.782	9470.360	10165.24	11229.48	11436.39	12166.14	13773.93	13788.82	13876.40	10968.37
PRESSURE+ DW + THERMAL + OBE +SHRINKAGE											
MEMBRANE		9576.716	9830.556	10382.12	11019.18	11339.10	12288.64	14082.90	14509.00	15353.16	15379.40
(PM+PB)/SM		0.564998	0.579973	0.612514	0.650099	0.668973	0.724994	0.830849	0.855988	0.905791	0.907339
PRESSURE+ DW + THERMAL + SSE +SHRINKAGE											
MEMBRANE		9679.506	9948.940	10519.02	11181.13	11515.48	12489.93	14329.41	14780.33	15662.89	15675.77
(PM+PB)/SM		0.571062	0.586958	0.620591	0.659653	0.679379	0.736869	0.845393	0.871996	0.924064	0.924824

TABLE 3-2

Summary of Applied Stress at Weld KR-2-36

LOAD CASES	BRANCH MOMENTS Myy (FT-LBS)	Mzz (FT-LBS)
DW	1922	-3539
THERMAL	12385	38810
OBE-XY	5097	5999
OBE-ZY	5050	4797
SSE-XY	7355	8454
SSE-ZY	7524	7042
SHRINKAGE	325	146

12" PIPE

PRESSURE=	1150	PSI
THK=	0.579	IN
OD=	12.75	IN
Z=	64.5	IN**3
SM=	16950	PSI

STRESSES NORMAL TO WELD DUE TO BRANCH MOMENTS (PSI)

	LOAD CASES	ANGLE (DEGREE) 0	10	20	30	40	50	60	70	80	90
	SCF MOMENT	1	1	1.05	1.17	1.24	1.42	1.8	2.12	2.69	3
	SCF PRES	0.6	0.61	0.64	0.67	0.69	0.75	0.86	0.89	0.95	1
INSIDE SURFACE	PRESSURE	7597.150	7723.769	8103.626	8483.484	8736.722	9496.437	10889.24	11269.10	12028.82	12661.91
	DW	658.4186	710.5091	778.0617	876.3275	910.4412	989.9481	1149.990	1189.763	1254.836	1072.744
	THERMAL	7220.465	7510.887	7951.750	8664.083	8695.251	9096.994	10090.28	9825.714	9476.872	6912.558
	SHRINKAGE	27.16279	37.24978	48.51520	62.89478	73.99592	90.56599	118.7022	140.1507	172.8682	181.3953
	OBE	2008.558	2305.859	2659.752	3139.542	3412.614	3886.860	4750.513	5217.176	5939.294	5663.441
	SSE	2882.976	3319.868	3838.681	4540.564	4944.926	5642.647	6909.854	7605.033	8679.970	8304.558
OUTSIDE SURFACE	PRESSURE	7597.150	7723.769	8103.626	8483.484	8736.722	9496.437	10889.24	11269.10	12028.82	12661.91
	DW	-438.945	-473.672	-518.707	-584.218	-606.960	-659.965	-766.660	-793.175	-836.557	-715.162
	THERMAL	-4813.64	-5007.25	-5301.16	-5776.05	-5796.83	-6064.66	-6726.85	-6550.47	-6317.91	-4608.37
	SHRINKAGE	-18.1085	-24.8331	-32.3434	-41.9298	-49.3306	-60.3773	-79.1348	-93.4338	-115.245	-120.930
	OBE	-1339.03	-1537.23	-1773.16	-2093.02	-2275.07	-2591.24	-3167.00	-3478.11	-3959.52	-3775.62
	SSE	-1921.98	-2213.24	-2559.12	-3027.04	-3296.61	-3761.76	-4606.56	-5070.02	-5786.64	-5536.37
PRESSURE + DW + THERMAL + SHRINKAGE	MEMBRANE	8914.824	9100.210	9566.681	10084.03	10350.00	11192.68	12782.41	13128.37	13846.25	14023.03
	BENDING	6588.372	6882.205	7315.272	8002.754	8066.407	8481.257	9465.818	9296.357	9087.147	6806.581
PRESSURE+ DW + THERMAL + OBE +SHRINKAGE	MEMBRANE	9249.584	9484.520	10009.97	10607.29	10918.77	11840.49	13574.16	13997.90	14836.13	14966.94
	(PM+PB)/SM	0.545698	0.559558	0.590558	0.625798	0.644175	0.698554	0.800835	0.825835	0.875288	0.883005
PRESSURE+ DW + THERMAL + SSE +SHRINKAGE	MEMBRANE	9395.320	9653.521	10206.46	10840.79	11174.15	12133.13	13934.05	14395.88	15292.91	15407.12
	(PM+PB)/SM	0.554296	0.569529	0.602151	0.639574	0.659242	0.715818	0.822068	0.849314	0.902236	0.908975

STRUCTURAL INTEGRITY ASSOCIATES, INC.

TABLE 3-3

Summary of Applied Stress at Weld KR-2-41

	BRANCH MOMENTS	
LOAD CASES	Myy (FT-LBS)	Mzz (FT-LBS)
DW	-3331	2985
THERMAL	-6752	42081
OBE-XY	6591	4514
OBE-ZY	2745	2853
SSE-XY	8216	5786
SSE-ZY	3989	4155
SHRINKAGE	40	19

12" PIPE		
PRESSURE=	1150	PSI
THK=	0.579	IN
OD=	12.75	IN
Z=	64.5	IN**3
SM=	16950	PSI

STRESSES NORMAL TO WELD DUE TO BRANCH MOMENTS (PSI)

	LOAD CASES	ANGLE (DEGREE) →	0	10	20	30	40	50	60	70	80	90
		SCF MOMENT	1	1	1.05	1.17	1.24	1.42	1.8	2.12	2.69	3
		SCF PRES	0.6	0.61	0.64	0.67	0.69	0.75	0.86	0.89	0.95	1
INSIDE SURFACE	PRESSURE		7597.150	7723.769	8103.626	8483.484	8736.722	9496.437	10889.24	11269.10	12028.82	12661.91
	DW		555.3488	654.5252	770.5049	925.2437	1021.475	1181.021	1465.863	1637.249	1901.134	1859.162
	THERMAL		7829.023	7928.217	8175.842	8667.624	8438.002	8512.464	9004.321	8179.198	6984.846	3768.558
	SHRINKAGE		3.534883	4.773446	6.160318	7.935208	9.289353	11.32162	14.78210	17.38837	21.36566	22.32558
	OBE		1370.604	1651.396	1976.112	2404.868	2686.362	3140.434	3941.150	4454.024	5241.587	5210.790
	SSE		1849.488	2215.693	2640.303	3202.351	3566.694	4158.162	5204.206	5864.598	6879.300	6812.093
OUTSIDE SURFACE	PRESSURE		7597.150	7723.769	8103.626	8483.484	8736.722	9496.437	10889.24	11269.10	12028.82	12661.91
	DW		-370.232	-436.350	-513.669	-616.829	-680.983	-787.347	-977.242	-1091.49	-1267.42	-1239.44
	THERMAL		-5219.34	-5285.47	-5450.56	-5778.41	-5625.33	-5674.97	-6002.88	-5452.79	-4656.56	-2512.37
	SHRINKAGE		-2.35658	-3.18229	-4.10687	-5.29013	-6.19290	-7.54774	-9.85473	-11.5922	-14.2437	-14.8837
	OBE		-913.736	-1100.93	-1317.40	-1603.24	-1790.90	-2093.62	-2627.43	-2969.34	-3494.39	-3473.86
	SSE		-1232.99	-1477.12	-1760.20	-2134.90	-2377.79	-2772.10	-3469.47	-3909.73	-4586.20	-4541.39
PRESSURE + DW + THERMAL + SHRINKAGE												
	MEMBRANE		8995.134	9155.022	9595.711	10083.61	10314.85	11113.90	12636.74	12908.07	13513.37	13603.59
	BENDING		6989.922	7156.263	7460.422	8000.669	7890.639	8087.339	8737.472	8194.863	7422.788	4708.372
PRESSURE+ DW + THERMAL + OBE +SHRINKAGE												
	MEMBRANE		9223.568	9430.254	9925.063	10484.42	10762.57	11637.31	13293.60	13650.41	14386.97	14472.05
	(PM+PB)/SM		0.544163	0.556357	0.585549	0.618550	0.634960	0.686567	0.784283	0.805334	0.848789	0.853808
PRESSURE+ DW + THERMAL + SSE +SHRINKAGE												
	MEMBRANE		9303.382	9524.304	10035.76	10617.34	10909.29	11806.93	13504.11	13885.51	14659.92	14738.94
	(PM+PB)/SM		0.548872	0.561905	0.592080	0.626391	0.643616	0.696574	0.796702	0.819204	0.864892	0.869554

TABLE 3-4

ALLOWABLE END-OF-EVALUATION PERIOD FLAW DEPTH[1] TO THICKNESS RATIO FOR CIRCUMFERENTIAL FLAWS — NORMAL OPERATING (INCLUDING UPSET AND TEST) CONDITIONS

$\frac{P_m + P_b}{S_m}$ [Note (2)]	Ratio of Flaw Length, ℓ_f, to Pipe Circumference [Note (3)]					
	0.0	0.1	0.2	0.3	0.4	0.5 or More
1.5	(4)	(4)	(4)	(4)	(4)	(4)
1.4	0.75	0.40	0.21	0.15	(4)	(4)
1.3	0.75	0.75	0.39	0.27	0.22	0.19
1.2	0.75	0.75	0.56	0.40	0.32	0.27
1.1	0.75	0.75	0.73	0.51	0.42	0.34
1.0	0.75	0.75	0.75	0.63	0.51	0.41
0.9	0.75	0.75	0.75	0.73	0.59	0.47
0.8	0.75	0.75	0.75	0.75	0.68	0.53
0.7	0.75	0.75	0.75	0.75	0.75	0.58
≤ 0.6	0.75	0.75	0.75	0.75	0.75	0.63

NOTES:

(1) Flaw depth = a_n for a surface flaw
  $2a_n$ for a subsurface flaw
 t = nominal thickness
 Linear interpolation is permissible.

(2) P_m = primary membrane stress
 P_b = primary bending stress
 S_m = allowable design stress intensity (in accordance with Section III)

(3) Circumference based on nominal pipe diameter.

(4) IWB-3514.3 shall be used.

TABLE 3-5

F for a Circumferentially Cracked Cylinder in Tension (t/R_i = 1/10)

a/t	1/8	1/4	1/2	3/4
F	1.19	1.32	1.82	2.49

TABLE 3-6

h_1 for a Circumferentially Cracked Cylinder in Tension (t/R_i = 1/10)

a/t	n=1	n=2	n=3	n=5	n=7	n=10
1/8	4.00	5.13	6.09	7.69	9.09	11.1
1/4	4.17	5.35	6.09	6.93	7.30	7.41
1/2	5.40	5.90	5.63	4.51	3.49	2.47
3/4	5.18	3.78	2.57	1.59	1.31	1.10

TABLE 3-7

F for a Circumferential, Through-Wall Crack in a Cylinder of t/R = 1/10 in Tension

a/b	1/16	1/8	1/4	1/2
F	1.077	1.259	1.802	4.208

TABLE 3-8

h_1 for a Circumferential Through-Wall Crack in a Cylinder of t/R = 1/10 in Tension

a/b	n=1	n=2	n=3	n=5	n=7
1/16	2.979	3.967	4.655	5.576	6.104
1/8	3.221	4.157	4.708	5.163	5.102
1/4	3.677	4.159	4.032	3.238	2.605
1/2	3.091	2.220	1.713	1.137	0.816

TABLE 3-9

Material Stress-Strain Properties of Base and Weldment Materials Used in Analysis

	304 75°F	304 550°F	TIG 75°F	TIG 550°F
True strain at P_m	0.546*	0.347	0.299	0.103
stress at P_{max}	149,380	88,650	121,890	70,100
α	30.7	17.3	13.63	2.83
n	1.92	2.49	4.00	11.84
σ_o	38,200	24,800	68,900	53,900
Range of Fit	0.166-0.888	0.04-0.888	0.114-.299	0.022-0.114
YS+	43,000	24,800	68,900	53,900
TS	86,000	62,600	90,500	63,400
Elong. %	80.3	45	55	28
% RA	81	70	69	69

* Diametral gage

\+ Cross-head measurements

o 0.4" Gage length

$E = 30 \times 10^6$ psi

$\nu = 0.3$

Table 3-10

Three Commonly Used Ramberg-Osgood Constants for Weldment Materials

	σ_0	α	n
Primary Curve	53.9	2.83	11.84
Alternate Curve A	44.8	3.39	6.89
Alternate Curve B	49.4	9.0	9.8

TABLE 3-11

WELDING PROCESSES

FOR STAINLESS STEEL PIPE

- SUBMERGED ARC WELD (SAW)
  - AUTOMATIC PROCESS
  - ARC BETWEEN BARE METAL CONSUMABLE ELECTRODE (WIRE) AND WORKPIECE
  - ARC SHIELDED BY GRANULAR AND FUSIBLE FLUX WHICH BLANKETS MOLTEN WELD METAL
  - HIGH WELD DEPOSITION RATE AND SPEED
  - DISADVANTAGES
    - SLAG MUST BE REMOVED AFTER EACH PASS TO AVOID ENTRAPMENT IN WELD METAL
    - HIGH HEAT INPUT CAN GIVE SLOW COOLING RATES AND COARSE, LOW TOUGHNESS MICROSTRUCTURE
    - PICKUP FROM THE FLUX CAN CHANGE COMPOSITION OF DEPOSIT
    - RISK OF MICROFISSURING
  - USED FOR MOST SHOP WELDS - NOT IN FIELD
  - RELATION TO WELD METAL TOUGHNESS
    - RELATIVELY HEAVY SLAG/INCLUSION CONTENT
    - COARSE MICROSTRUCTURE
    - HIGH HEAT INPUT CAN GIVE HIGHER FERRITE CONTENTS
    - THE ABOVE CAN LEAD TO REDUCED TOUGHNESS - PROBABLY THE LOWEST FOR THE WELD PROCESSES CONSIDERED HERE

TABLE 3-11
(Continued)

- SHIELDED METAL ARC WELD (SMAW)
  - MANUAL PROCESS
  - ARC BETWEEN FLUX-COVERED CONSUMABLE ELECTRODE AND WORKPIECE
  - SHIELDING BY GASEOUS SHIELD AND MOLTEN FLUX OR SLAG FROM ELECTRODE COVERING
  - MOST VERSATILE PROCESS - POSITIONS, ETC.
  - DISADVANTAGES
    - SLAG BLANKET - SOURCE OF INCLUSIONS
    - VISIBILITY IMPAIRED BY SLAG
    - SLAG REMOVAL BETWEEN PASSES IS NECESSARY
    - MOISTURE PICKUP IN ELECTRODES
    - LOW DEPOSITION EFFICIENCY
  - USED FOR REPAIRS AND FOR CERTAIN PORTIONS OF FIELD AND SHOP WELDS
  - RELATION TO WELD METAL TOUGHNESS
    - INTERMEDIATE TO HEAVY INCLUSION CONTENT
    - INTERMEDIATE HEAT INPUT AND DILUTION
    - EXPECT INTERMEDIATE TOUGHNESS

TABLE 3-11
(Concluded)

GAS TUNGSTEN ARC WELD (GTAW), OR TUNGSTEN INERT GAS (TIG)

- AUTOMATIC OR MANUAL PROCESS
- ARC BETWEEN NONCONSUMABLE ELECTRODE (TUNGSTEN) AND WORKPIECE - FILLER METAL (WELD WIRE) CAN BE ADDED TO WELD POOL - SHIELDED BY INERT GAS (ARGON OR HELIUM)
- MULTI-POSITION, HIGH QUALITY WELD, BUT LOW DEPOSITION RATES
- NO FLUX USED - NO SLAG
- INSIGNIFICANT CHANGES IN FILLER COMPOSITION DURING DEPOSIT - LOW PICKUP OF CONTAMINANTS
- USED MOSTLY FOR FIELD WELDS, SOME SHOP WELDS, AND ALL WELD OVERLAYS
- RELATION TO WELD METAL TOUGHNESS
    - REDUCED HEAT INPUT THROUGH PULSING GIVES FINER, TOUGHER MICROSTRUCTURE AND POTENTIALLY LOWER FERRITE
    - NO SLAG-METAL REACTIONS AND RESULTANT NONMETALLIC INCLUSIONS
    - INSIGNIFICANT PICKUP OF CONTAMINANTS
    - THE ABOVE CAN LEAD TO THE HIGHEST TOUGHNESS FOR THE WELD PROCESSES CONSIDERED HERE

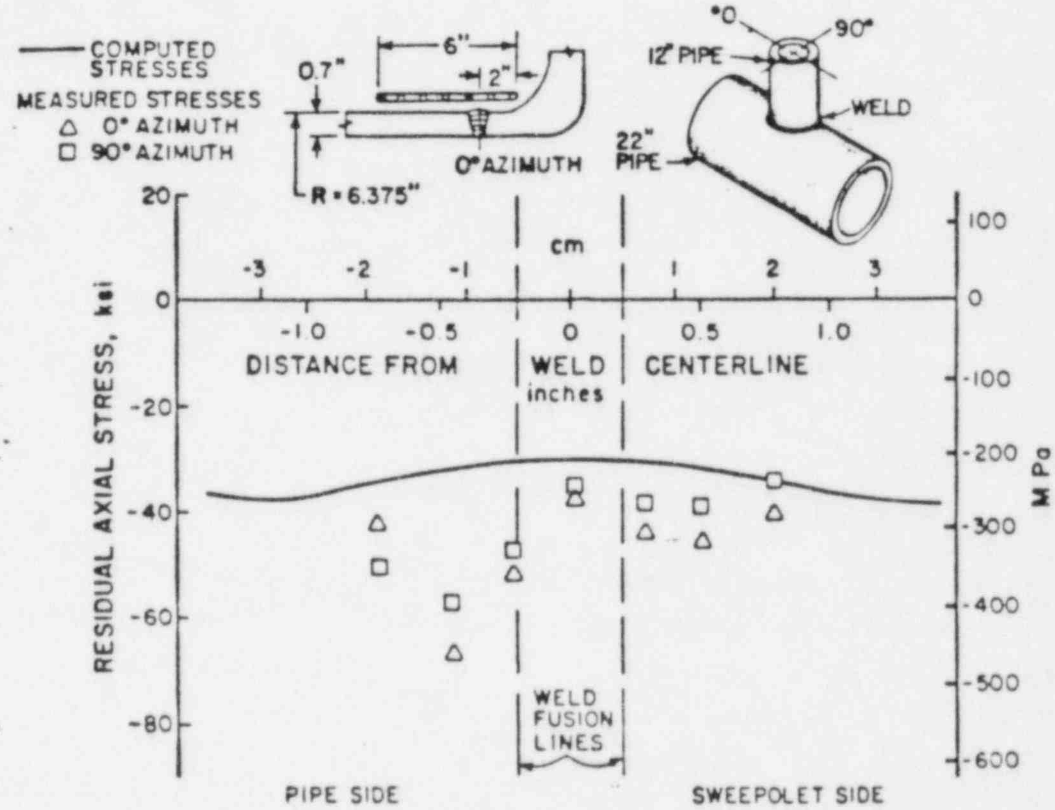

Figure 3-1. Comparison of Measured and Computed Residual Axial Stresses Along Inner Surface of a Welded, IHSI Treated 12-Inch Sweepolet

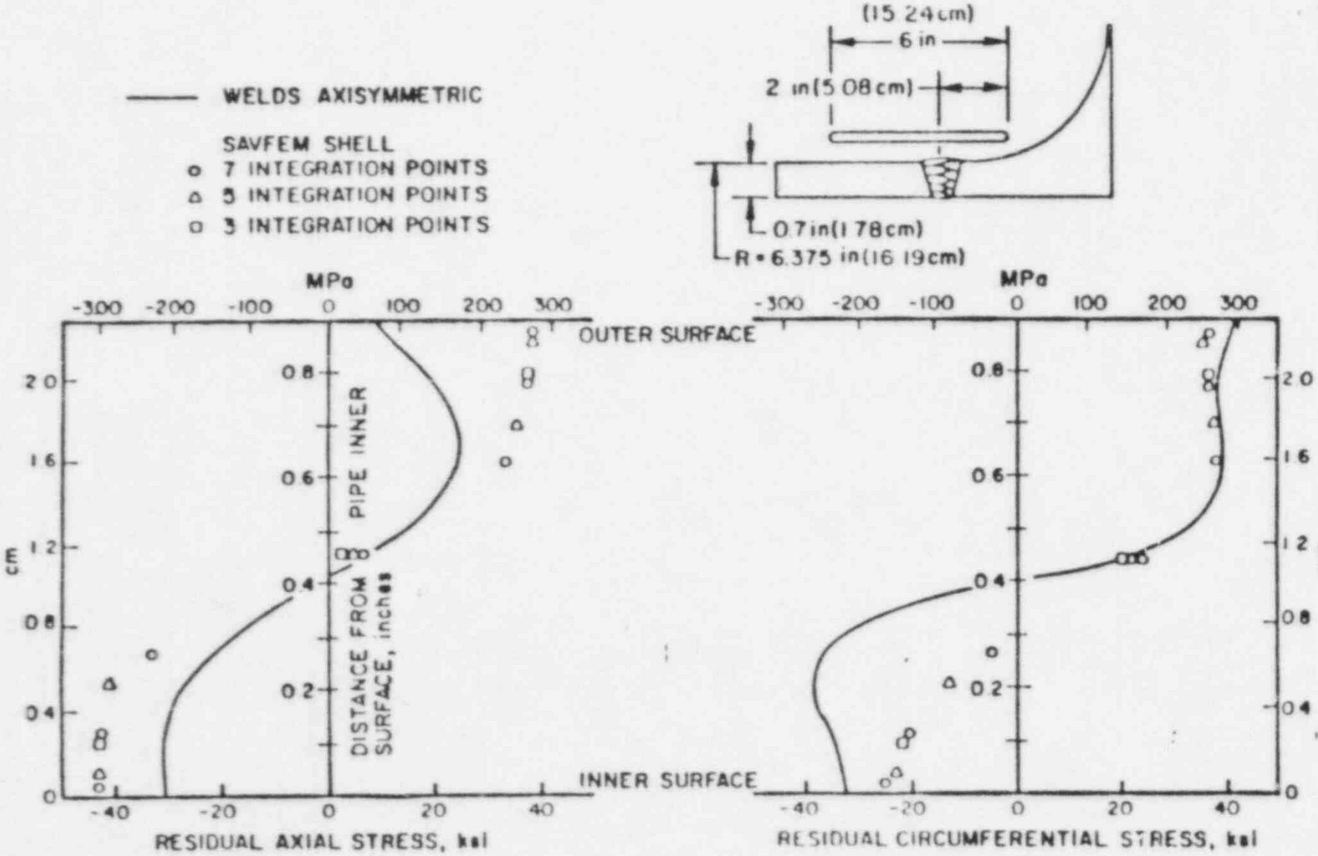

Figure 3-3. Computed Residual Stresses at Weld Centerline for IHSI Treatment of a 12-Inch Sweepolet

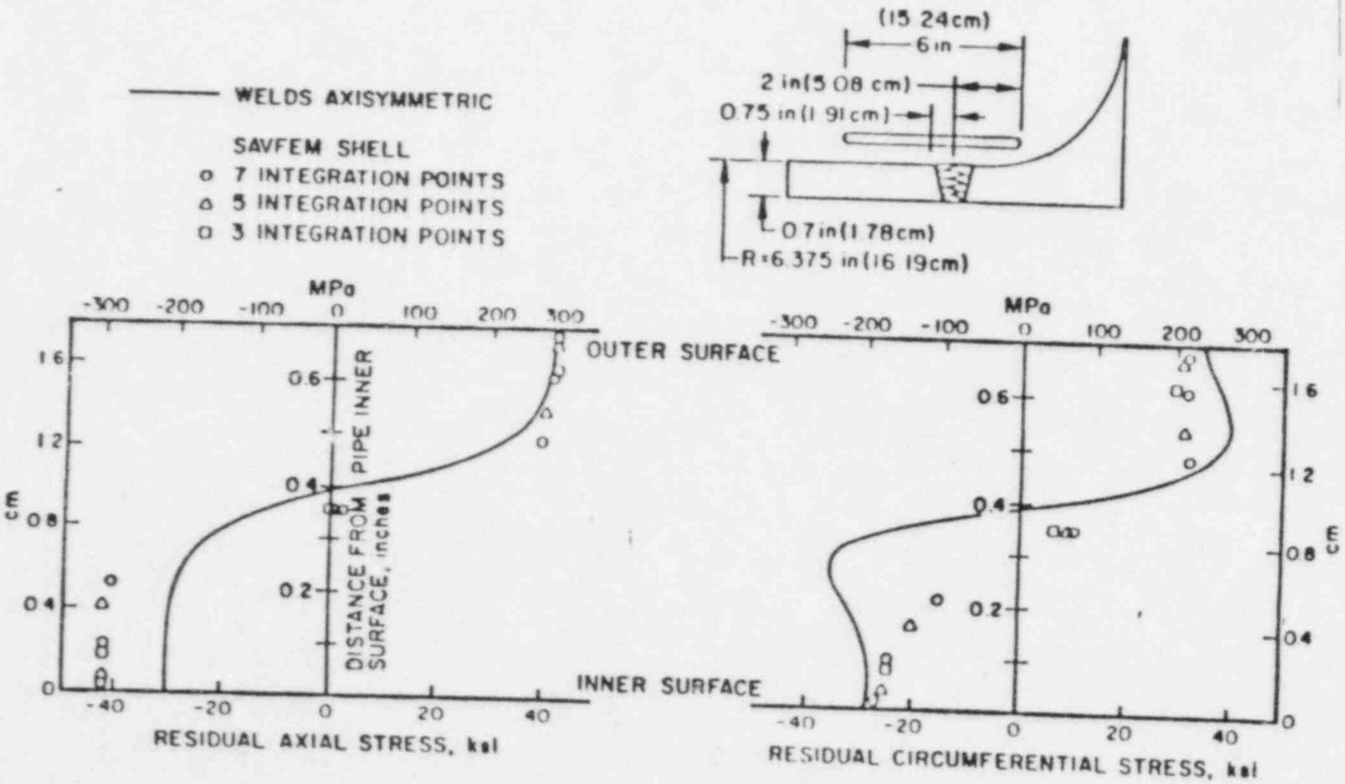

Figure 3-4. Computed Residual Stresses 0.75 Inch (1.9 cm) from Weld Centerline, 0.25 Inch (0.64 cm) from Coil Centerline, for IHSI Treatment of a 12-Inch Sweepolet

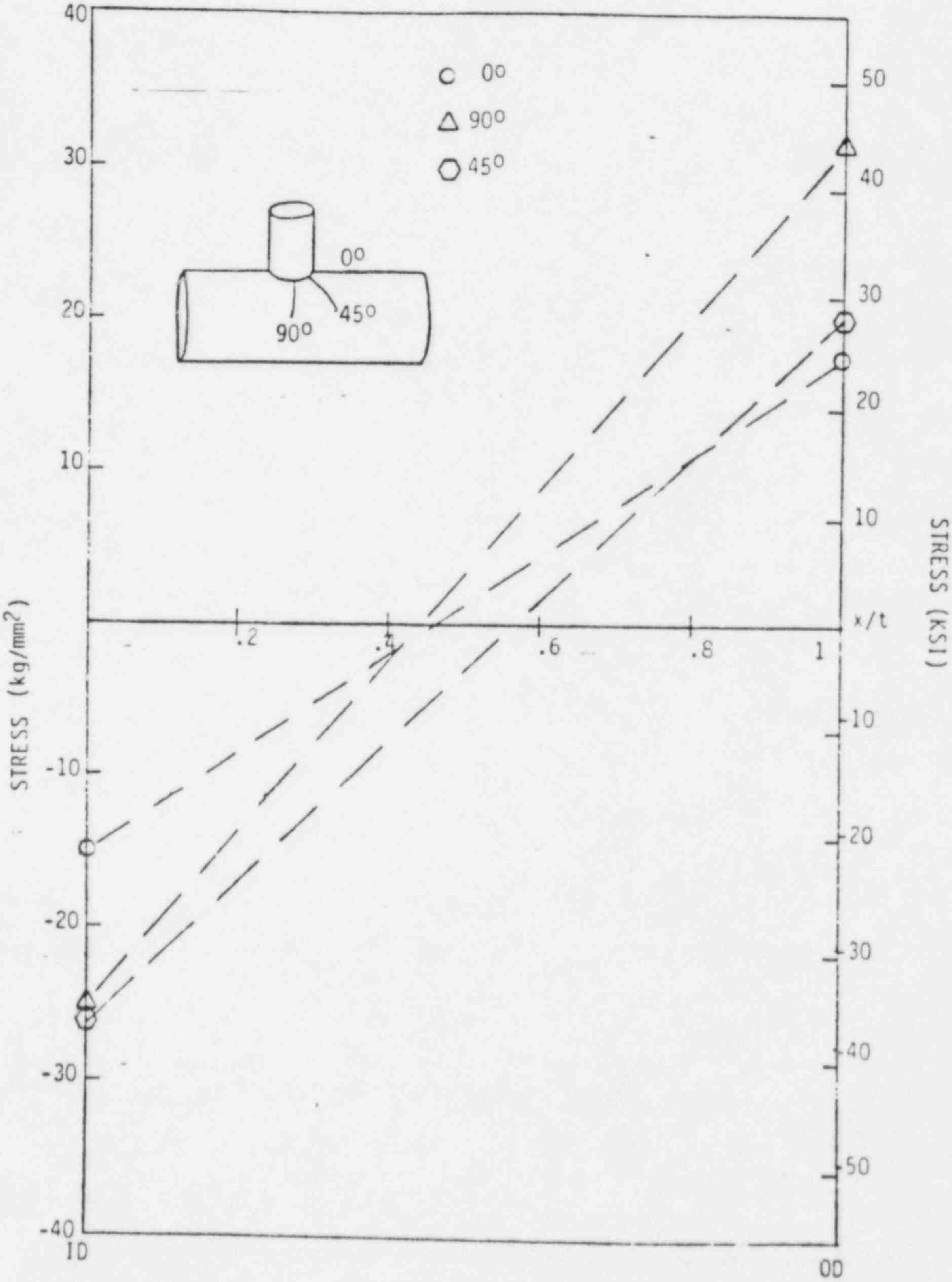

Figure 3-5. Post-IHSI Residual Stress Distribution

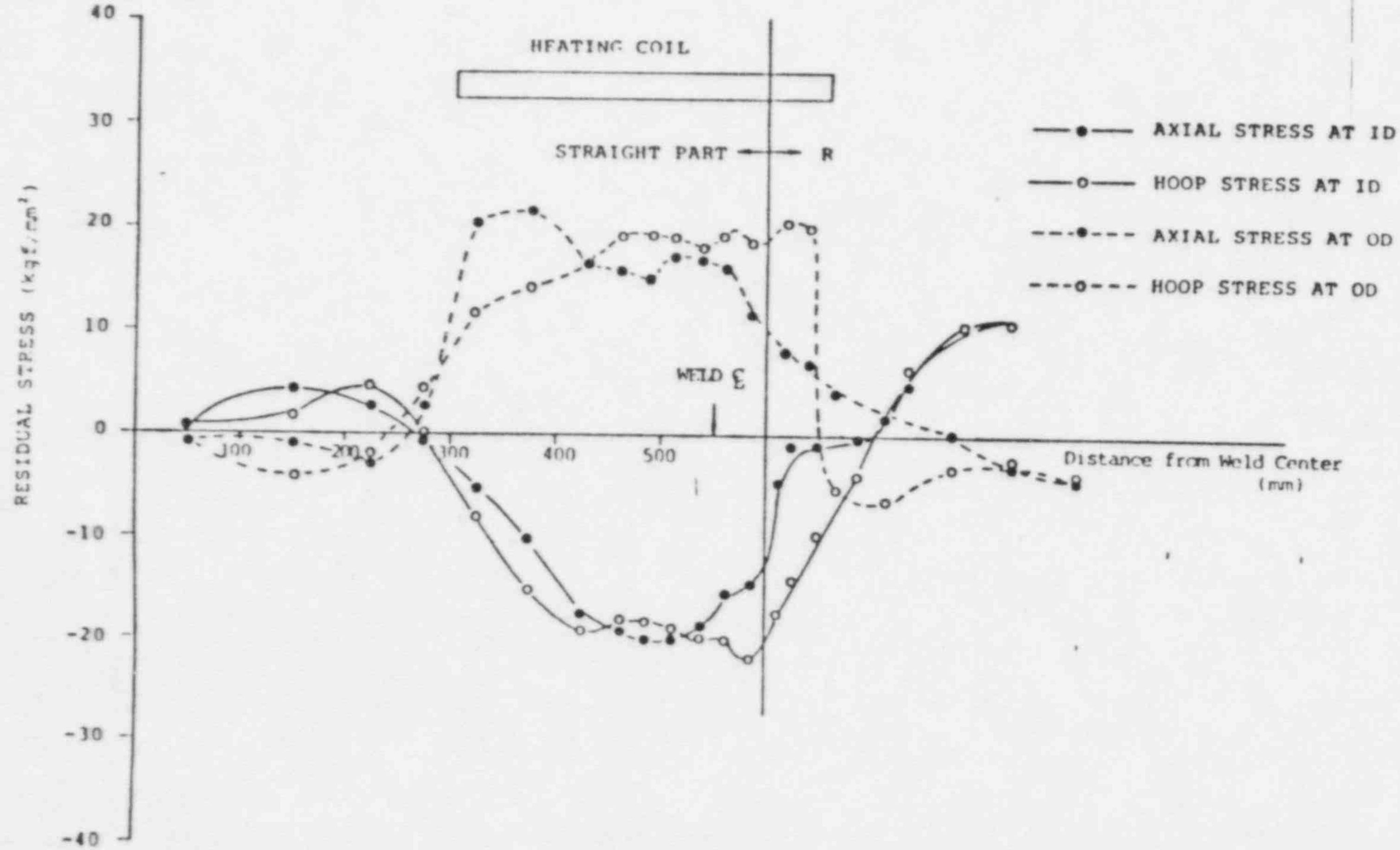

Figure 3-7. Post-IHSI Residual Stress Distribution

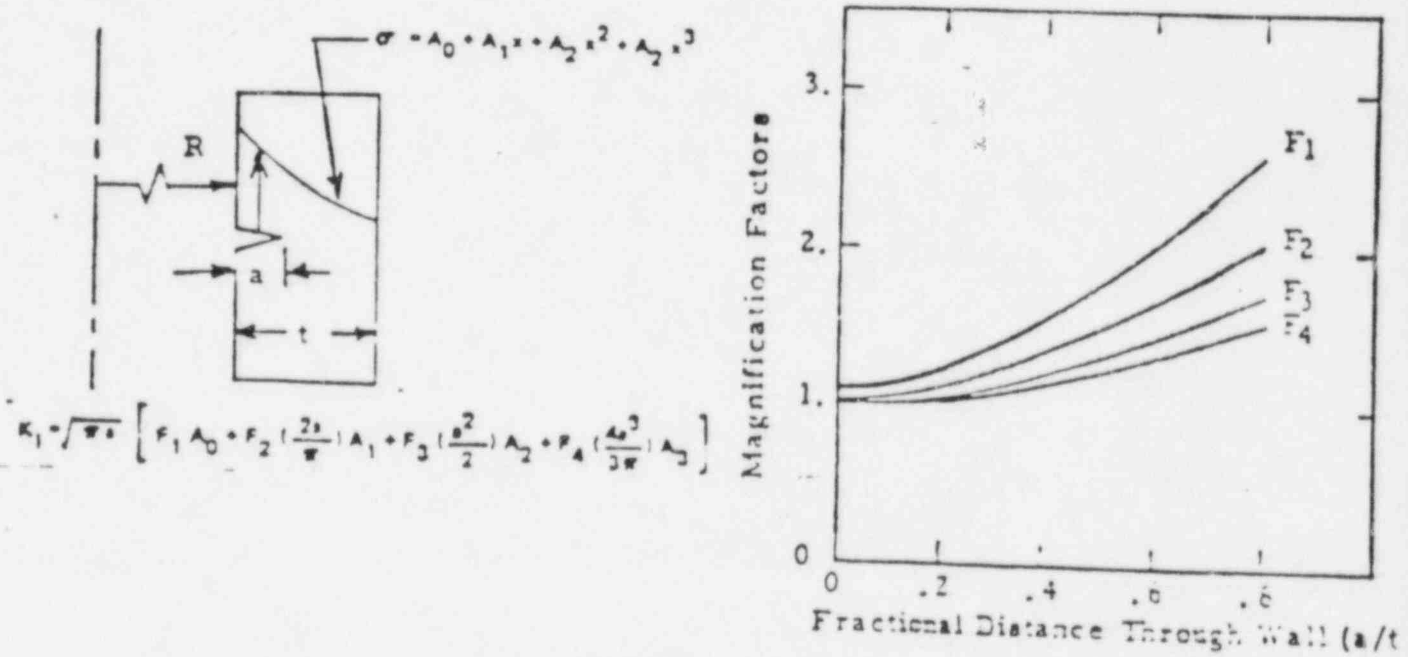

Figure 3-8. Magnification Factors of Circumferential Crack in a Cylinder (a/t = 0.1)

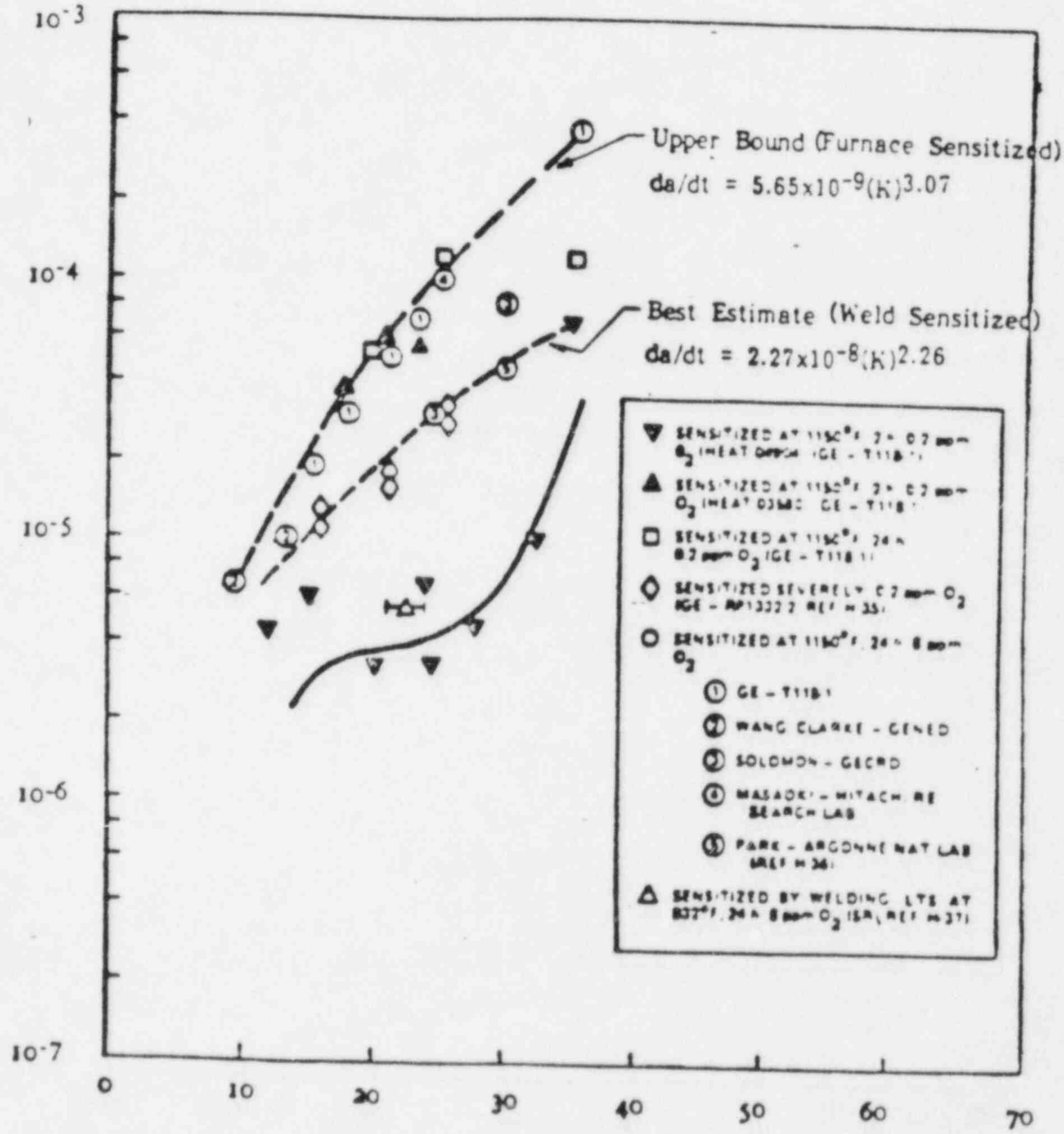

Figure 3-9. Stress Corrosion Crack Growth Data for Sensitized Stainless Steel in BWR Environment (Ref. 7)

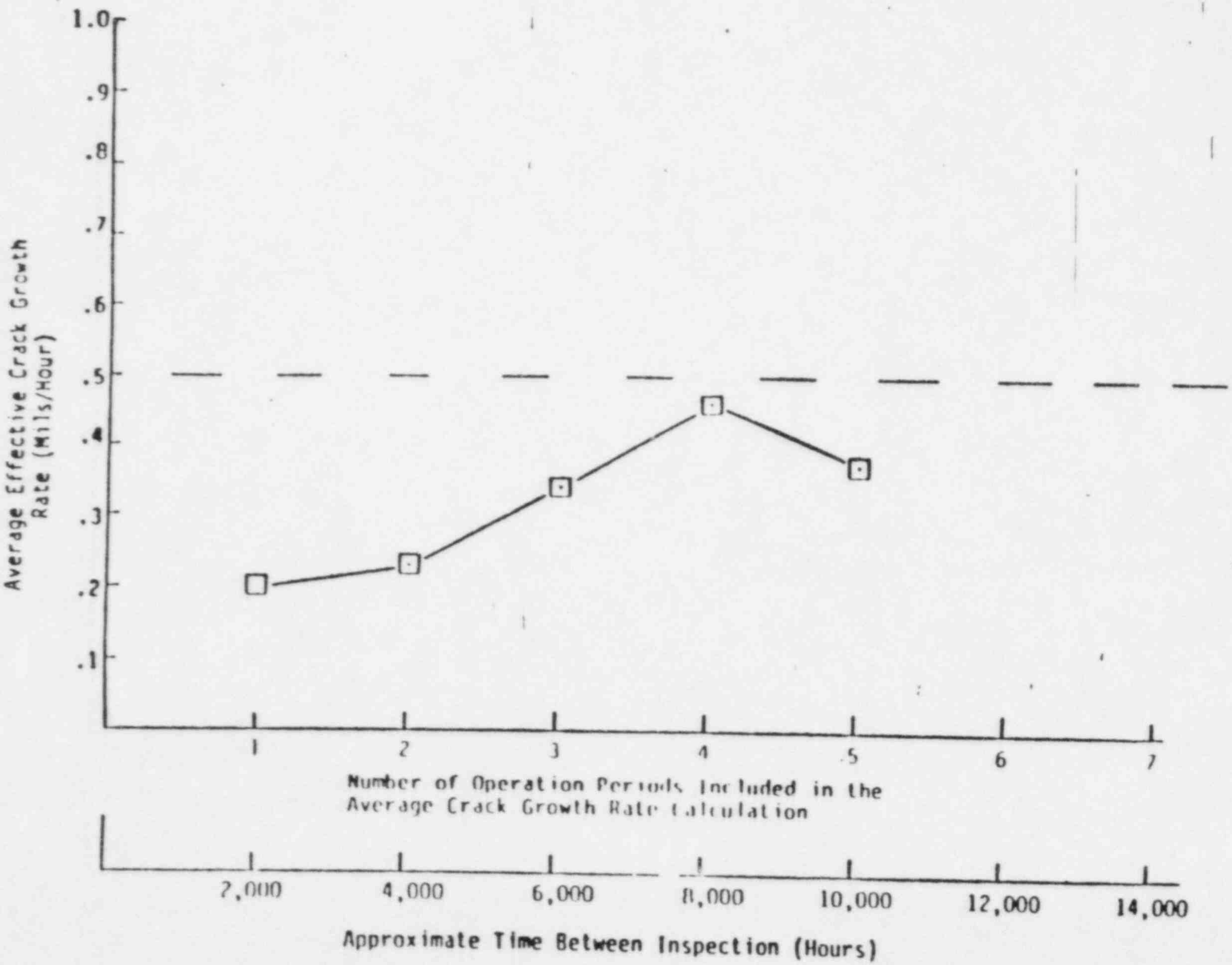

Figure 3-11. Average Effective Circumferential Crack Growth Rate As a Function of Operation Periods Used in Calculation of Time Between Inspections

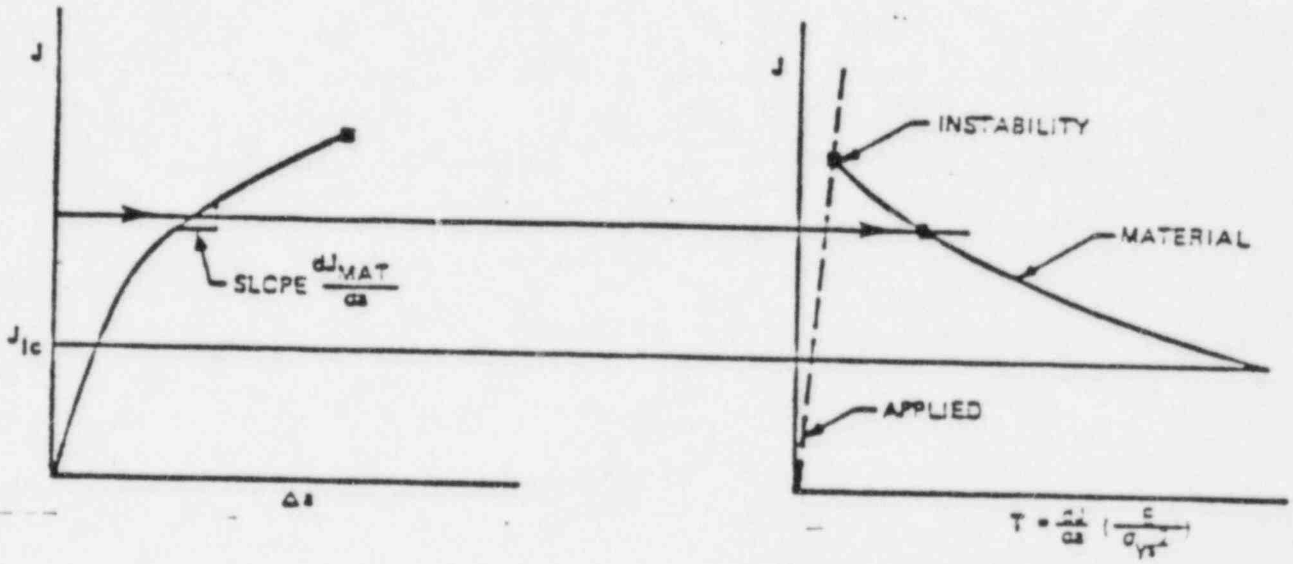

Figure 3-12. Tearing Modulus Concept for Stable Crack Growth

STRUCTURAL INTEGRITY ASSOCIATES, INC.

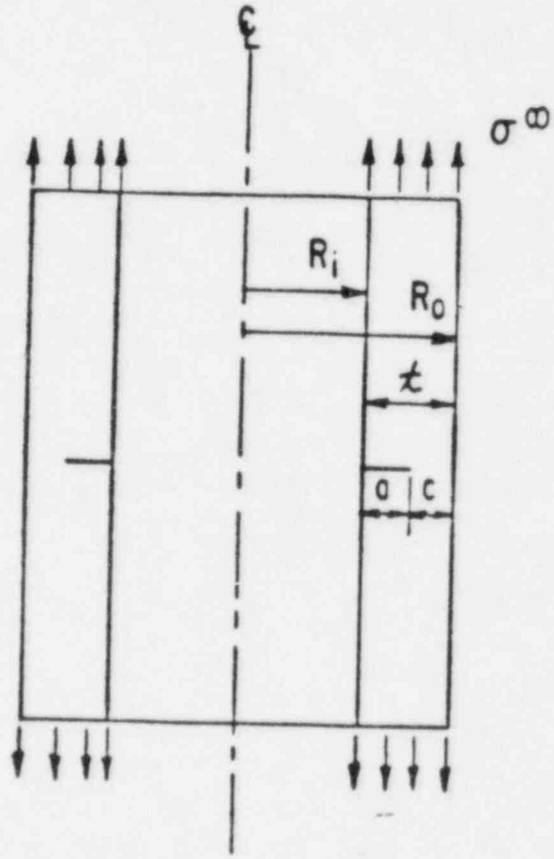

Figure 3-13. Circumferentially Cracked Cylinder in Tension

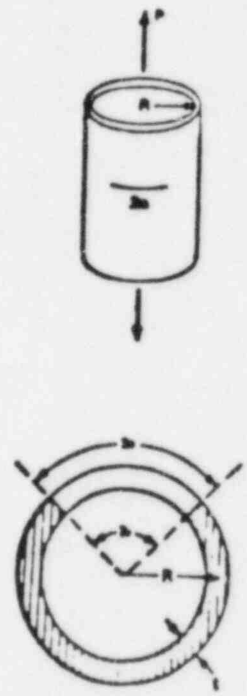

Figure 3-14. Through-Wall Flawed Cylinder Under Remote Tension

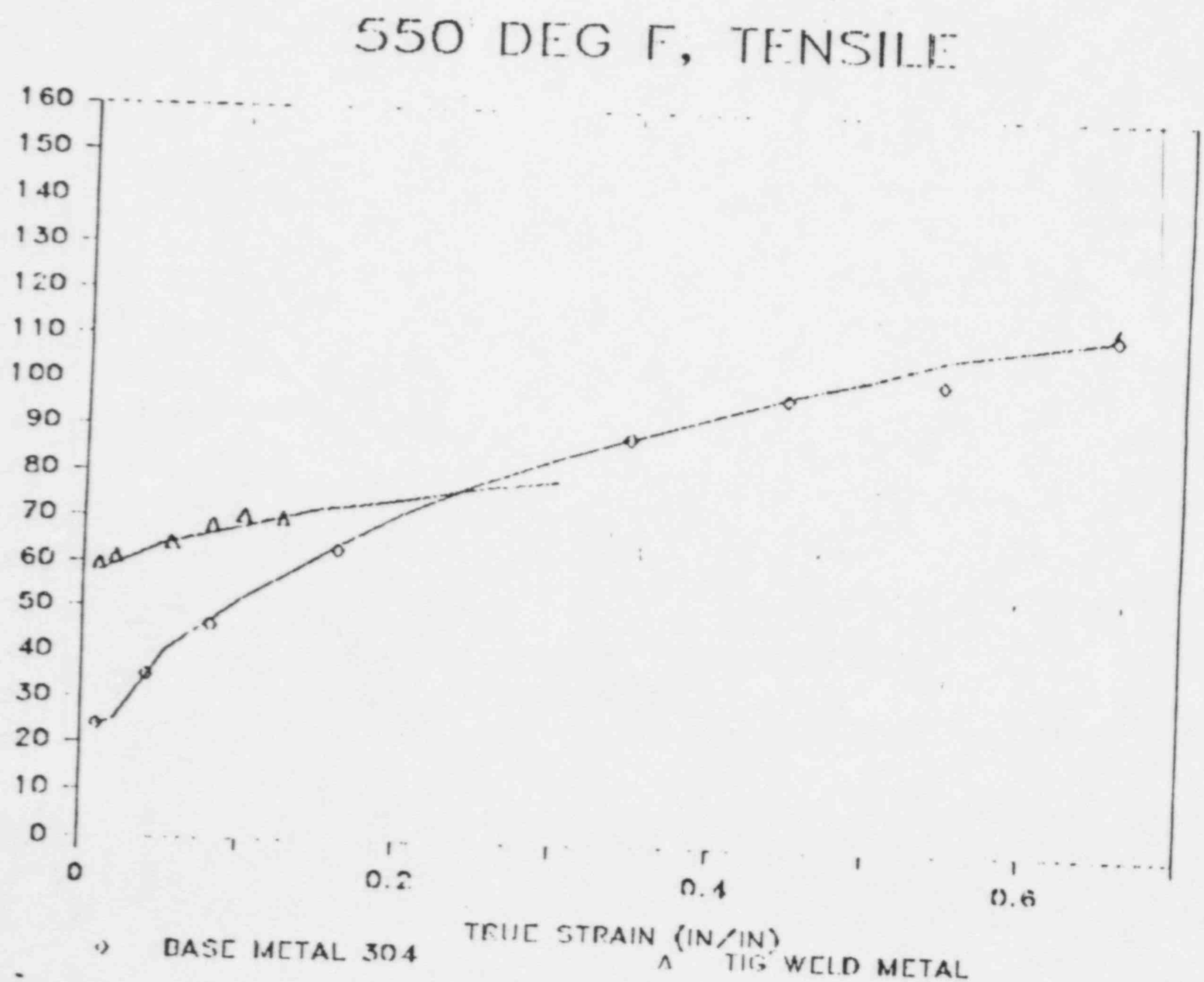

Figure 3-15. Ramberg-Osgood Characterization Stress-Strain Curves

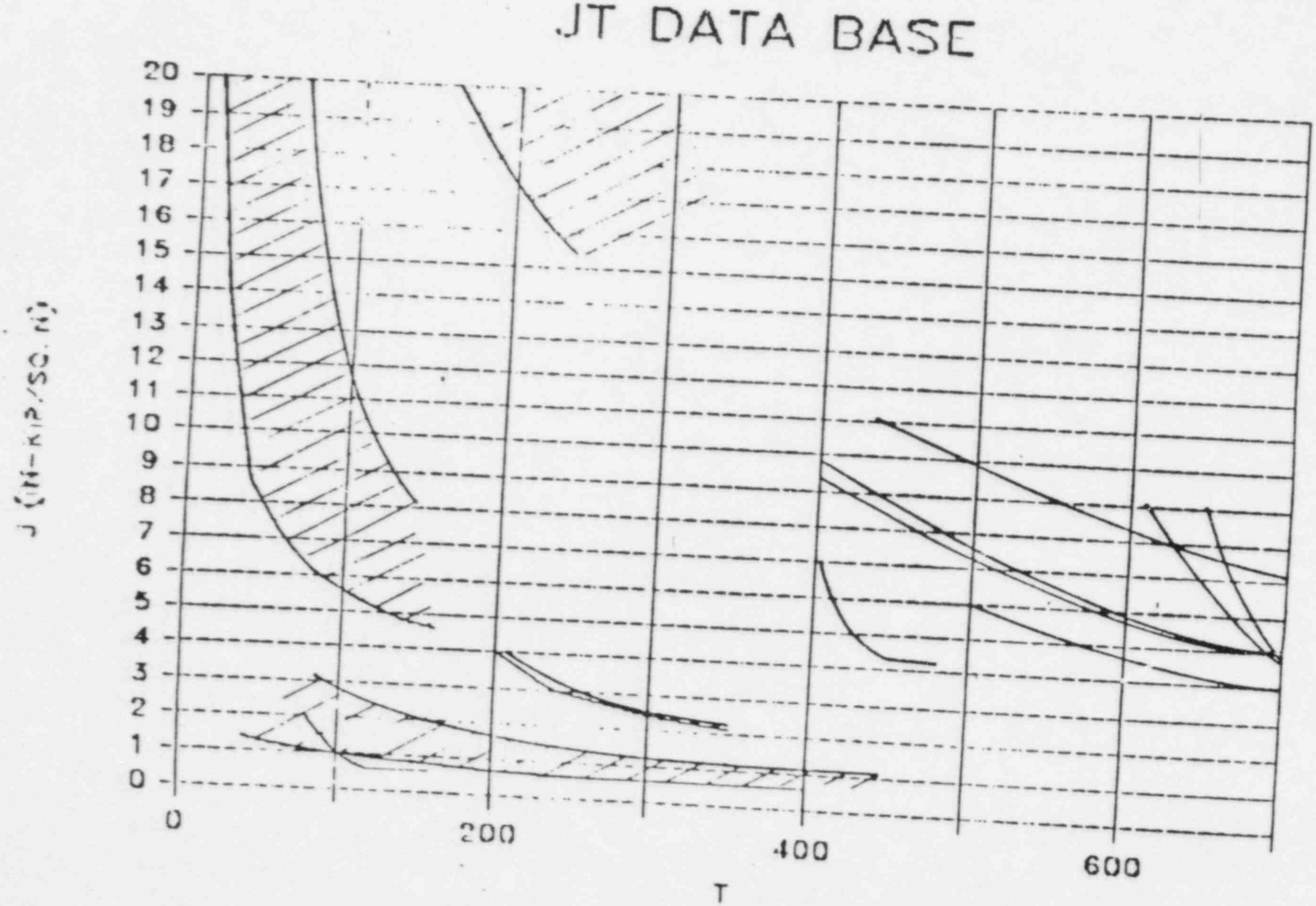

Figure 3-16. Compilation of Material Toughness J-T Curves (from data of Refs. 17 to 21)

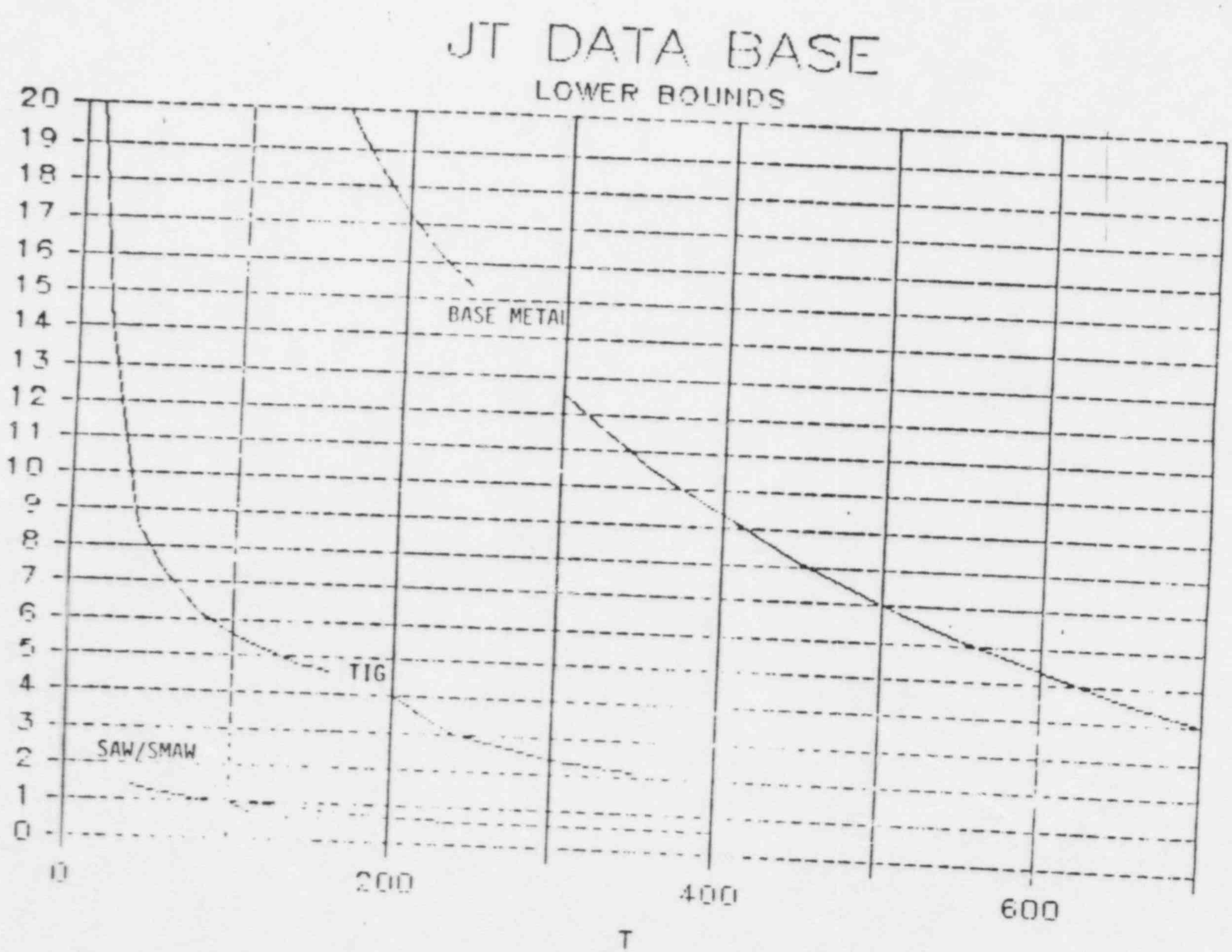

Figure 3-17. Lower Bounds of J-T Data for Wrought Stainless Steel Base Metal and for Stainless Steel Weld Metal from TIG, SMAW and SAW Welding Processes

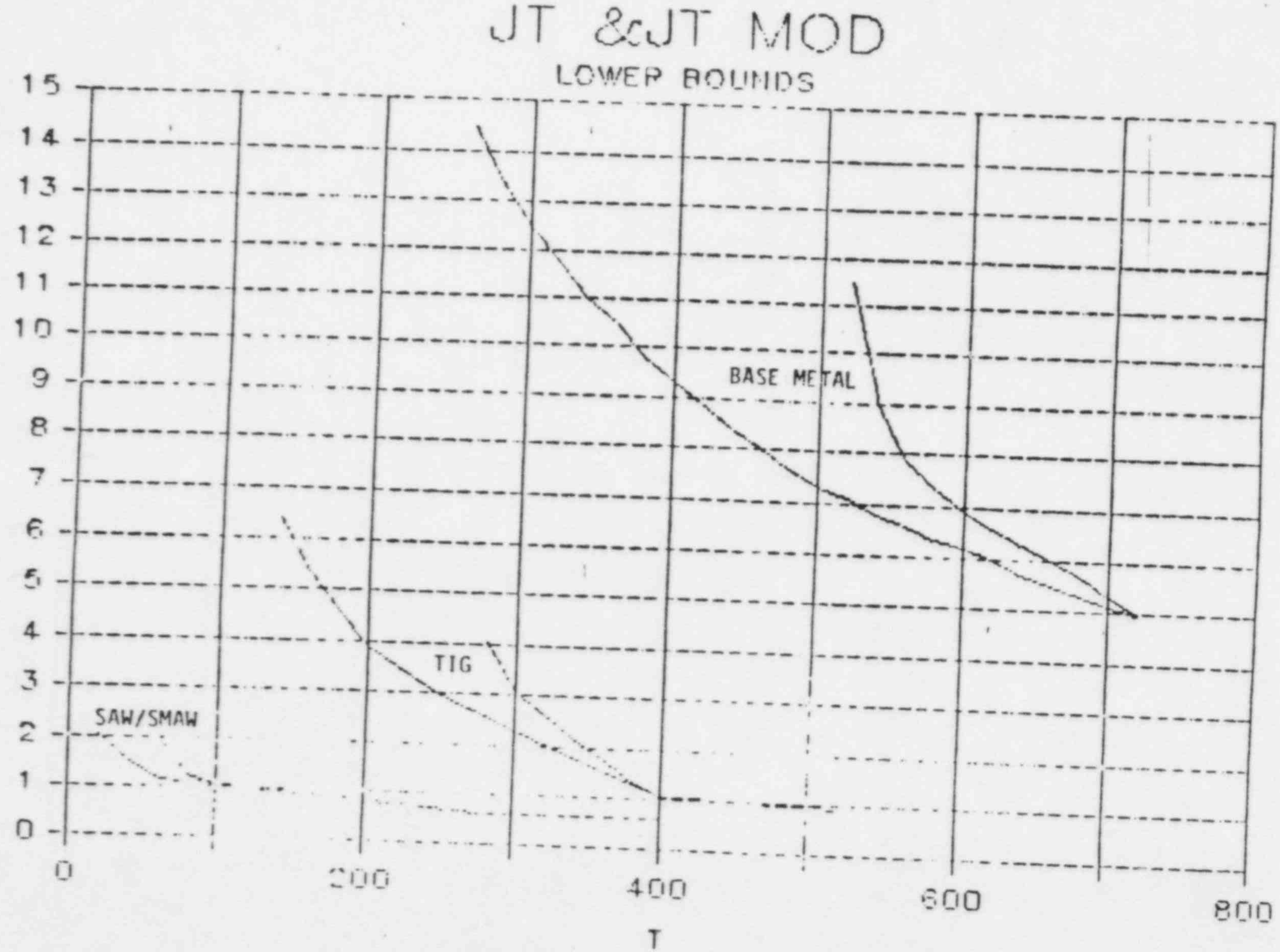

Figure 3-18. Effect of Ernst Correction on Lower Bound Weld and Base Plate J-T Curves

STRUCTURAL INTEGRITY ASSOCIATES, INC.

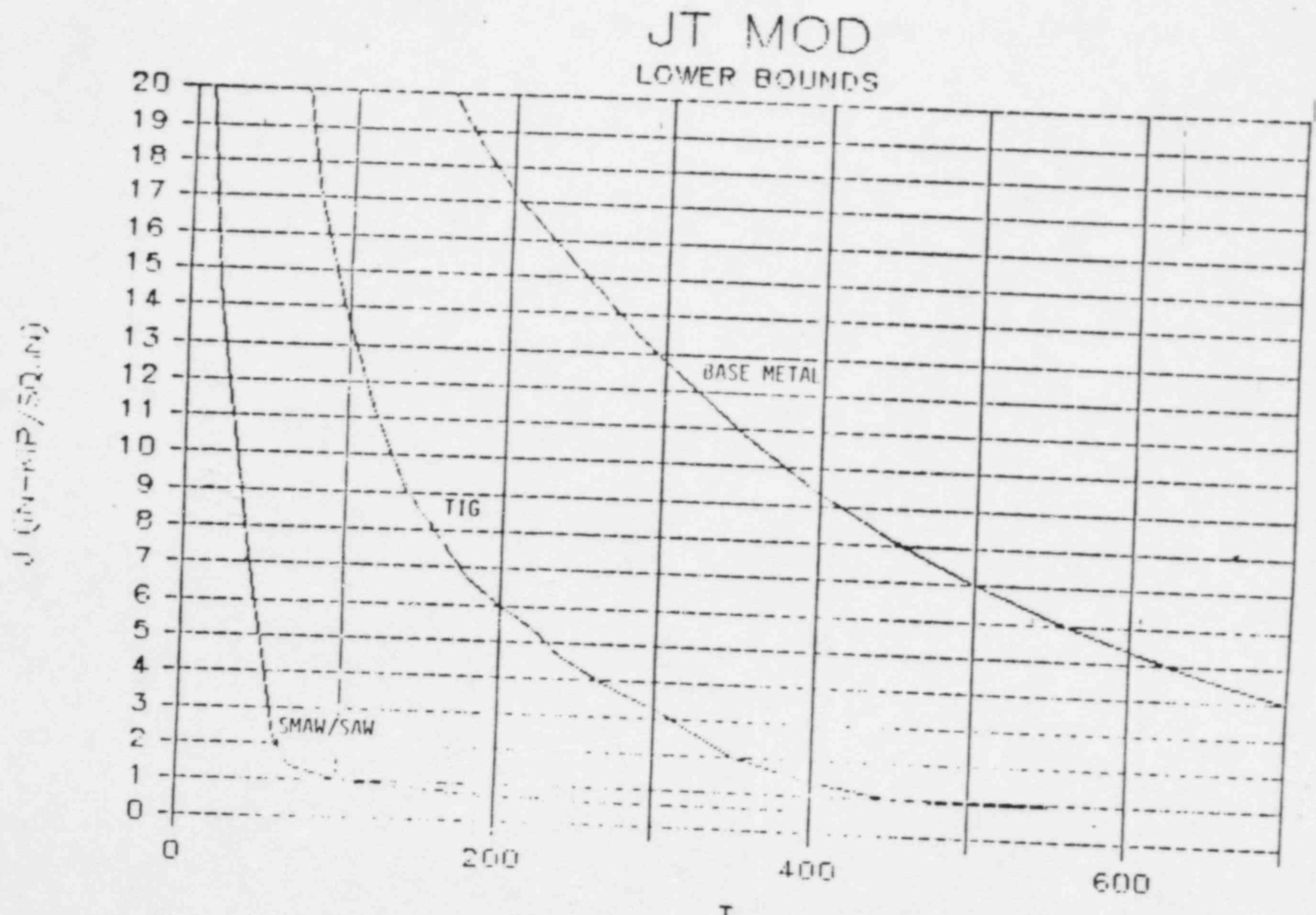

Figure 3-19. Lower Bound J-T Reference Curves for Use in Elastic-Plastic Fracture Mechanics Analysis of Austenitic Stainless Steel Pipes

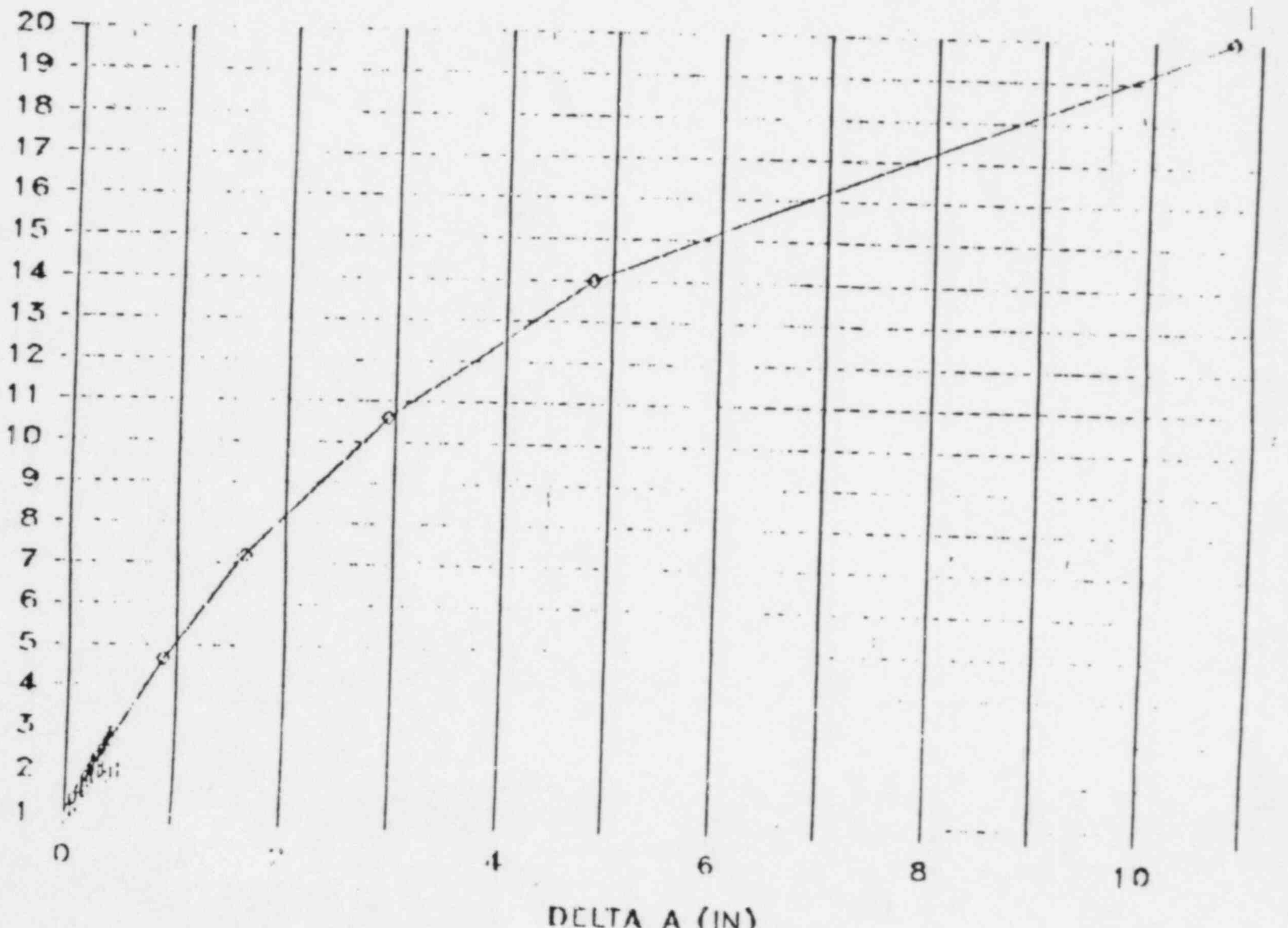

Figure 3-20. Material J-R Curve Derived from Lower Bound J-T Diagram for SAW/SMAW Weldment Material

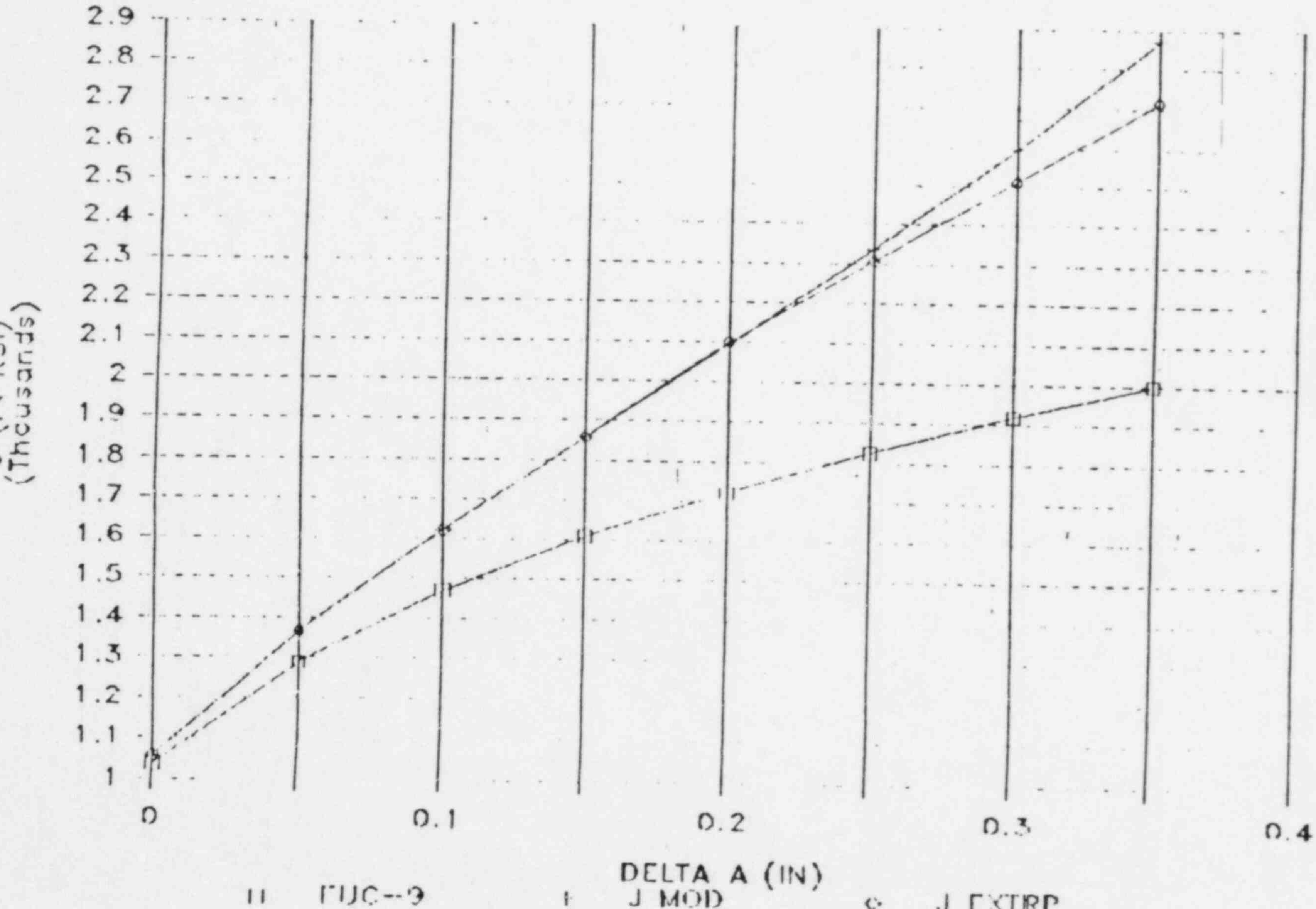

Figure 3-21. Material J-R Curve from Lower Bound J-T Diagram for SAW/SMAW Weldment Material (Expanded Scale)

STRUCTURAL INTEGRITY ASSOCIATES, INC.

4.0 EVALUATIONS AND RESULTS

4.1 Weld KR-2-14

Input to the flaw evaluation for this weld was as follows:

Indication Length = 2.1 inches
Indication Depth = 0.1418 inch

Pipe O.D. = 12.75 inches/22 inches
(Riser circumference used in normalizing crack length for conservatism)
Pipe Wall Thickness = 1.125 inches

Applied Stresses (Table 3-1)
Pressure + DW + Thermal + Shrinkage = 14.80 ksi membrane, 13.88 ksi bending
Pressure + DW + Thermal + Shrinkage + Seismic = 15.38 ksi membrane

Residual Stresses (Figure 3-5)

Figure 4-1 provides applied stress intensity factor versus crack depth data for the two load cases used in the evaluation (piping loads and IHSI residual stress). Assuming the indication to be IGSCC, these stress intensity curves were used to perform post-IHSI IGSCC crack growth estimates and the resulting crack growth predictions are illustrated in Figure 4-2. The analysis results in no predicted crack growth for the balance of plant life.

The allowable end-of-cycle flaw size was determined in accordance with ASME Section XI, Article IWB-3640, and using the J-T procedure described in Section 3.5. The results are illustrated in Figure 4-3 in terms of allowable flaw depth versus length. Note that, although not required by IWB-3640, thermal expansion stresses have been included in the evaluation to account for the possible effects of low toughness weldment material. Also, in accordance with the recommendations of NRC Generic Letter 84-11, a maximum allowable flaw size of 2/3 of the IWB-3640 limit (shown as a dashed line in Figure 4-3) is used to allow for uncertainty in flaw depth sizing.

Also shown in Figure 4-3 are allowable flaw size curves calculated by elastic-plastic fracture mechanics (EPFM) for the three different sets of Ramberg-Osgood constants of Table 3-10. It is seen that the EPFM results yield somewhat more conservative allowable flaw size, but compare favorably to the 2/3 of IWB-3640 limit.

Referring to Figure 4-3, it is seen that the 2/3 of IWB-3640 limit is satisfied indefinitely by the analysis, since no crack propagation is predicted. To add further assurance, the IGSCC crack growth analysis has been repeated assuming various initial flaw sizes ranging upward from the observed UT depth. No crack propagation is predicted in the post-IHSI condition for initial crack depths up to 0.414 inch, or 37% of the pipe wall. It is also noteworthy that, given the relatively short length of the observed indication (5.3% of circumference), it would not lead to rupture of the pipe joint even if the above crack growth or initial flaw size estimates are significantly in error. Leak-before-break is clearly the appropriate hypothetical failure mode for this indication.

On the basis of the above evaluation, it is concluded that continued operation of the plant with this weld, considering the observed indication and the IHSI treatment which has been applied, will not lead to a reduction in plant safety margins, or a plant operational concern.

4.2 Weld KR-2-36

Input to the flaw evaluation for this weld was as follows:

Indication Length = 2.2 inches
Indication Depth = 0.2813 inch

Pipe O.D. = 12.75 inches/22 inches
(Riser circumference used in normalizing crack length for conservatism)
Pipe Wall Thickness = 1.125 inches

Applied Stresses (Table 3-2)

Pressure + DW + Thermal + Shrinkage = 13.85 ksi membrane, 9.09 ksi bending

Pressure + DW + Thermal + Shrinkage + Seismic = 14.97 ksi membrane

Residual Stresses (Figure 3-5)

Figure 4-4 provides applied stress intensity factor versus crack depth data for the two load cases used in the evaluation (piping loads and IHSI residual stress). Assuming the indication to be IGSCC, these stress intensity curves were used to perform post-IHSI IGSCC crack growth estimates and the resulting crack growth predictions are illustrated in Figure 4-5. The analysis results in no predicted crack growth for the balance of plant life.

The allowable end-of-cycle flaw size was determined in accordance with ASME Section XI, Article IWB-3640, and using the J-T procedure described in Section 3.5. The results are illustrated in Figure 4-6 in terms of allowable flaw depth versus length. Note that, although not required by IWB-3640, thermal expansion stresses have been included in the evaluation to account for the possible effects of low toughness weldment material. Also, in accordance with the recommendations of NRC Generic Letter 84-11, a maximum allowable flaw size of 2/3 of the IWB-3640 limit (shown as a dashed line in Figure 4-6) is used to allow for uncertainty in flaw depth sizing.

Also shown in Figure 4-6 are allowable flaw size curves calculated by elastic-plastic fracture mechanics (EPFM) for the three different sets of Ramberg-Osgood constants of Table 3-10. It is seen that the EPFM results yield somewhat more conservative allowable flaw sizes, but compare favorably to the 2/3 of IWB-3640 limit.

Referring to Figure 4-6, it is seen that the 2/3 of IWB-3640 limit is predicted to be satisfied indefinitely by the analysis, since no crack propagation is predicted. To add further assurance, the IGSCC crack growth analysis has been repeated assuming various initial flaw sizes ranging upward from the observed UT depth. No crack propagation is predicted in the post-IHSI condition for initial crack depths up to 0.612 inch, or 54% of the pipe wall. It is also noteworthy that, given the relatively short length of the observed indication (5.5% of circumference), it would not lead to rupture of the pipe joint even if the above crack growth or initial flaw size estimates are significantly in error. Leak-before-break is clearly the appropriate hypothetical failure mode for this indication.

On the basis of the above evaluation, it is concluded that continued operation of the plant with this weld, considering the observed indication and the IHSI treatment which has been applied, will not lead to a reduction in plant safety margins, or a plant operational concern.

4.3 Weld KR-2-41

Input to the flaw evaluation for this weld was as follows:

Indication Length = 4 inches
Indication Depth = 0.2138 inch

Pipe O.D. = 12.75 inches/22 inches
(Riser circumference used in normalizing crack length for conservatism)
Pipe Wall Thickness = 1.125 inches

Applied Stresses (Table 3-3)
Pressure + DW + Thermal + Shrinkage = 12.64 ksi membrane, 8.74 ksi bending
Pressure + DW + Thermal + Shrinkage + Seismic = 14.47 ksi membrane

Residual Stresses
Zero and Post-IHSI (Figure 3-5)

Figure 4-7 provides applied stress intensity factor versus crack depth data for the two load cases used in the evaluation (piping loads and IHSI residual stress). Assuming the indication to be IGSCC, these stress intensity curves were used to perform post-IHSI IGSCC crack growth estimates and the resulting crack growth predictions are illustrated in Figure 4-8. The analysis results in no predicted crack growth for the balance of plant life.

The allowable end-of-cycle flaw size was determined in accordance with ASME Section XI, Article IWB-3640 and using the J-T procedure described in Section 3.5. The results are illustrated in Figure 4-9 in terms of allowable flaw depth versus length. Note that, although not required by IWB-3640, thermal expansion stresses have been included in the evaluation to account for the possible effects of low toughness weld material. Also, in accordance with the recommendations of NRC Generic Letter 84-11, a maximum allowable crack size of 2/3 of the IWB-3640 limit is used to allow for uncertainty in crack depth sizing.

Also shown in Figure 4-9 are allowable flaw size curves calculated by elastic-plastic fracture mechanics (EPFM), for the three different sets of Ramberg-Osgood constants of Table 3-10. It is seen that the EPFM results yield somewhat more conservative allowable flaw sizes, but compare favorably to the 2/3 of IWB-3640 limit.

Referring to Figure 4-9, it is seen that the flaw is predicted to remain at its present size indefinitely, and thus satisfy the allowable flaw size limit by a large margin for the balance of plant life. To add further assurance, the IGSCC crack growth analysis has been repeated assuming various initial flaw sizes ranging upward from the observed UT depth. No crack propagation is predicted in the post-IHSI condition for initial crack depths up to 0.6S4 inch or 61% of the pipe wall.

On the basis of the above evaluation, it is concluded that continued operation of the plant with this weld, considering the observed indication, will not lead to a reduction in plant safety margins, or a plant operational concern.

4.4 Weld KR-2-37

Input to the flaw evaluation for this weld was as follows:

Indication Length = 5 inches
Indication Depth = 0.135 inch

Pipe O.D. = 22 inches
Pipe I.D. = 19.75 inches
Pipe Wall Thickness = 1.125 inches

Applied Stresses
Pressure = 5.622 ksi

Residual Stresses (Figure 3-7)

Figure 4-10 provides applied stress intensity factor versus crack depth data for the two load cases used in the evaluation (pressure and IHSI residual stresses). Assuming the indication to be IGSCC, these stress intensity curves were used to perform IGSCC crack growth estimates for both cases, and the resulting crack growth predictions are illustrated in Figure 4-1. The analysis case results in no predicted crack growth for the balance of plant life.

The allowable end-of-life flaw size was determined in accordance with ASME Section XI, Article IWB-3640, and using the J-T procedure described in Section 3.5. The results are illustrated in Figure 4-12 in terms of allowable flaw depth versus length. Also, in accordance with the recommendations of NRC Generic Letter 84-11, a maximum allowable crack size of 2/3 of the IWB-3640 limit is used to allow for uncertainty in crack depth sizing.

Also shown in Figure 4-12 are allowable flaw size curves calculated by elastic-plastic fracture mechanics (EPFM) for the three different sets of Ramberg-Osgood constants of Table 3-10. It is seen that the EPFM results yield less conservative allowable flaw sizes in this weld.

Referring to Figure 4-12, it is seen that the flaw is predicted to remain at its present size indefinitely, and thus satisfy the allowable flaw size limit by a large margin for the balance of plant life. To add further assurance, the IGSCC crack growth analysis has been repeated assuming various initial flaw sizes ranging upward from the observed UT depth. No crack propagation is predicted in the post-IHSI condition for crack depths up to 0.81 inches, or 72% of the pipe wall.

On the basis of the above evaluation, it is concluded that continued operation of the plant with this weld, considering the observed indication, will not lead to a reduction in plant safety margins, or a plant operational concern.

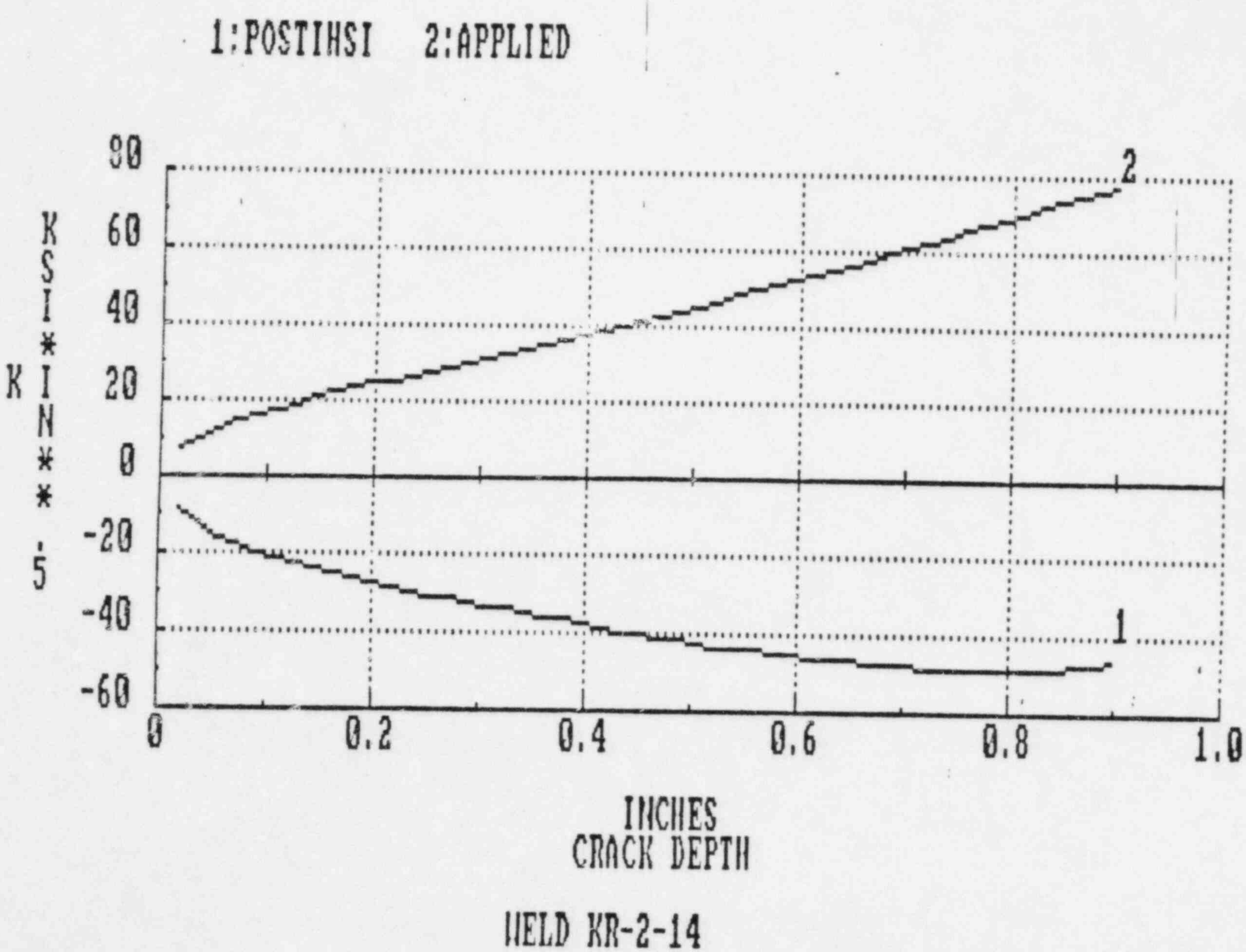

Figure 4-1. Stress Intensity Factor Versus Crack Depth for Weld KR-2-14

STRUCTURAL INTEGRITY ASSOCIATES, INC

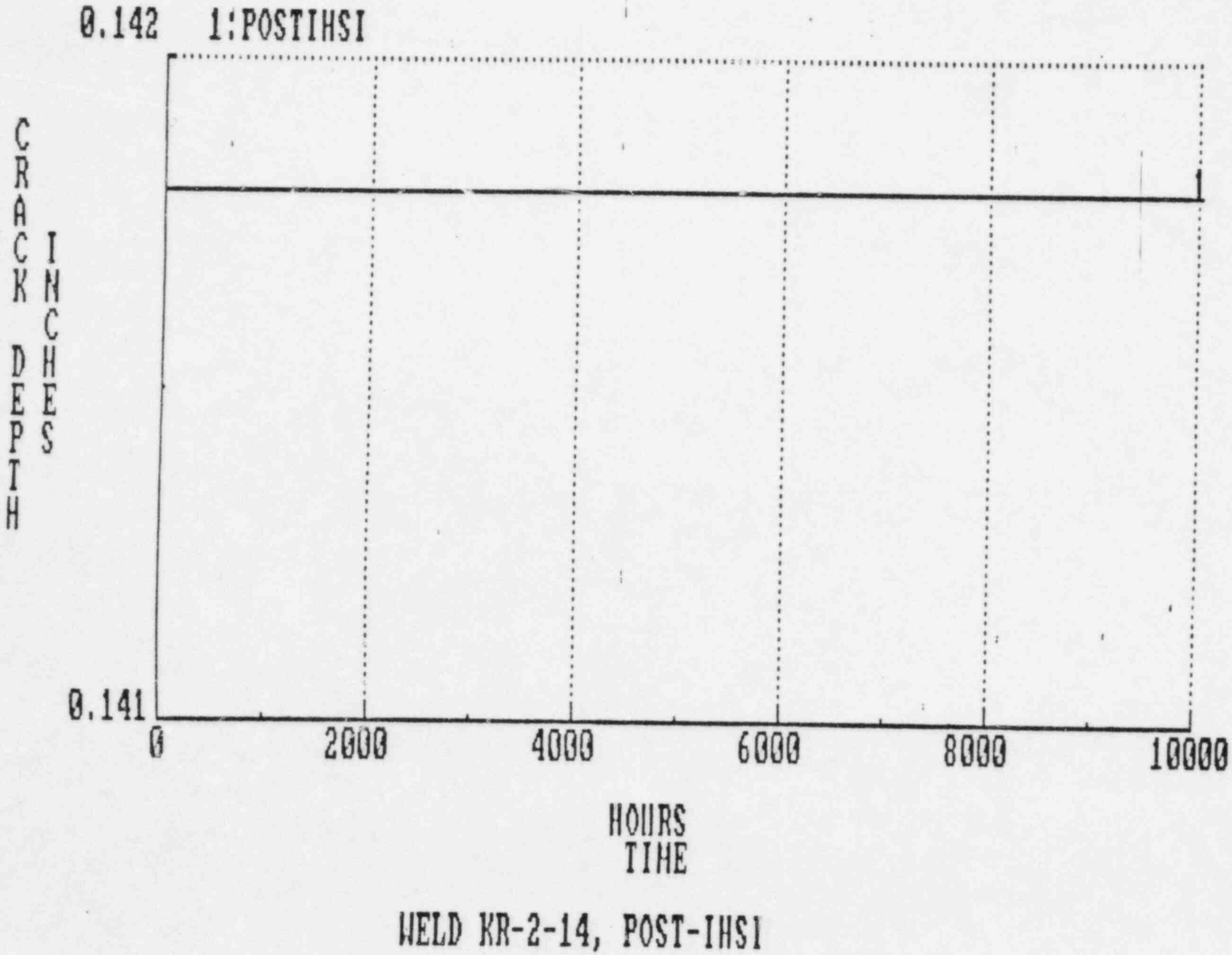

Figure 4-2. Predicted Stress Corrosion Crack Growth for Observed Ultrasonic Flaw Indication - Weld KR-2-14

STRUCTURAL INTEGRITY ASSOCIATES INC

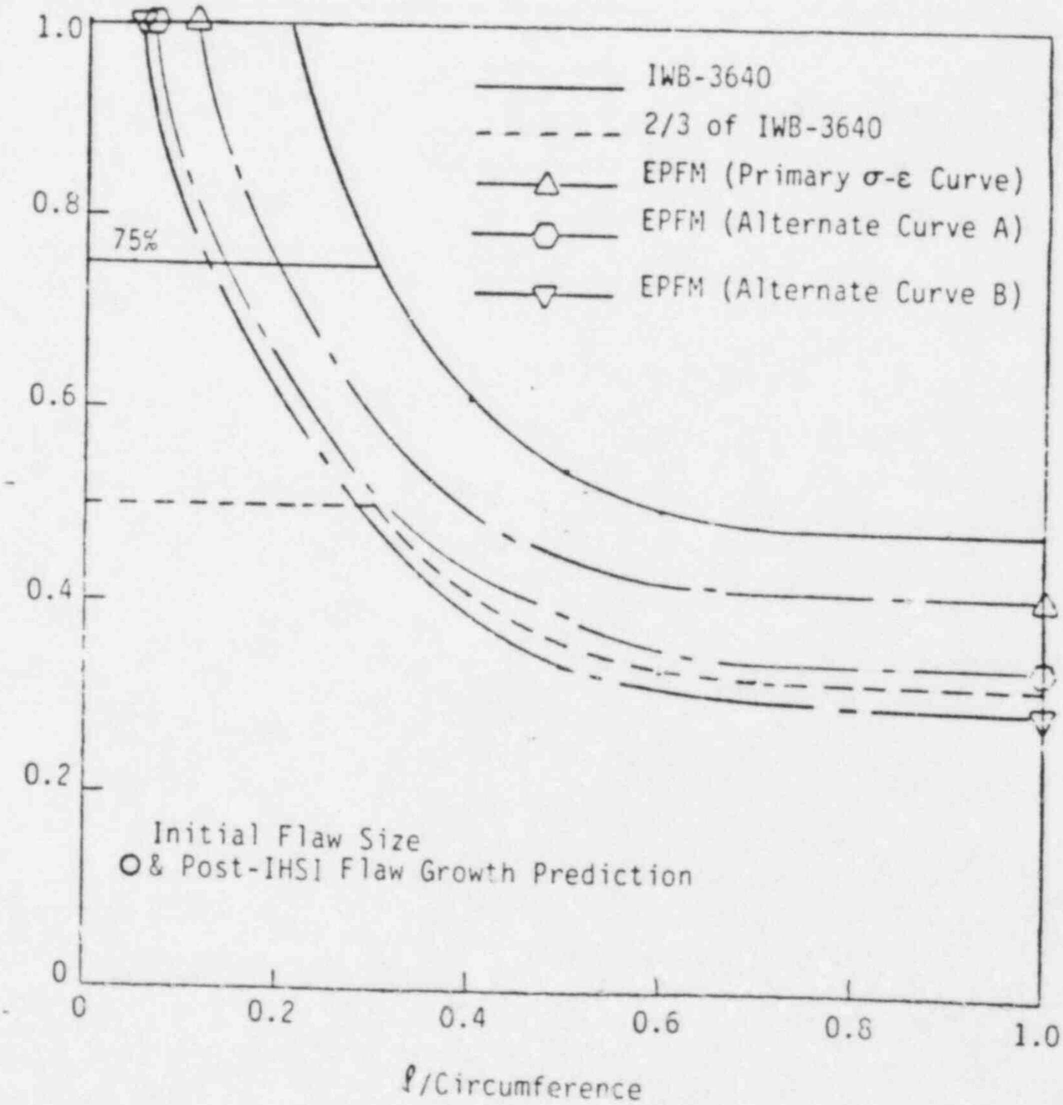

Figure 4-3. Comparison of Predicted Crack Growth with Allowable Flaw Size Limits - Weld KR-2-14

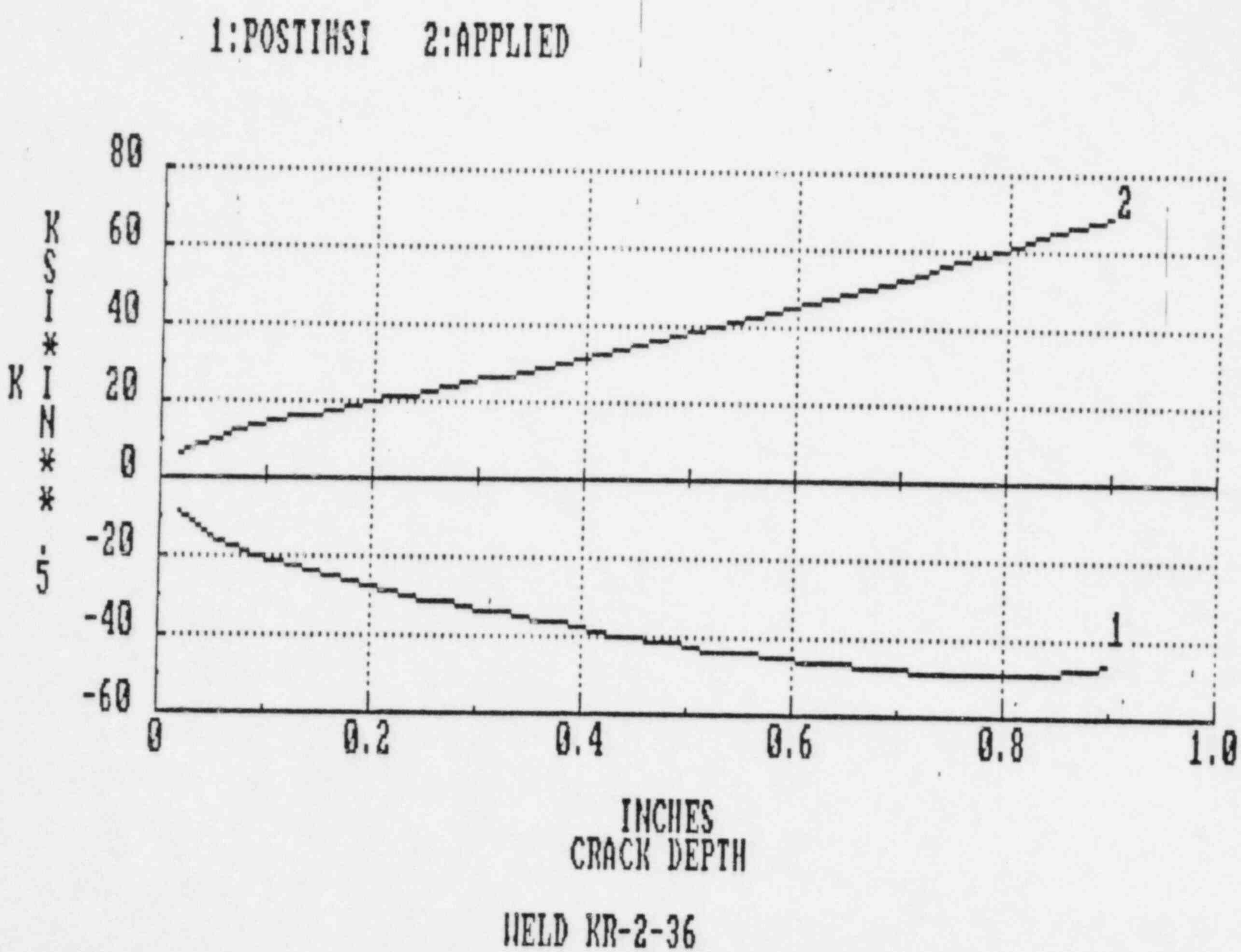

Figure 4-4. Stress Intensity Facotr Versus Crack Depth for Weld KR-2-36

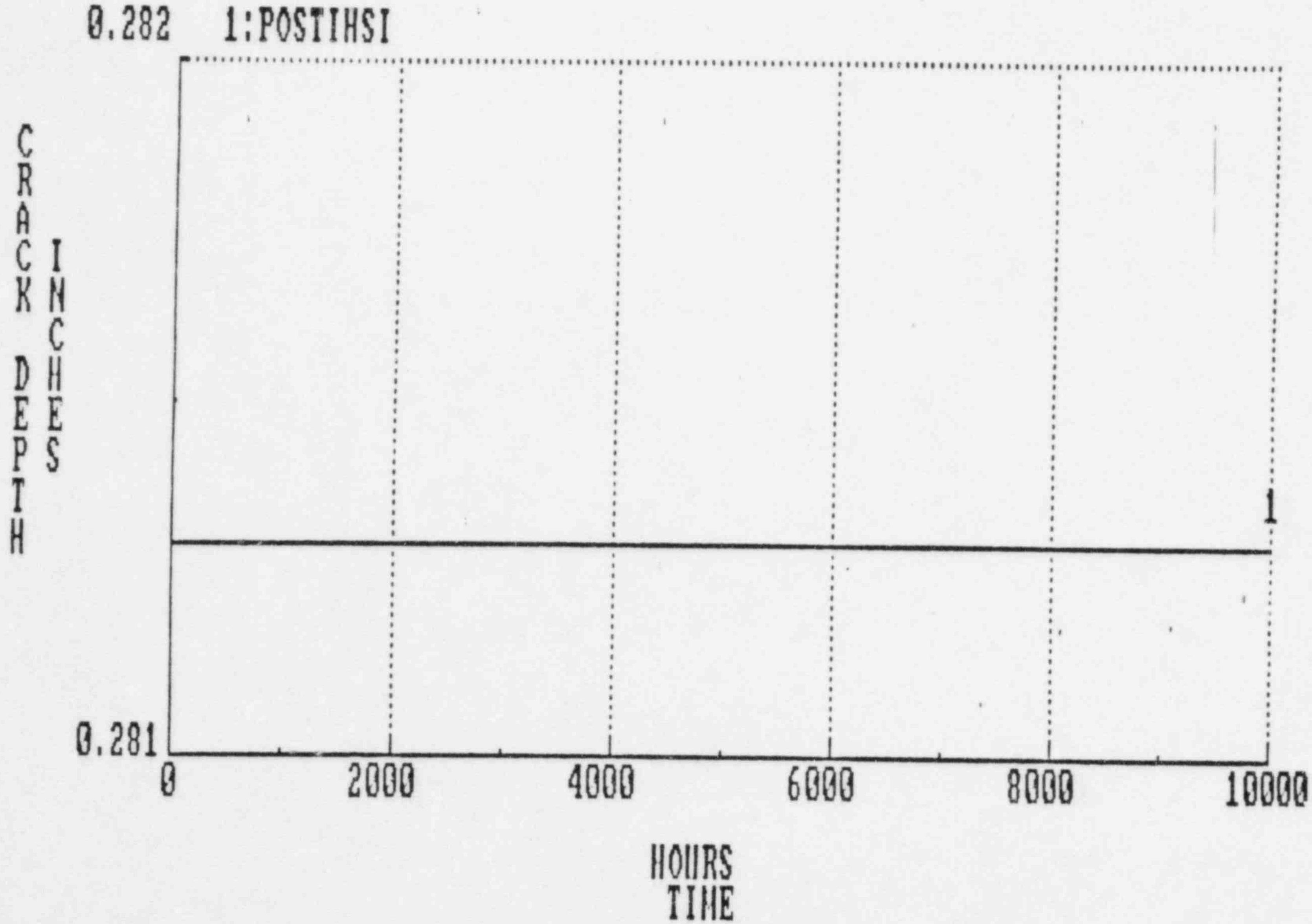

WELD KR-2-36, POST-IHSI

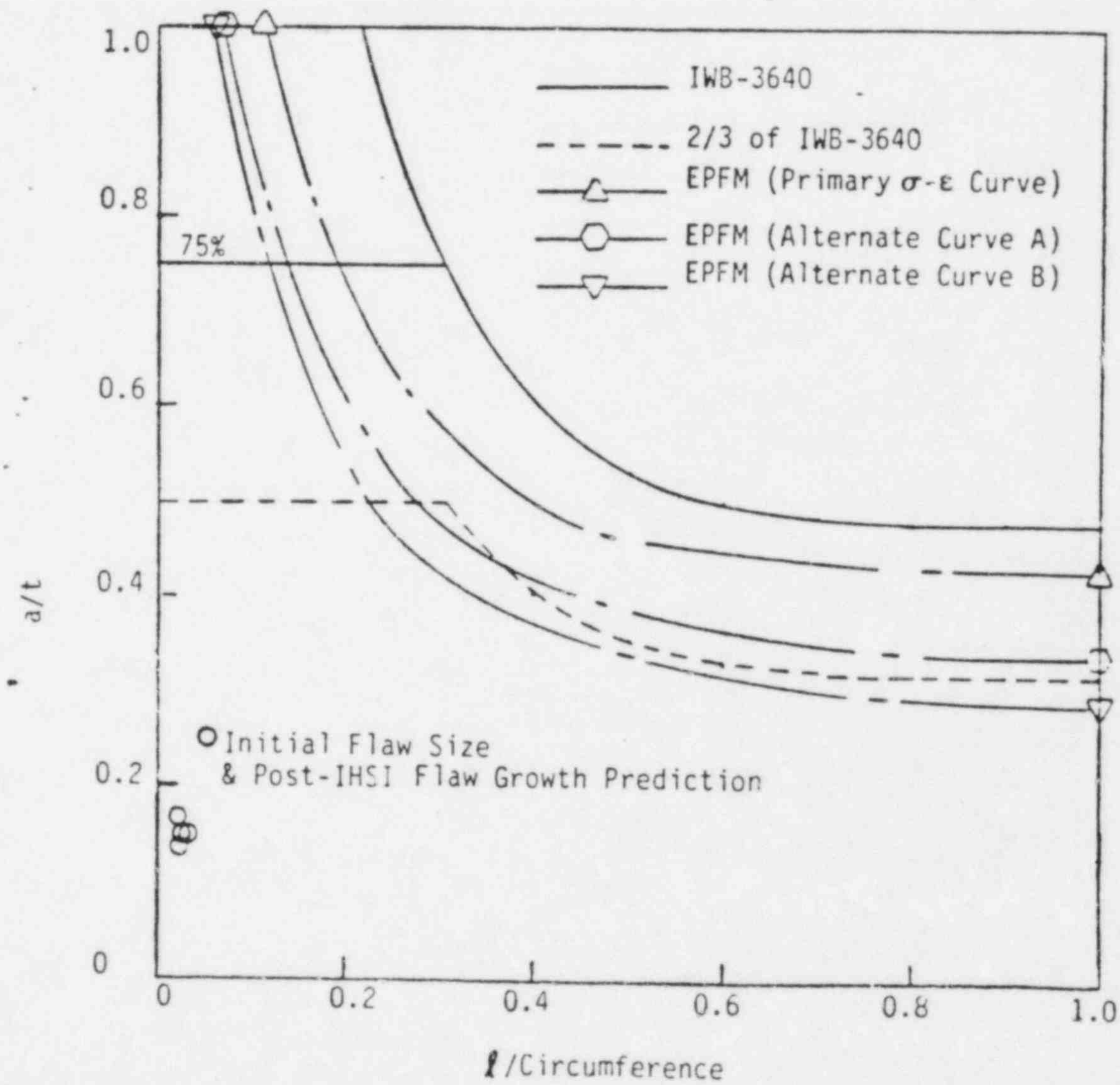

Figure 4-6. Comparison of Predicted Crack Growth with Allowable Flaw Size Limits - Weld KR-2-36

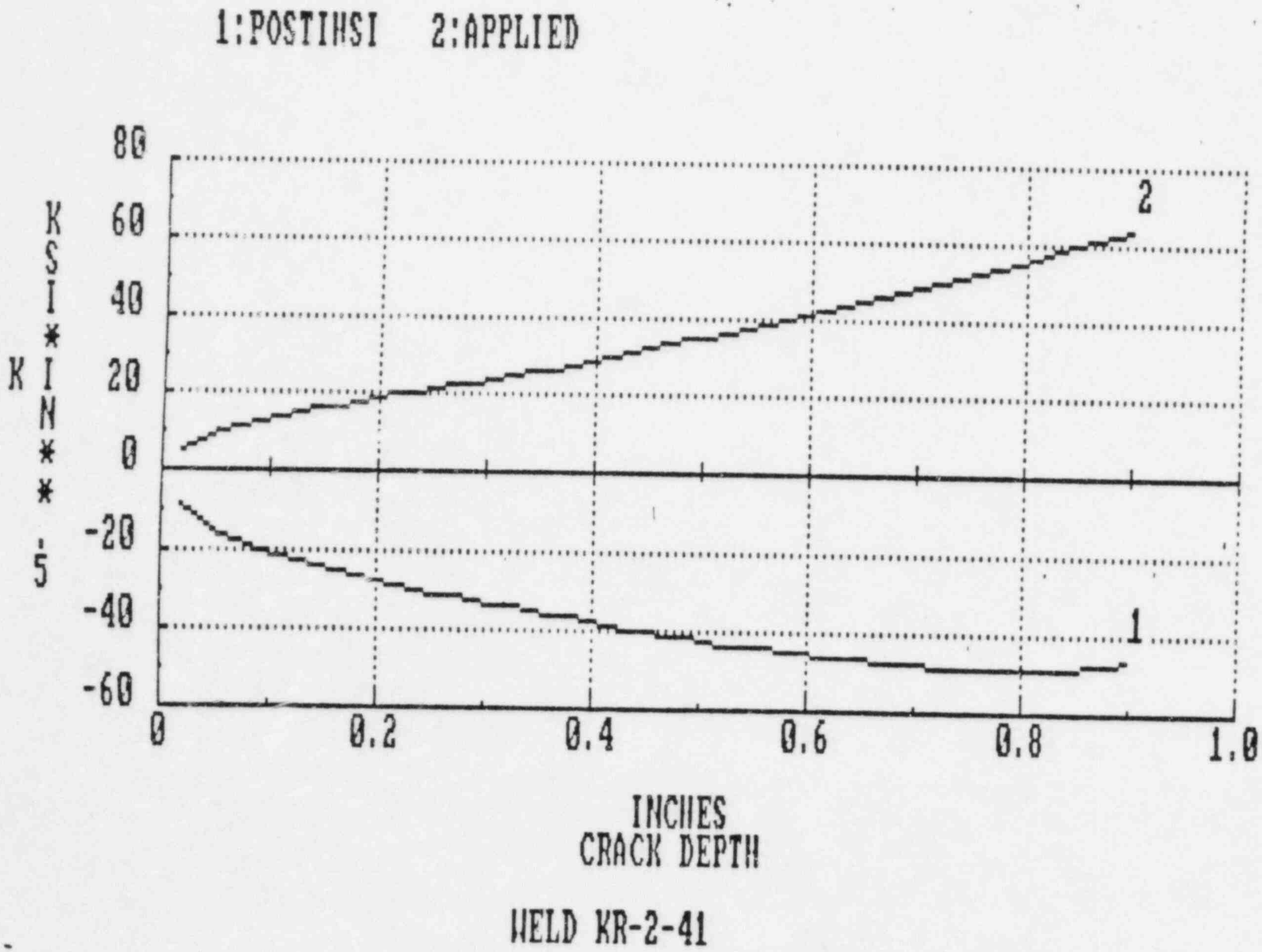

Figure 4-7. Stress Intensity Factor Versus Crack Depth for Weld KR-2-41

STRUCTURAL INTEGRITY ASSOCIATES, INC.

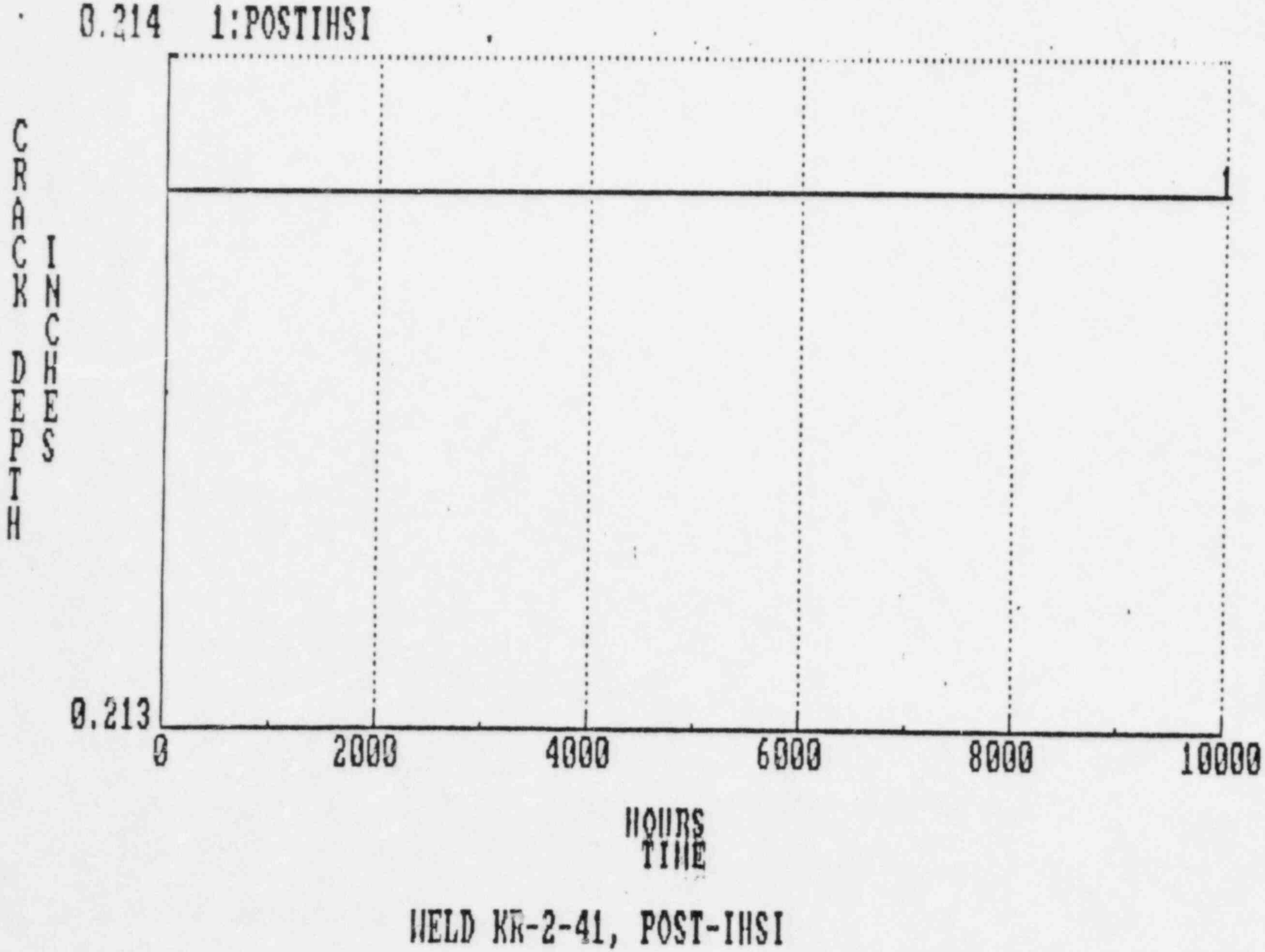

Figure 4-8. Predicted Stress Corrosion Crack Growth for Observed Ultransonic Flaw Indication -

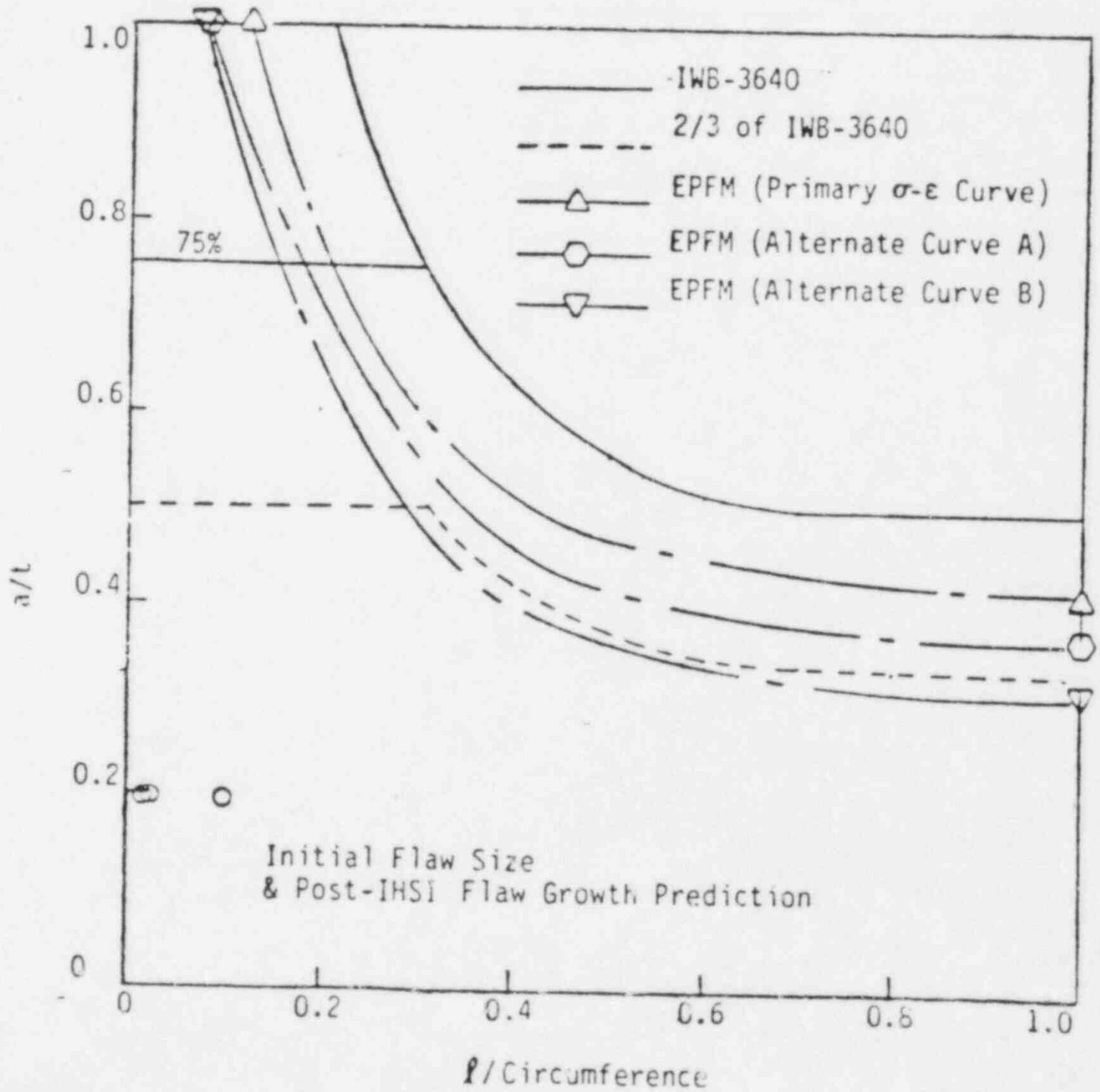

Figure 4-9. Comparison of Predicted Crack Growth with Allowable Flaw Size Limits - Weld KR-2-41

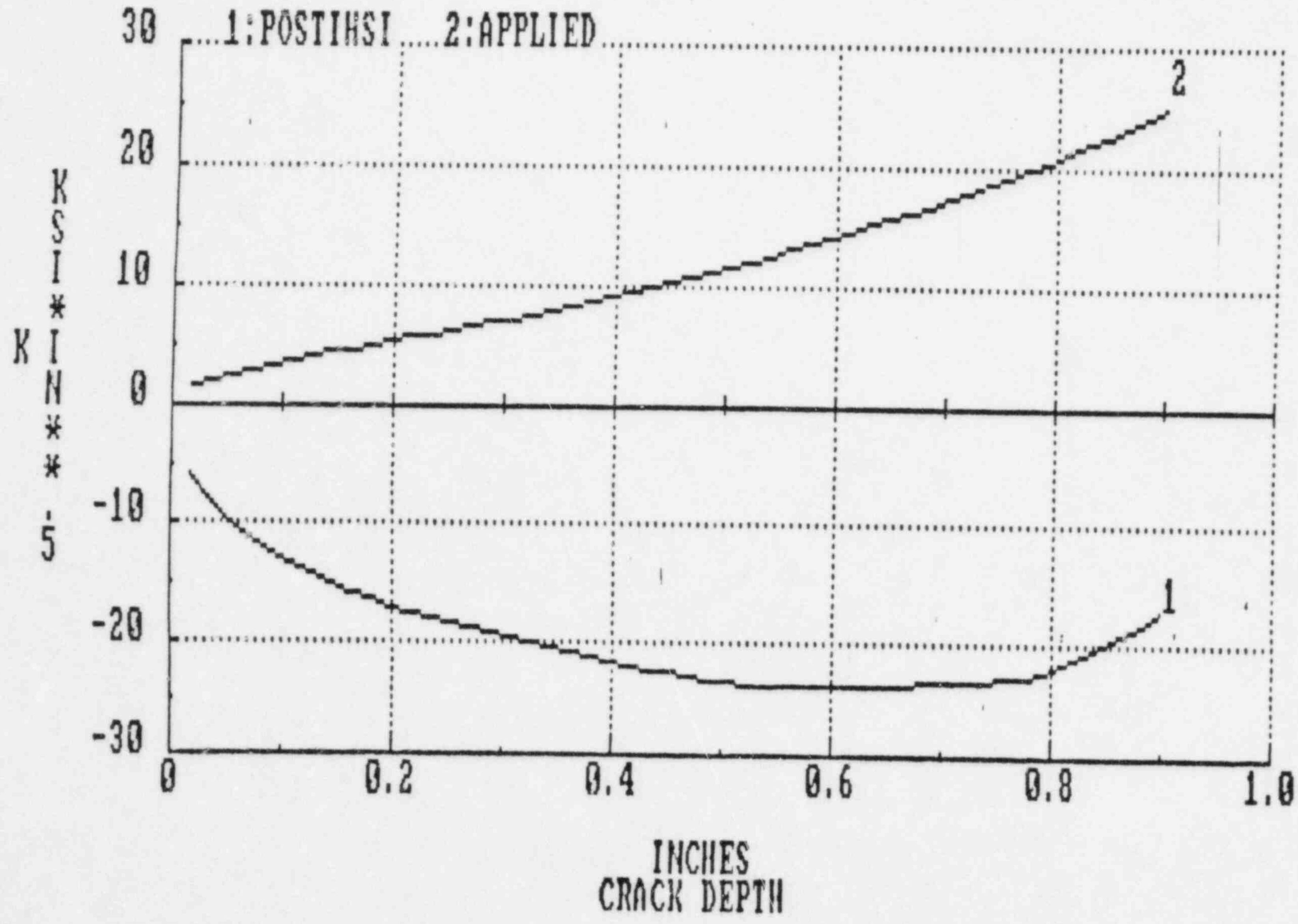

4-17

STRUCTURAL INTEGRITY ASSOCIATES, INC

Figure 4-10. Stress Intensity Factor Versus Crack Depth for Weld KR-2-37

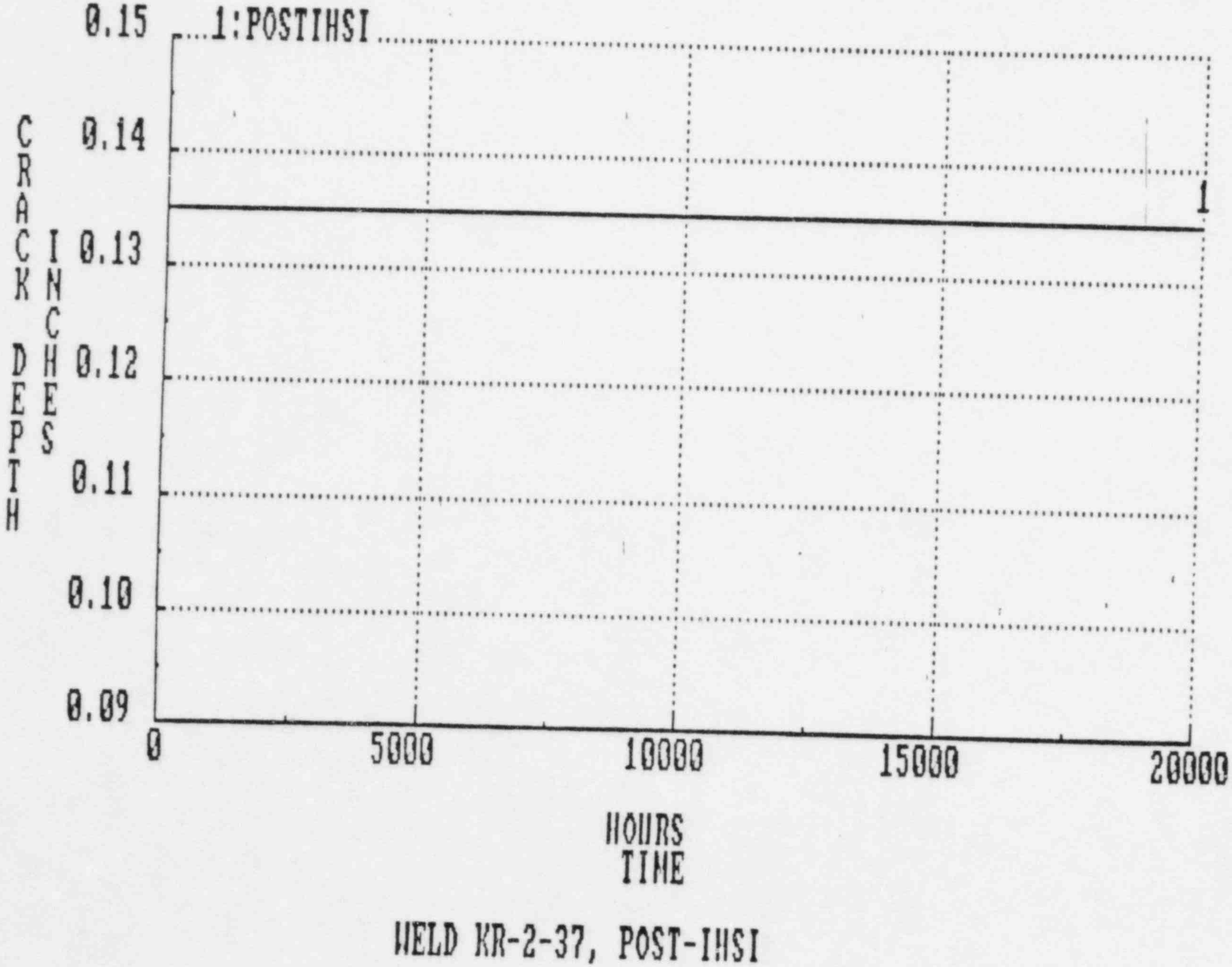

Figure 4-11. Predicted Stress Corrosion Crack Growth for Ob[illegible]

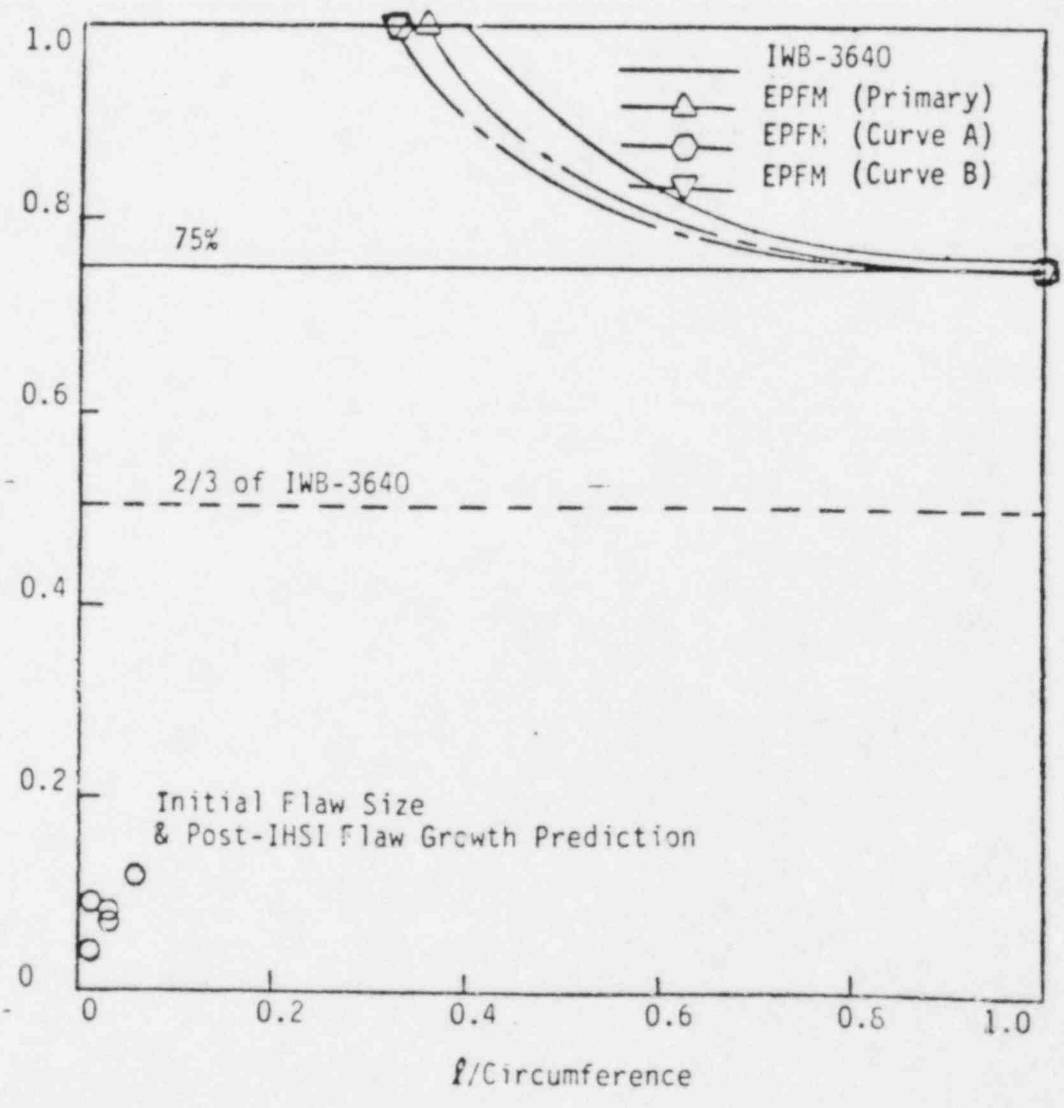

Figure 4-12. Comparison of Predicted Crack Growth with Allowable Flaw Size Limits - Weld KR-2-37

5.0 DISCUSSION AND CONCLUSIONS

This report presents fracture mechanics flaw evaluations for four welds in the Browns Ferry Unit 2 recirculation piping system (three sweep-o-let to ring header welds, and one ring header to end cap weld).

The four welds contained relatively small, crack-like indications. These welds, along with the other, uncracked welds in the plant, were treated by Induction Heating Stress Improvement (IHSI) to produce a favorable residual stress pattern and thus reduce their susceptability to IGSCC degradation. The flaw evaluations were based on the post-IHSI indication sizes, which differed somewhat from the pre-IHSI inspections, but not significantly.

The evaluations presented in this report were performed in accordance with ASME Section XI, IWB-3640 and the recommendations of NRC Generic Letter 84-11. These conventional approaches were also supplemented by Elastic Plastic Fracture Mechanics Tearing Instability analyses to account for the possible effects of low toughness weld metal. The results of the analyses for all four welds indicate that design basis safety margins are maintained in the welds, by a large margin, considering the worst case effects of the observed flaws; and that these margins are maintained indefinitely during the life of the plant, due to the beneficial effects of the IHSI treatment, which is expected to inhibit further IGSCC propagation. It is also noteworthy that all of the indications had circumferential lengths less than 10% of pipe circumference. Thus, even in the event of large uncertainties in UT depth sizing or crack growth predictions, the governing failure mode would still be leak-before-break.

On the basis of these factors, it is concluded that the inspection results and corrective actions taken should not result in any reduction in design basis safety margins or increase in the probability of a pipe rupture at the plant.

One final point of significance is that the IHSI treatments, which were performed on a large percentage of the remaining uncracked welds, should greatly reduce the probability of future IGSCC in these welds. Thus, it is reasonable to expect that the plant will operate for a long period of time with no further degradation due to IGSCC, and no reduction in leak-before-break margins relative to plants with piping not susceptable to IGSCC.

6.0 REFERENCES

1. Transmittals from E. Wilson, TVA, Jan. 29, 1985 and May 3, 1985.

2. SI Report, "Design Report for Recirculation Piping Sweep-o-lets Repair and Flaw Evaluation, Browns Ferry Nuclear Power Plant, Unit 1", SIR-83-006, Sept. 1984.

3. EPRI Report NP-2662-LD, "Computational Residual Stress Analysis for Induction Heating of Welded BWR Pipes", December 1982.

4. EPRI Report, NP-81-4-LD, "Residual Stress Improvement by Means of Induction Heating", March 1981.

5. BWROG IGSCC Research Program Status Report presented by T. Umemoto and A. Tanaka, "Application of Induction heating Stress Improvement to Pipe Branches", December 9, 1980.

6. Buchalet, C.B., and Bamford, W. H., "ASTM 8th National Symposium on Fracture Mechanics, 1974", ASTM STP-590, pp. 385-402, 1975.

7. NUREG 1061, "Investigation and Evaluation of Stress Corrosion Cracking in Piping of Boiling Water Reactor Plants", U.S. Nuclear Regulatory Commission, March, 1984.

8. "Guidelines for Flaw Evaluation and Remedial Actions for Stainless Steel Piping Susceptible to IGSCC", Final Report for EPRI Project T303-1, Report No. SIR-84-005, April 13, 1984.

9. Bickford, R. L., et al, "Nondestructive Evaluation Instrument Surveillance Test on 26-Inch Pipe", EPRI NP-3393, January, 1984.

10. Ranganath, S., and Norris, D.M., "Evaluation Procedure and Acceptance Criteria for Flaws in Austenitic Steel Piping", Draft No. 10, Subcommittee on Piping, Pumps, and Values of the PVRC of the WRC, July 1983.

11. Ranganath, S., Mehta, H. S., and Norris, D.M., "Structural Evaluation of Flaws in Power Plant Piping", ASME PVP-Vol. 94, Circumferential Cracks in Pressure Vessels and Piping - Vol. I, pp. 91-116, 1984.

12. ASME Boiler and Pressure Vessel Code, Section XI, 1983.

13. ASME Section XI Meeting Minutes, May 25, 1984.

14. Kumar, V., et al., "An Engineering Approach for Elastic-Plastic Fracture Analysis", EPRI NP-1931, July, 1981.

15. Kumar, V., et al., "Advances in Elastic-Plastic Fracture Analysis", EPRI NP-3607, Aug., 1984.

16. Hutchinson, J. W., and Paris, P. C., "Stability Analysis of J-Controlled Crack Growth", in Elastic-Plastic Fracture, ASTM 668, American Society for Testing and Materials, 1979, pp. 37-64.

17. Westinghouse Test Data, presented by J. Landes at the meeting of ASME Boiler & Pressure Vessel Code Section XI, Task Group on Piping Flaw Evaluation, San Antonio, Texas, April 23, 1984.

18. Gudas, J.P., and Anderson, D. R., "J_1-R Curve Characteristics of Piping Material and Welds", NSRDC, presented at U.S. NRC 9th Water Reactor Safety Research Information Meeting, Washington, D.C., Oct. 29, 1981.

19. NSRDC Test Data, presented by M. Vassileros at the meeting of ASME Boiler & Pressure Vessel Code Section XI, Task Group on Piping Flaw Evaluation, San Antonio, Texas, April 23,1984.

20. Paris, P.C., Brunetti, J. V., and Cotter, K. H., "The Effect of Large Crack Extension on the Tearing Resistance of Stainless Steel Piping Materials", Presented at the CSNI Specialist Meeting on "Leak-Before-Break in Nuclear Reactor Piping Systems", Sept. 1-2, 1983, Monterey, CA.

21. McCabe, D. E., Westinghouse letter to J. F. Copeland, Stainless Pipe Weldment Tests, Aug. 29, 1984.

22. Metals Handbook - Ninth Edition, Volume 6 - Welding, Brazing, and Soldering, American Society for Metals, Metals Park, Ohio, c. 1983.

23. Tetelman, A.S., and McEvily, Jr., A. J., Fracture of Structural Materials, John Wiley & Sons, Inc., New York, c. 1967, pp. 212-222.

24. Landes, J. D., et al, "Elastic-Plastic Methodology to Establish R-Curves and Instability Criteria", Sixty Semi-annual Report, Jan. 1, 1982 to June 30, 1982, EPRI Contract No. RP 1238-2, Aug. 4, 1982.

25. Ernst, H. A., "Material Resistance and Instability Beyond J Controlled Crack Growth", presented at the Second International Symposium on Elastic-Plastic Fracture Mechanics, Philadelphia, PA, Oct. 1981.

STRUCTURAL INTEGRITY ASSOCIATES, INC.

ATTACHMENT 3

Browns Ferry Nuclear Plant Unit 2, Cycle 5
Induction Heating Stress Improvement (IHSI)
of IGSCC Susceptible 304 Stainless Steel (SS) Welds

1.0 Introduction

The results of the ultrasonic (UT) examinations performed on the recirculation, residual heat removal (RHR), core spray, and reactor water cleanup (RWCU) piping systems indicated that only five welds contained IGSCC. It was decided to perform induction heating stress improvement (IHSI) on all accessible, susceptible 304 SS Class 1 welds in those systems to prevent the initiation of IGSCC. IHSI was also performed on four of the welds with IGSCC indications to prevent the propagation of cracking.

General Electric Company was contracted to perform IHSI under a two-phase workplan. Phase I consisted of a site survey to evaluate the implementation of IHSI on candidate welds. Phase II included coil development, scheduling, equipment setup, and all other work necessary to complete the IHSI treatments on welds identified as treatable in Phase I.

2.0 Phase I - Site Survey

The site survey was conducted from December 10, 1984 through December 20, 1984. The following work was performed during the survey:

- evaluation of candidate welds designated by TVA for treatment
- collection of weld contour data
- verification of weld accessibility and identification of obstructions
- measurement of piping systems - study of potential IHSI equipment locations

The survey information was then evaluated and a workplan for Phase II was laid out.

2.1 IHSI Workscope

It was determined that IHSI could be implemented on 156 welds. The treatable welds are listed in Tables 1 through 5. During the course of IHSI implementation, welds DSRWC-2-7 and DRWC-2-4 were deleted from the workscope. The elbow containing these welds was cut out and replaced to effect repair of the crack in weld DRWC-2-4. The total number of welds in the IHSI workscope was therefore reduced to 154. Twelve recirculation, 22 core spray, and 6 RHR welds were excluded from the workscope; these are listed in table 6. The recirculation nozzle-to-safe end welds and welds DCS-2-12, DCS-2-3, DRHR-2-12, and DRHR-2-3 were excluded because they were untreatable by the IHSI methods generally available when the requisition was prepared. As IHSI techniques to treat these configurations become available, these welds will be treated. The other core spray and RHR welds which were excluded are carbon steel or low-carbon SS and are not considered susceptible to IGSCC. They will require no further disposition.

2.2 Induction Coils

The survey results indicated that 62 induction coils would be needed to perform the 154-weld IHSI work scope. This required 3 new coils in addition to the 59 coils already available to GE.

2.3 Interferences

Sixty-seven interferences were identified during the site survey. The list below gives the type and number of each obstruction identified.

Type	No. of Obstructions
Structural Steel	2
Hanger Lug	5
Hanger Pad	6
Hanger Rod	8
Hanger Clamp	6
Electrical Conduit	8
Chain Falls and Wire Rope	8
Snubber Lug	5
Lead Blanket	2
Pipe Bracket	8
Penetration Insulation	1
Chain	1
Pump Housing	2
Thermocouples	2
Instrument Lines	2
Painted Pipe	1

All interferences were removed prior to the treatment of each weld. Plant equipment, such as hanger components and conduit, was restored following treatment of the associated weld.

2.4 Equipment

The equipment locations were also determined during the survey. Equipment needed for IHSI consisted of a 4160/480V three-phase transformer, a frequency converter (power supply), work stations, a cooling water system, and a data acquisition system. Each work station consisted of a voltage-reducing transformer, a capacitor bank, and a variable transformer that matches the converter output power to the impedance of the induction coil. The cooling water system was a self-contained closed loop supplying cooling water to the frequency converter, work station, coils and electrical cables. The data acquisition system monitored and documented the pipe temperature during each IHSI treatment. Thermocouples were attached to the pipe's outer surface and connected to the data acquisition system.

Two work stations were located outside of the drywell, one at each equipment hatchway. The IHSI control room, which housed the data aquisition hardware as well as the process control panel, was located at the personnel air lock. The power supply and cooling supply system pump skid were placed on elevation 593.

In addition, a direct line communication system was established between the power supply, pump skid, heat station, and IHSI control room. A communication line between the IHSI control station and the reactor control room was also established.

3.0 Phase II - IHSI Treatments

The IHSI treatments were performed from January 14 through March 31, 1985. The following table shows the time taken to complete each system.

System	No. of Successful Treatments	Date First Thermocouple Installed	Date Last Thermocouple Removed
RWCU	12	1/10	3/24
CS	9	1/15	1/24
Recirc	99	1/21	3/31
RHR	29	3/6	3/29

An overall average of 2.9 treatments were performed each day. GE was unsuccessful in treating recirculation welds KR-2-4, KR-2-1, KR-2-26, KR-2-23, and RWCU weld DRWC-2-5A. A total of 149 welds were treated successfully.

In general, the treatment sequence for each weld included thermocouple (TC) installation, coil installation, low-power idle run, coil adjustment, treatment, coil removal, TC removal, and PT of TC tack welds. Selected welds were also ultrasonically examined following the IHSI treatment.

3.1 Thermocouples

Eleven TCs were attached to each weld to record temperature data during IHSI treatment. Five TCs were positioned on one azimuth, parallel to the center axis of the pipe, with one centered on the weld crown and two on either side placed in the heat-affected zone (HAZ) and at the edge of the IHSI heat zone. Two TCs were also attached on the HAZ on the three remaining azimuths spaced 90° apart. On some welds, a twelfth TC was used to monitor the temperature of permanent obstructions positioned close to the IHSI heat zone. The data acquisition system had a 12-channel input, allowing all data to be recorded on tapes, and provided individual TC temperature printouts every 4 seconds. A temperature profile plot was also provided during each IHSI treatment.

The TCs were resistance welded to the pipe in accordance with ASME Section III, NB4311-3. Following the IHSI treatment, the TCs were removed and the affected areas were blended smooth and liquid penetrant examined in accordance with ASME Section III NB5000.

3.2 Low-Power Idle Run

A low-power pre-treatment at 250°C±50°C (482°F±90°F) was performed on each weld just prior to the full IHSI treatment to verify that the TCs were operative, the coil was positioned correctly, the water was cooling effectively, and load controls were operative. On some welds several low-power tests were required to precisely align the coil.

3.3 IHSI Treatment

To obtain a successful IHSI treatment, the minimum throughwall temperature difference of 275°C (527°F) was effected within the treatment zone for the minimum heating time (see Table 7 for process control parameters). This was achieved by heating the pipe outer surface within the treatment zone to between 400°C (752°F) and 575°C (1067°F) while simultaneously cooling the inner surface with system water flowing at the specified rates. Several welds required more than one attempt to obtain a successful treatment. In the treatment of 14 welds, there were deviations from the process control parameters; these were all analyzed by GE engineering and documented on NCRs and FDDRs. The analyses showed that all fourteen welds obtained sufficient comprehensive stress to qualify for full treatment. TVA disagreed with the GE disposition of welds KR-2-36 and KR-2-37. These welds were retreated within the specified process control parameter limits.

3.4 Post IHSI Ultrasonic Examination

A 25-percent sample of IGSCC susceptible welds were ultrasonically examined following the IHSI treatments. The welds were selected for examination based on the following factors:

1. Welds which had recordable indications and/or underwent evaluation and were found to have geometric reflectors during initial examination for IGSCC.

2. Welds in the same location where defects were found during the unit 1, cycle 5 IGSCC examinations.

The welds in the sample are listed in Attachment 1.

4.0 Conclusions

Despite schedule delays caused by labor shortages, weather, and loss of cooling water, the IHSI program undertaken on Browns Ferry unit 2 was successfully completed. Most of the IGSCC susceptible 304 ss welds in board of the penetrations on the subject systems received successful IHSI treatments. The susceptible welds which were excluded from the scope and those that were unsuccessfully treated have complicated or unconventional configurations. These welds which are listed in table 8 will be treated as the technology becomes available.

IHSI has been shown to offer a level of mitigation against IGSCC. Treatment of these recirculation, RHR, core spray, and RWCU will be cost effective by providing one or more cycles of operation with relative freedom from cracking and associated repair activities. Current speculation is that IHSI combined with other mitigation measures, e.g., alternate water chemistry is required to provide life-of-plant immunity.

TABLE 1

RECIRCULATION LOOP A

SIZE (IN.)	CONFIGURATION	TVA-WELD IDENTIFICATION
28	STP/SE	GR-2-53
28	STP/LREL	KR-2-45
28	STP/LREL	GR-2-54
28	STP/LREL	KR-2-47
28	STP/LREL	KR-2-2
28	STP/TEE	GR-2-55
28	STP/TEE	KR-2-46
28	STP/TEE	KR-2-3
28	VLV/LREL	GR-2-56
28	VLV/LREL	GR-2-3
28	VLV/STP	GR-2-57
28	VLV/STP	GR-2-2
28	STP/SREL	KR-2-48
28	PMP/SREL	GR-2-58
28	STP/PMP	GR-2-1
28	CRS/RED	KR-2-11
28	CRS/TEE	GR-2-8
22	HDR/ECP	KR-2-15
22	HDR/CRS	KR-2-12
22	HDR/CRS	GR-2-18

TABLE 1

RECIRCULATION LOOP A (Continued)

SIZE (IN.)	CONFIGURATION	TVA-WELD IDENTIFICATION
22	HDR/VLV	GR-2-25
22	HDR/VLV	GR-2-26
22	HDR/SOL	KR-2-14*
22	HDR/SOL	KR-2-13
22	HDR/SOL	KR-2-19
22	HDR/SOL	KR-2-20
12	STP/SOL	GR-2-9
12	STP/SOL	GR-2-12
12	STP/SOL	GR-2-19
12	STP/SOL	GR-2-22
12	STP/SE	GR-2-11
12	STP/SE	GR-2-14
12	STP/SE	GR-2-17
12	STP/SE	GR-2-21
12	STP/SE	GR-2-24
12	STP/RED	GR-2-15**
12	STP/LREL	GR-2-10
12	STP/LREL	GR-2-13
12	STP/LREL	GR-2-16
12	STP/LREL	GR-2-20
12	STP/LREL	GR-2-23
12	STP/LREL	KR-2-16
12	STP/LREL	KR-2-17
12	STP/LREL	KR-2-18

TABLE 1

RECIRCULATION LOOP A (Continued)

SIZE (IN.)	CONFIGURATION	TVA-WELD IDENTIFICATION
12	STP/LREL	KR-2-21
12	STP/LREL	KR-2-22
4	ECP/WLT	GR-2-7
4	ECP/WLT	GR-2-4
4	WLT/STP	KR-2-4
4	WLT/STP	KR-2-1
6	FLN/STP	KR-2-49

* Weld with indication of crack

** Throughwall crack discovered after IHSI

TABLE 1

RECIRCULATION LOOP B

SIZE (IN.)	CONFIGURATION	TVA-WELD IDENTIFICATION
4	WLT/ECP	GR-2-33
4	WLT/ECP	GR-2-30
4	WLT/STP	KR-2-26
4	WLT/STP	KR-2-23
6	FLN/STP	KR-2-53
22	HDR/SOL	KR-2-41*
22	HDR/SOL	KR-2-42
12	STP/SOL	GR-2-35
12	STP/SOL	GR-2-38
12	STP/SOL	GR-2-45
12	STP/SOL	GR-2-48
12	STP/SE	GR-2-37
12	STP/SE	GR-2-40
12	STP/SE	GR-2-43
12	STP/SE	GR-2-47
12	STP/SE	GR-2-50
12	STP/RED	GR-2-41
12	STP/LREL	GR-2-49
12	STP/LREL	GR-2-46
12	STP/LREL	GR-2-42
12	STP/LREL	GR-2-39
12	STP/LREL	GR-2-36
12	STP/LREL	KR-2-44

TABLE 1

RECIRCULATION LOOP B (Continued)

SIZE (IN.)	CONFIGURATION	TVA-WELD IDENTIFICATION
28	STP/SE	GR-2-59
28	STP/LREL	KR-2-50
28	STP/LREL	GR-2-60
28	STP/LREL	KR-2-51
28	STP/LREL	KR-2-24
28	STP/TEE	KR-2-25
28	STP/STP	GR-2-61
28	VLV/LREL	GR-2-62
28	VLV/LREL	GR-2-29
28	VLV/STP	GR-2-63
28	VLV/STP	GR-2-28
28	STP/SREL	KR-2-52
28	PMP/SREL	GR-2-64
28	STP/PMP	GR-2-27
28	CRS/TEE	GR-2-34
28	CRS/RED	KR-2-33
22	HDR/ECP	KR-2-37*
22	HDR/CRS	KR-2-34
22	HDR/CRS	GR-2-44
22	HDR/VLV	GR-2-51
22	HDR/VLV	GR-2-52
22	HDR/SOL	KR-2-35
22	HDR/SOL	KR-2-36*

TABLE 1

RECIRCULATION LOOP B (Continued)

SIZE (IN.)	CONFIGURATION	TVA-WELD IDENTIFICATION
12	STP/LREL	KR-2-43
12	STP/LREL	KR-2-40
12	STP/LREL	KR-2-39
12	STP/LREL	KR-2-38
5	WLT/ECP	GR-2-63A
5	WLT/STP	GR-2-63B

* Weld with indication of crack

TABLE 2

RHR LOOP A (SUCTION)

SIZE (IN.)	CONFIGURATION	TVA-WELD IDENTIFICATION
20	STP/TEE	DRHR-2-19
20	STP/LREL	DSRHR-2-9
20	STP/LREL	DSRHR-2-10
20	STP/LREL	DSRHR-2-11
20	LREL/VLV	DRHR-2-21
20	STP/VLV	DRHR-2-22
20	STP/VLV	DRHR-2-23
20	STP/SOL	DSRHR-2-8

TABLE 3

RHR LOOP B (DISCHARGE

SIZE (IN.)	CONFIGURATION	TVA-WELD IDENTIFICATION
24	TEE/STP	DRHR-2-18
24	STP/VLV	DRHR-2-17
24	VLV/SREL	DRHR-2-16
24	SREL/STP	DSRHR-2-7
24	STP/STP	DSRHR-2-6
24	STP/VLV	DRHR-2-15
24	SREL/VLV	DRHR-2-14
24	SREL/STP/SREL	DSRHR-2-5A
24	SREL/STP/SREL	DSRHR-2-5
24	STP/SREL	DRHR-2-13

RHR LOOP A (DISCHARGE

SIZE (IN.)	CONFIGURATION	TVA-WELD IDENTIFICATION
24	STP/TEE	DRHR-2-9
24	STP/VLV	DRHR-2-8
24	SREL/VLV	DRHR-2-7
24	SREL/LREL	DSRHR-2-4A
24	STP/LREL	DSRHR-2-4
24	STP/STP	DSRHR-2-3
24	STP/VLV	DRHR-2-6
24	VLV/LREL	DRHR-2-5
24	STP/LREL	DSRHR-2-2
24	STP/SREL	DSRHR-2-1
24	STP/SREL	DRHR-2-4

TABLE 4

CORE SPRAY

SIZE (IN.)	CONFIGURATION	TVA-WELD IDENTIFICATION
12	STP/STP	DCS-2-13
12	STP/LREL	DCS-2-13A
12	LREL/LREL	DCS-2-7
12	STP/LREL	DSCS-2-9
12	STP/VLV	DCS-2-14
12	STP/STP	DCS-2-4
12	STP/LREL	DSCS-2-1
12	STP/LREL	DSCS-2-2
12	STP/VLV	DCS-2-5

TABLE 5

REACTOR WATER CLEAN-UP

SIZE (IN.)	CONFIGURATION	TVA-WELD IDENTIFICATION
6	SOL/VLV	*DRWC-2-1A/DSRWC-2-1B
6	VLV/STP	DRWC-2-1
6	STP/LREL	DSRWC-2-1
6	LREL/VLV	DRWC-2-2
6	VLV/STP	DRWC-2-3
6	STP/LREL	DSRWC-2-1A
6	LREL/STP	DSRWC-2-2
6	STP/LREL	DSRWC-2-3
6	STP/LREL	DSRWC-2-4
6	STP/LREL	DSRWC-2-5
6	LREL/STP	DSRWC-2-6
6	STP/LREL	DSRWC-2-7
6	STP/LREL	DRWC-2-4
6	FLUED HEAD/STP	DRWC-2-5A
6	STP/VALVE	DRWC-2-5B

*/ONE WELD ONLY

TABLE 6

WELDS EXCLUDED FROM IHSI WORKSCOPE

Recirculation N-2 Nozzle-to-Safe End Welds (10)

Recirculation N-1 Nozzle-to-Safe End Welds (2)

Core Spray System

DCS-2-12	TCS-2-422	TCS-2-402
DCS-2-3	TCS-2-423	TSCS-2-404
TCS-2-417	TSCS-2-424	TCS-2-405
TSCS-2-418	TSCS-2-425	TCS-2-406
TCS-2-419	TCS-2-426	TCS-2-407
TSCS-2-420	TCS-2-401	TSCS-2-408
TCS-2-421	TCS-2-403	TSCS-2-409
		TCS-2-410

RHR System

TRHR-2-191

TRHR-2-192

DRHR-2-12

DRHR-2-3

TRHR-2-194

TRHR-2-193

TABLE 7

IHSI PROCESS CONTROL PARAMETERS - STAINLESS TO STAINLESS STEEL JOINTS

1.	Pipe Outer Surface Temperature within Treatment Zone (Notes 1, 2)	$500^{o}(+75^{o},-100^{o})$
1A.	Maximum Weld Crown Temperature	$600^{o}C$
2.	Minimum Throughwall Temperature Difference (ΔT)	$275^{o}C$
3.	Minimum Width of Zone Heated to T Minimum (Note 3)	$1.5\sqrt{Rt}$ or coil length/2, whichever is less (R = Radius to mid-wall, t = wall thickness)
4.	Minimum Distance from Weld Center to Boundary of ΔT Minimum	15 mm (0.6 inch) or t/2 (whichever is larger, but not less than edge of weld crown)
5.	Minimum Heating Time to Temperature	$0.7\ t^2/a$ seconds (a = Thermal diffusivity, t = wall thickness)
6.	Maximum total time for outer surface above temperature of $425^{o}C$	20 minutes
7.	Nominal Frequency	3 to 4 kHz
8.	Minimum Induction Coil Length	$3\sqrt{Rt}$ (R = Radius to mid-wall, t = wall thickness)

TABLE 8

WELDS STILL REQUIRING IHSI TREATMENT

Recirculation

N-1 nozzle to safe end (2)

N-2 nozzle to safe end (10)

KR-2-23

KR-2-26

KR-2-4

KR-2-1

Core Spray

DCS-2-12

DCS-2-3

RHR

DRHR-2-12

DRHR-2-3

RWCU

DRWC-2-5A

STRUCTURAL JUSTIFICATION FOR THE OVERLAY REPAIR ON WELD GR-2-15

Overlay Sizing Calculations

Weld overlay sizing calculations were performed based on a 360° through-wall circumferential crack in the 12-inch end of the 28 X 12-inch reducer. The thickness at this joint is 0.579 inch. The resultant overlay is 0.35-inches thick and is depicted in Figure 1. The 0.35-inch thickness is in addition to the seal weld which is applied over the crack and the first weld layer that clears dye-penetrant testing (PT) inspection.

Axial stresses at this joint are given as:

Pressure	=	6,321 psi
Dead Weight	=	1,990 psi
Seismic	=	6,000 psi
Thermal Expansion	=	14,000 psi

The primary stresses include pressure, dead weight, and seismic stresses; thus the resultant stress is 14,311 psi. The allowable stress, S_m, at the design temperature of 575°F is 16,675 psi.

The primary stress ratio, $(P_m + P_b)/S_m$, is about 0.858, which results in an allowable flaw depth to thickness ratio, a/t, of 0.495 for a 360° crack, from ASME Section XI, Table IWB-3641-1. Therefore, the unrepaired joint is unacceptable; however, an overlay repair of 0.35-inch thickness results in several effects which render the repaired joint acceptable. The a/t ratio is reduced from 1 to 0.6232, and the primary stress ratio is reduced from 0.858 to 0.5348 because of the increased pipe wall thickness. For this stress ratio of 0.5348, an allowable a/t ratio of 0.6626 is obtained from IWB-3641-1 for a 360° crack, and the allowed crack depth, a, is determined to be 0.6155-inch deep.

Fatigue Crack Growth

Consideration of fatigue crack growth during service is required to show that the original 360° crack of 0.579-inch depth will not extend past the allowed 0.6155-inch depth. Thus, the allowance for fatigue crack growth is 0.0365 inch.

Axial stresses at this joint for heatup/cooldown cycles include pressure, and thermal stresses, thus the resultant stress is 20,321 psi. This stress can be reduced by the unoverlaid-to-overlaid-thickness ratio, 0.6232, and this reduced stress is 12,665 psi. The EPRI DRIVE Computer Program was used to compute the stress intensity factor, K, for a 360°, 0.579-inch deep flaw having a stress of 12,665 psi. The resulting stress intensity factor is approximately 38 ksi $\sqrt{\text{inch}}$.

A weld metal fatigue crack growth curve is assumed equal to the upper bound of solution annealed Type 304 for BWR environments, as shown in the attached figure from EPRI Report NP-2423-LD. The crack growth rate corresponding to K=38 ksi $\sqrt{\text{inch}}$ is about 4×10^{-4} in/cycle. Because changes in K are negligible for small amounts of crack growth, it is estimated that it would take 91 heatup/cooldown cycles to use up the 0.0365 inch allowance for fatigue.

Conclusion

Based on a conservative estimate of 10 heatup/cooldown cycles per year, it would take about 9 years for the crack to extend from 0.579 inch to the limit of 0.6155 inch. Thus, the joint is suitable for service with the weld overlay for at least 2 fuel cycles which is the maximum that is currently accepted by NRC.

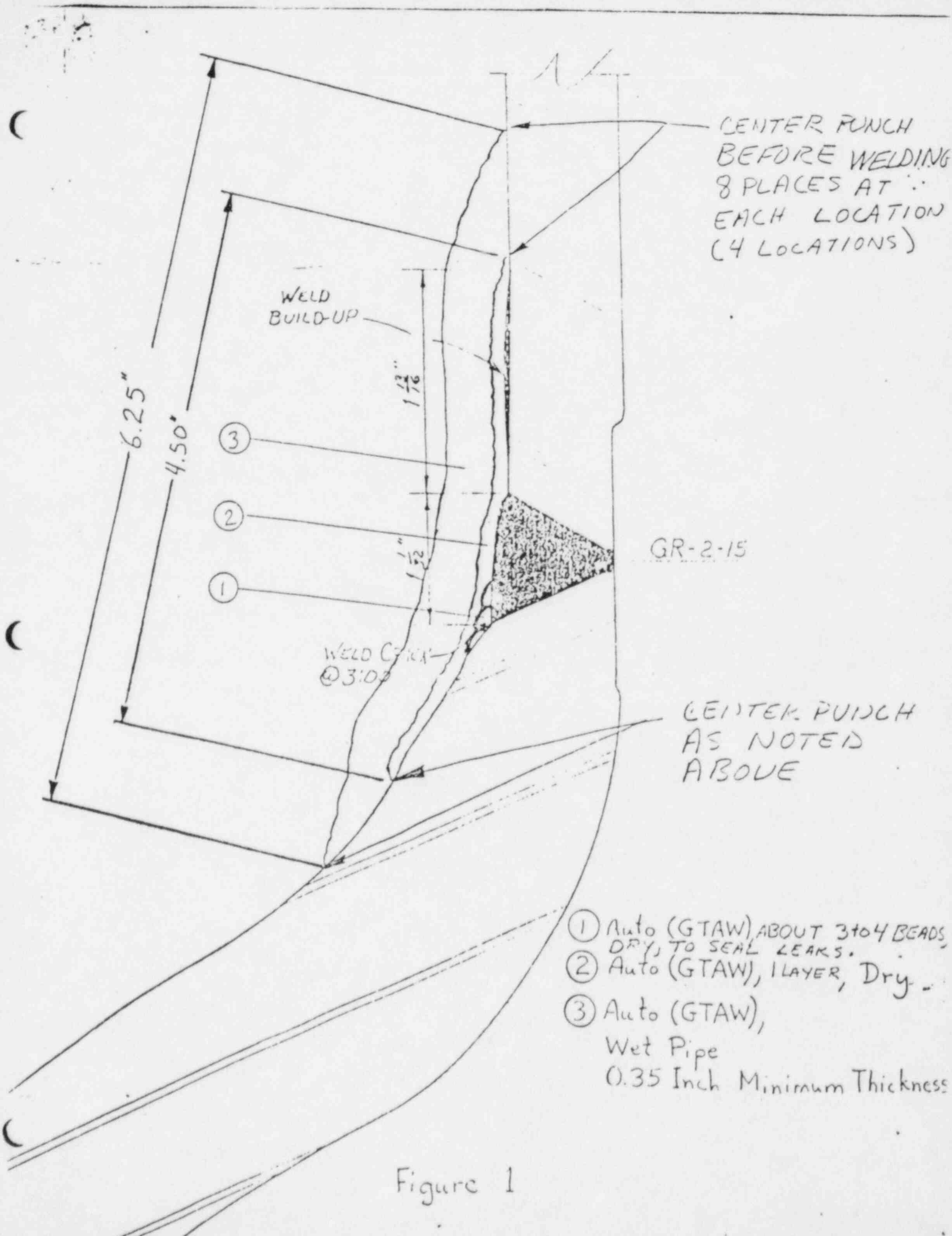
CENTER PUNCH BEFORE WELDING 8 PLACES AT EACH LOCATION (4 LOCATIONS)
WELD BUILD-UP
6.25"
4.50"
3
2
1
GR-2-15
CENTER PUNCH AS NOTED ABOVE
1 Auto (GTAW), ABOUT 3 to 4 BEADS, DRY, TO SEAL LEAKS.
2 Auto (GTAW), 1 LAYER, Dry.
3 Auto (GTAW), Wet Pipe 0.35 Inch Minimum Thickness

Figure 1

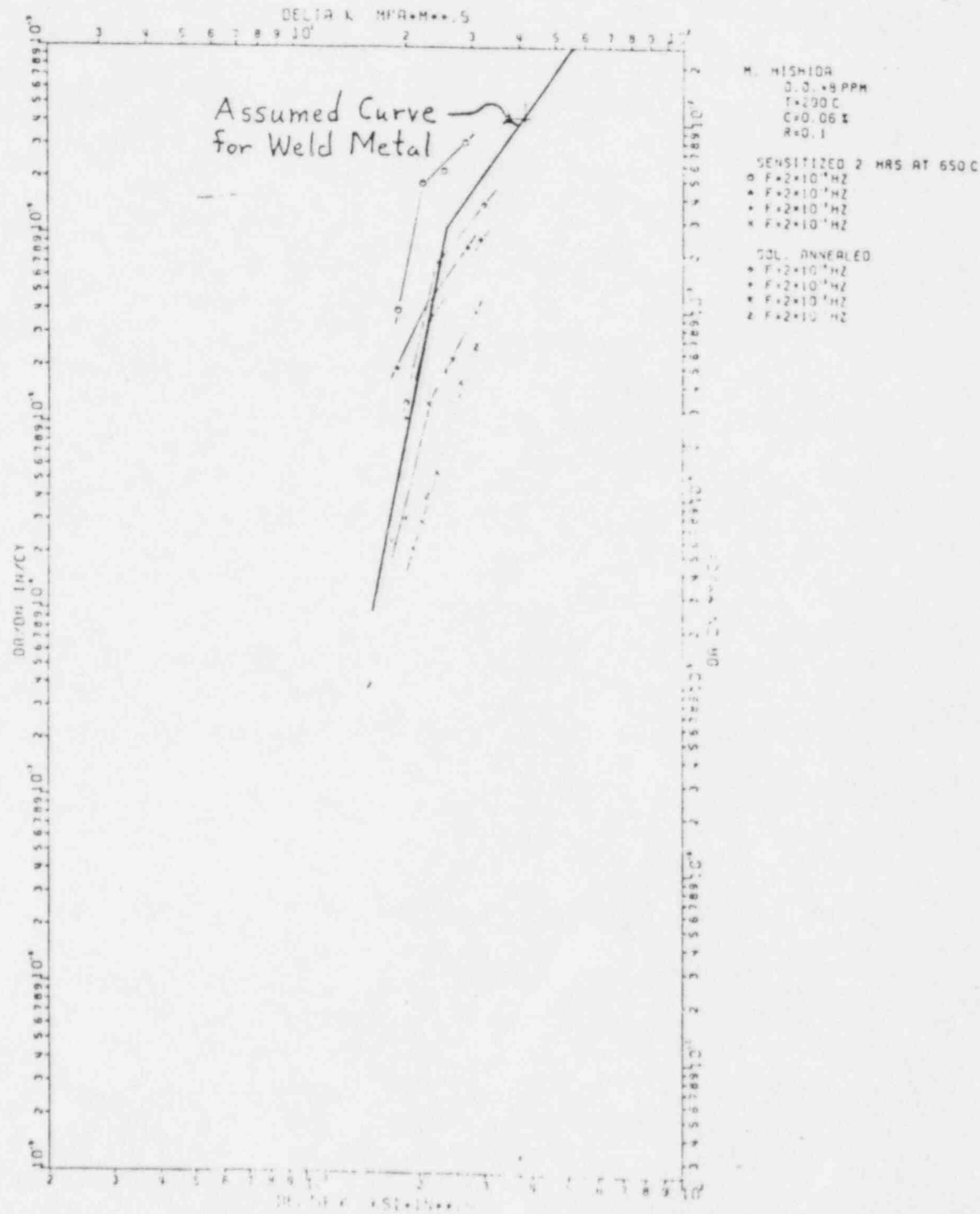

Figure 2-19. Hishida's Data, 8 ppm Oxygen (da/dN vs. ΔK)

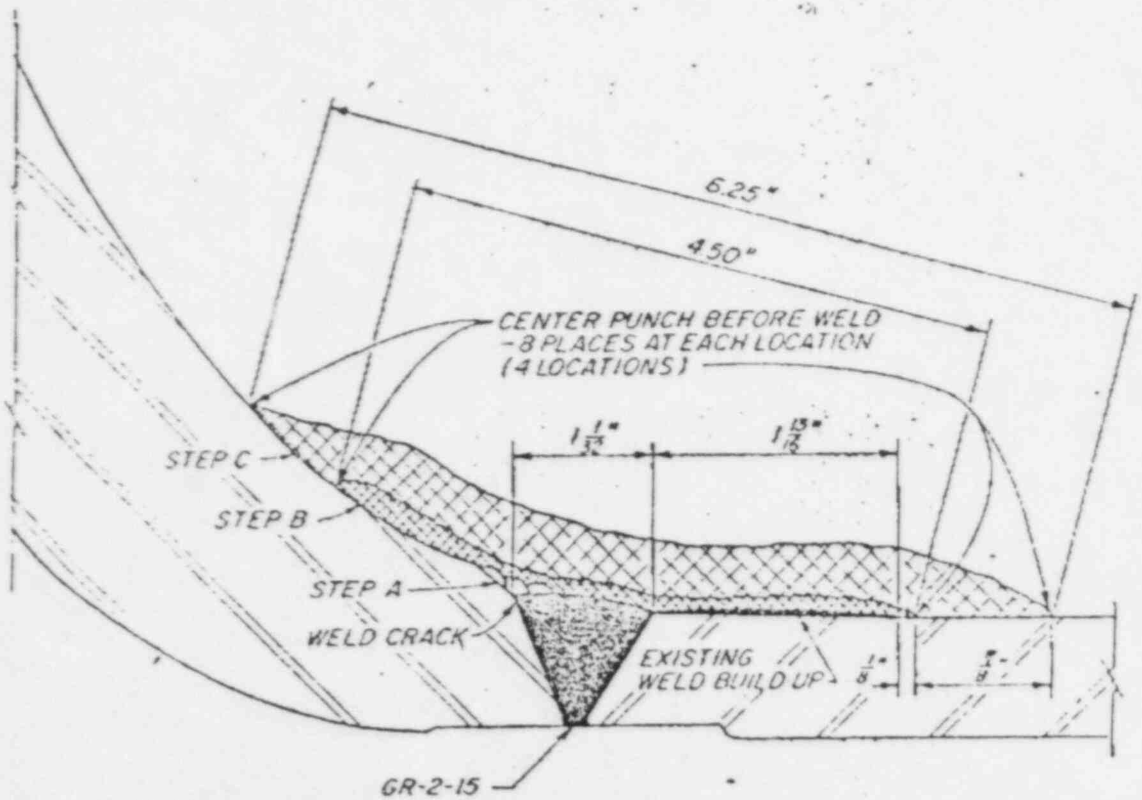

STEPS

- A DEPOSIT ABOUT 3 TO 4 BEADS TO DRY SEAL (PT REQ'D)
- B AUTO (GTAW), ONE LAYER, DRY (PT REQ'D)
- C AUTO (GTAW), WET PIPE, 0.35 INCH MIN. THICKNESS (EXCLUDING LAYERS A & B)

GENERAL NOTES PERTAINING TO WELDING AND NDE FOR OVERLAY OF WELD GR-2-15

1. WELDING AND NON DESTRUCTIVE EXAMINATION SHALL BE PERFORMED IN ACCORDANCE WITH ASME SECTION XI, 1974 WITH SUMMER 1975 ADDENDA, AND THE ADDITIONAL REQUIREMENTS OF THIS DRAWING.
2. WELDING PROCEDURES, WELDERS AND WELDING OPERATORS SHALL BE QUALIFIED TO THE REQUIREMENTS OF ASME SECT. IX. WELDING PROCEDURE SHALL BE APPROVED BY TVA PRIOR TO USE.
3. ALL WELDING EXCEPT AS PROVIDED IN NOTE 5 SHALL BE DONE BY THE GAS TUNGSTEN ARC WELDING PROCESS USING ER308L FILLER METAL CONFORMING TO ASME SFA 5.9. DELTA FERRITE CONTENT OF DEPOSITED WELD METAL SHALL BE 8FN MIN. AS DETERMINED BY THE MAGNETIC INSTRUMENT METHOD OF ASME SECT III, NB-2400.
4. DURING WELDING, A MAXIMUM INTERPASS TEMPERATURE OF 350°F AND A MAXIMUM HEAT INPUT OF 50 KILOJOULES PER INCH SHALL BE OBSERVED.
5. PRIOR TO DEPOSITION OF THE STRUCTURAL OVERLAY TO DESIGN DIMENSIONS, THE AREA CONTAINING THRU WALL CRACKS SHALL BE SEALED BY WELDING. THICKNESS OF THE SEAL WELD NEED NOT EXCEED ONE LAYER PROVIDED THE REQUIREMENTS OF NOTE 6 ARE MET. PIPE INTERIOR SHALL BE DRY DURING SEAL WELDING. SEAL WELD MAY BE MADE BY THE PROCESS OF NOTE 3 OR BY THE SHIELDED METAL ARC PROCESS USING E308L-15 OR -16 ELECTRODES OF ASME SFA 5.4. THE FERRITE REQUIREMENTS OF NOTE 3 APPLY.
6. THE SEAL WELD LAYER AND ADJACENT SURFACE TO BE OVERLAYED SHALL BE LIQUID PENETRANT EXAMINED PRIOR TO START OF THE STEP B OVERLAY LAYER. THE STEP B LAYER SHALL ALSO BE LIQUID PENETRANT EXAMINED PRIOR TO BEGINNING THE STRUCTURAL OVERLAY (STEP C).
7. THE FIRST LAYER OF THE STRUCTURAL OVERLAY SHALL BE MADE WITH PIPE INTERIOR DRY. DURING DEPOSITION OF SUBSEQUENT LAYERS REQUIRED TO DEVELOPE NECESSARY OVERLAY THICKNESS, PIPE INTERIOR SHALL CONTAIN STANDING OR FLOWING WATER.
8. COMPLETED OVERLAY SHALL BE EXAMINED BY LIQUID PENETRANT AND BY ULTRASONIC TESTS APPROPRIATE FOR DETERMINATION OF WELD SOUNDNESS AND BOND TO THE ORIGINAL PIPE/WELD SURFACE.
9. ALL WELD LAYERS INCLUDING SEAL WELD TO EXTEND 360° AROUND PIPE CIRCUMFERENCE.

R0 ISSUE FOR ECN P5215

NOT TO SCALE

POWERHOUSE
REACTOR BUILDING - UNIT 2

MECHANICAL
RECIRCULATION SYSTEM
WELD GR-2-15 OVERLAY

BROWNS FERRY NUCLEAR PLANT

67M 47B2408-1

STRUCTURAL INTEGRITY ASSOCIATES, INC.

'SOCIATES
J. Frederick Copeland, Ph.D.
Thomas L. Gerber, Ph.D.
Anthony J. Giannuzzi, Ph.D.
Anthony N. Mucciardi, Ph.D.
Peter C. Riccardella, Ph.D.

PCR-85-032
March 27, 1985

Mr. James E. Wilson
Tennessee Valley Authority
1420 Chestnut Street Tower II
Chattanooga, TN 37401

Subject: Independent Review of the Overlay Repair for Weld GR-2-15, Browns Ferry, Unit 2

Dear Ed:

Our independent review of the overlay repair on weld GR-2-15 shows that the weld overlay design on the subject weld is adequate.

Highlights of the review for the subject weld overlay are summarized as follows:

- Axial stresses at this joint were calculated and tabulated in Table 1. Resulting stresses are very close to those used in the TVA analysis. We concur with your approach of not using Code stress indices, as this is the standard approach used on all Browns Ferry, Unit 1 overlays, as well as those at most other plants.
- Based on the stresses in Table 1, a minimum thickness of 0.31 inch is required for the overlay (Table 2). The 0.35 inch thick designed overlay provides an extra 0.04 inch allowance for fatigue crack growth.
- Stress intensity factor for a 0.929 inch thick cylinder with a 0.579 inch deep, 360° circumferential crack was calculated to be 35.1 $Ksi\sqrt{in}$ (Figure 1) which is compatible with 38 $Ksi\sqrt{in}$ given in the design analysis.
- The fatigue curve used in the design analysis was judged to be adequate and the 4×10^{-4} in/cycle crack growth rate was reconfirmed.

- Allowable flaw size after the 0.35 inch overlay repair was evaluated and tabulated in Table 3. It was also reconfirmed that fatigue crack growth from more than 90 heatup/cooldown cycles can be tolerated within the extra 0.04 inch thickness allowance. Additional margin on cycles could also be obtained by taking credit for part of the first weld overlay layer if needed.

Should you have any further questions, please call me.

Very truly yours,

P. C. Riccardella

/sl

enc.

cc: Frank Novak
Welding Services, Inc.

TABLE 1

Calculation of Applied Stresses

TVA-06 WELD GR-2-15

Pressure=1150 psi
OD=12.75 inches
Z =64.5 in**3

LOAD CASE	Mx (ft-lbf)	My (ft-lbf)	Mz (ft-lbf)	Mb (ft-lbf)	Axial Sig (psi)
PRESSURE					6330.96
DW	381.00	139.00	10661.00	10661.91	1983.61
TE1	3162.00	701.00	12598.00	12617.49	2347.44
TE2	6621.00	73762.00	3232.00	73832.77	13736.33
OBE-xy	1129.00	5317.00	31487.00	31932.77	5940.98
OBE-yz	549.00	2486.00	12560.00	12803.66	2382.08
SSE-xy	1618.00	7922.00	46871.00	47535.76	8843.86
SSE-yz	786.00	3509.00	17868.00	18209.30	3387.78

TABLE 2

Weld Overlay Sizing

pcCRACK
STRUCTURAL INTEGRITY ASSOCIATES, INC.
VERSION 1.0, APRIL 1985
SAN JOSE, CA (408)978-8200

WELD OVERLAY SIZING

OVERLAY SIZING FOR CIRCUMFERENTIAL CRACK:-

TVA-06, WELD GR-2-15

WALL THICKNESS= 0.5790
STRESS RATIO= 0.8550

	L/CIRCUMFERENCE					
	0.0	0.1	0.2	0.3	0.4	0.5-->1.0
FINAL A/T	0.7500	0.7500	0.7500	0.7500	0.7500	0.6514
OVERLAY THICKNESS	0.1930	0.1930	0.1930	0.1930	0.1930	0.3099

TABLE 3

Allowable Flaw Size for Pipes with 0.35" Weld Overlay

pcCRACK
STRUCTURAL INTEGRITY ASSOCIATES, INC.
VERSION 1.0, APRIL 1985
SAN JOSE, CA (408)978-8200

CRITICAL FLAW SIZE EVALUATION

CRITICAL FLAW SIZE FOR CIRCUMFERENTIAL CRACK:-

TVA-06, WELD GR-2-15

WALL THICKNESS= 0.9290
STRESS RATIO= 0.5330

	L/CIRCUM					
	.0	.1	.2	.3	.4	.5-->1.0
ALLOWABLE A/T	0.7500	0.7500	0.7500	0.7500	0.7500	0.6635

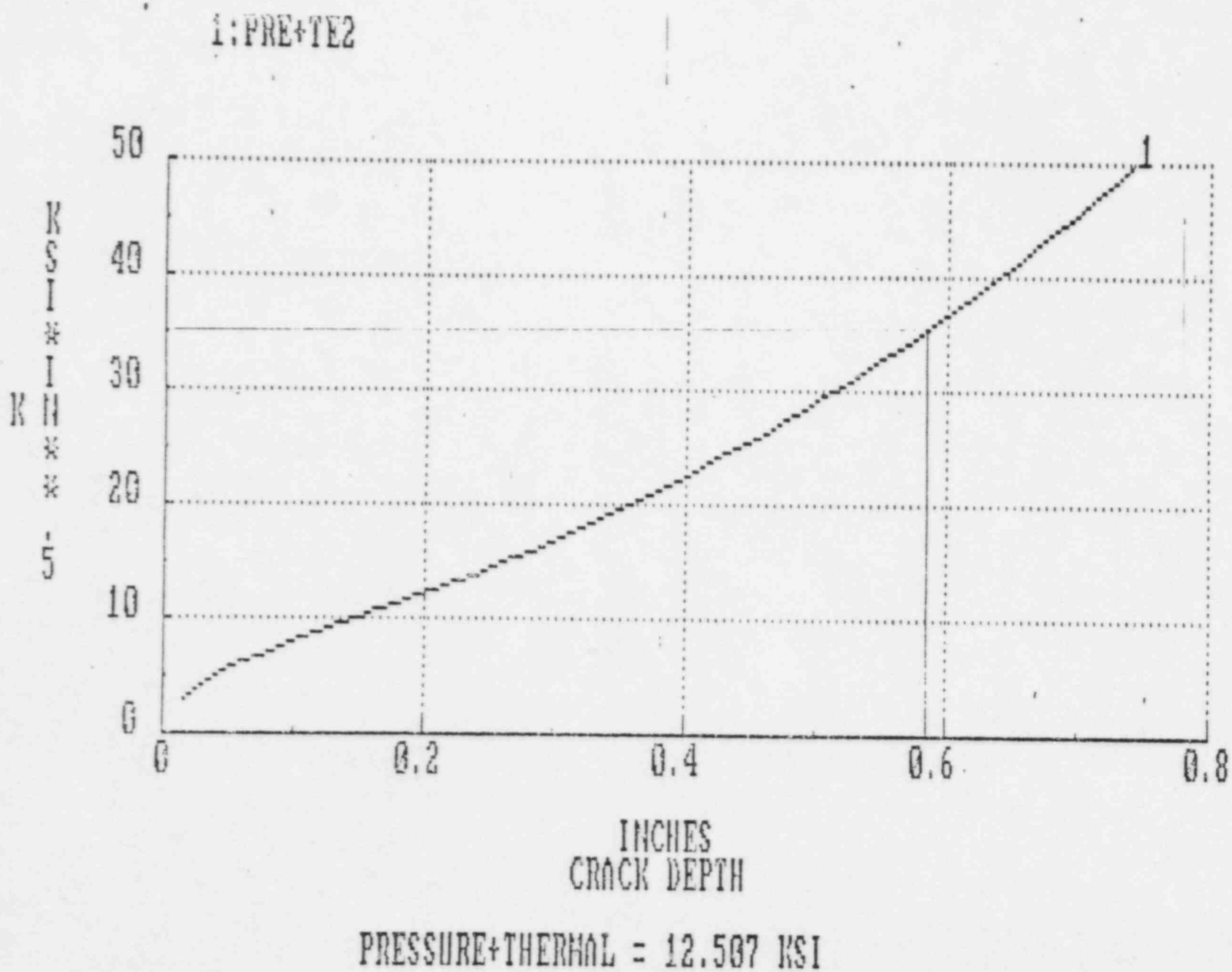

FIGURE 1. Stress Intensity Factor Versus Crack Depth for a 0.929" Thick Cylinder (R/t=10)